Bacterial Adhesion and Motility at Oil-Water Interfaces

by
Narendra Kumar Dewangan

A Dissertation submitted to the Department of Chemical & Biomolecular Engineering
Cullen College of Engineering
In partial fulfillment of the requirements for the degree of

DOCTOR OF PHILOSOPHY
in Chemical Engineering

Chair of Committee: Dr. Jacinta C. Conrad

Committee Member: Dr. Richard C. Willson

Committee Member: Dr. Patrick C. Cirino

Committee Member: Dr. Debora F. Rodrigues

Committee Member: Dr. Stacey M. Louie

University of Houston
December 2020

ACKWONLEDGEMENTS

I express my sincere gratitude to my advisor Dr. Jacinta Conrad for the continuous guidance and support I received during my five and half years of study at the UH. To Jaci, thank you for your motivation and inspiration during my entire project. You helped me to transition from the industry to the graduate school by teaching me how to be an experimentalist. You have not only helped in challenges that I faced in my project but also, helped me how to become a good teacher and a good presenter. Jaci, thank you for trusting me and I hope I will make you proud.

I would like to thank my committee members Dr. Richard Willson, Dr. Patrick Cirino, Dr. Debora Rodrigues, Dr. Stacey Louie, and my advisor for their time, discussion, and suggestions. Thank you for your encouragements and discussions that helped me to successfully finish my Ph.D. dissertation. Thank you to Vincent Donnelly, the department chair Dr. Michael Harold, and the admission committee for giving me the opportunity to pursue the graduate program at this department.

I thank Dr. Patrick Cirino for providing bacteria strains and for access to the lab facilities. I would like to thank Zhiqing Wang and Ryan McLay for helping me transition from an O/G engineer to a researcher by training me on different experiments. I thank Aarti Doshi for the discussion on motility project and her valuable time for running bacteria transformation experiments.

I would like to thank Dr. Richard Willson for the culture and storage facilities. I also would like to thank Dr. Gila Stein for access to the contact goniometer, and Dr. John Wolfe for access to the SEM facility. I thank Dr. Debora Rodrigues for providing bacteria strains.

I would like to thank Andrea Jaimes, Jinsu Kim, Mohammad Safari, Sumedha Sharma, and Nayoung Park for training me on various lab instruments. I thank my labmates; Ryan Roberts, Maxwell Smith, Deepak Mangal, Tzu-Han Li, Fahimeh Khakzad, Mariah Gallegos, Diego Soetrisno, and Gary Chan who helped in along the way in this journey. I would like to thank undergrad researchers Simone Alexandrova, Jing Wang-Reed, and Nhi Tran for contributing to my research work.

I extend my thanks to my parents and sisters for love and support and for believing in me. I thank you from the bottom of my heart for making me the person that I am today. I hope I will make you all proud one day.

ABSTRACT

Degradation of hydrocarbons by bacteria is one of the most important processes in oil spill cleanup. In attempt to increase the rate of biodegradation, chemical dispersants have been deployed in many oil spill scenarios to increase the surface area per unit volume available to bacteria. Biofilm formation is one of the important pathways in degradation of oil by bacteria. Because adhesion of bacteria to surface is one of the important steps in biofilm formation. It is important to study what factors affect the bacterial adhesion on oil/water interfaces. Adhesion of bacteria on solid surfaces is widely studied but surprisingly, how bacteria adhere on oil/water interface, and the effect of surfactants and bacterial motility on adhesion of bacteria on oil/water interface is not well studied.

First, we designed and fabricated a microfluidic device to produce denser monodispersed oil in water emulsion. We developed a method to be able to capture 3D images of bacteria adhering to oil droplets with minimal number of cells attached to imaging chamber and with minimizing the wetting (~ 180° contact angle) of oil droplet to the imaging chamber. We developed tracking algorithms to visualize the cells adhering on the droplet and to calculate the contact angle that each bacterium makes to the droplet surface. In the first part of the project, we studied the effect of surfactant chemistries (anionic [dioctyl sodium sulfosuccinate, dicyclohexyl sodium sulfosuccinate, dibutyl sodium sulfosuccinate], cationic [cetyltrimethylammonium bromide], and nonionic [Tween 20]) and surfactant concentration on adhesion of nonmotile *Marinobacter hydrocarbonoclasticus* SP17 on dodecane droplets.

Secondly, we found that motile bacteria *Halomonas titanicae* adhering to dodecane droplets were able to move the droplets in aqueous suspension. We explored the physics of droplet rotation driven by bacteria. Droplets rotate in clockwise direction when viewed from the liquid side, due to symmetry-breaking hydrodynamic interactions of bacteria with the surface. We examined the effect of droplet size on angular speed of droplets. We further investigated the effect of surfactant concentration and interfacial affinity of bacteria (by using three different bacteria species *Escherichia coli*, *Shewanella haliotis*, and *Halomonas titanicae*) on droplet rotation.

Thirdly, we investigated the effect of bacterial motility on adhesion of bacteria on hexadecane droplets. Here, we show that bacterial motility enhances adhesion to surfactant-decorated oil droplets dispersed in artificial sea water. Motile *Halomonas titanicae* adhered to hexadecane droplets stabilized with dioctyl sodium sulfosuccinate (DOSS) more rapidly and at greater surface densities compared to nonmotile *H. titanicae*, whose flagellar motion was arrested through addition of a proton decoupler. Increasing the concentration of DOSS reduced the surface density of both motile and nonmotile bacteria as a result of the reduced interfacial tension.

Finally, we investigated the effect of concentration of anionic surfactant dioctyl sodium sulfosuccinate (DOSS) and calcium chloride on aggregation of nonmotile *Marinobacter hydrocarbonoclasticus* and *Halomonas titanicae* in synthetic seawater. Bacteria aggregation may occur due to environmental stresses as a protective mechanism or it can occur as a first step towards biofilm formation and subsequent biodegradation. There are two physical mechanisms known in aggregation of bacteria: (1) aggregation by depletion attraction, and (2) aggregation by bridging attraction due to EPS or polymers.

In our study, we found that aggregation (size and number density) increases with increase in DOSS concentration and calcium chloride concentration. Motile *Halomonas titanicae* showed higher aggregation compared to nonmotile bacteria.

Together, we studied bacteria motility and adhesion interactions on cell-solid surface, on cell-liquid interfaces, and on cell/cell interfaces. Broadly, this research contributes to the fields of bioremediation and antifouling.

TABLE OF CONTENTS

List of Tables:

List of Figures:

Chapter 1: Introduction to bacterial adhesion

Bacterial adhesion is one of the important steps in biofilm formation.[1] Biofilm formation is seen in a variety of different surfaces such as industrial pipelines,[2] river rocks,[3] ship hulls,[4] kitchen sink,[5] plant roots,[6] teeth,[7] biomedical implants in human body.[8] Biofilm formation may be advantageous in fields such as in biofuel cells, removal of pollutants (e.g., oil spills), wastewater treatments or deleterious such as painted surface and medical implants. Because bacterial adhesion is the first step towards biofilm formation it is important to understand what factors influence bacterial adhesion.

More specifically, this work is primarily inspired from offshore oil-spills.[9] Many bacteria species are known to degrade various hydrocarbons of crude oil.[10] Chemical dispersants[11] are employed to break larger oil droplets into smaller droplets to provide larger surface access to bacteria. There are a lot of works published on how dispersants affect bacteria growth and biodegradation[12–15] but not much is known on how dispersants affect initial attachment of bacteria. This work is primarily focused on interaction of bacteria to oil/water interfaces in presence of surfactants.

1.1 Biofilm formation

Initial adhesion of bacteria is the first step of biofilm formation.[1] Bacteria may adhere to the surface reversibly or irreversibly. Adhered bacteria on surface may divide and produce extracellular polymeric substance (EPS). EPS helps in enhanced adhesion and formation of 3D cellular matrix. In the next stage the EPS matrix further develops and can prevent harmful effects of environmental stresses. In the final stage, some bacteria leave the cellular matrix and re-enter the planktonic state.

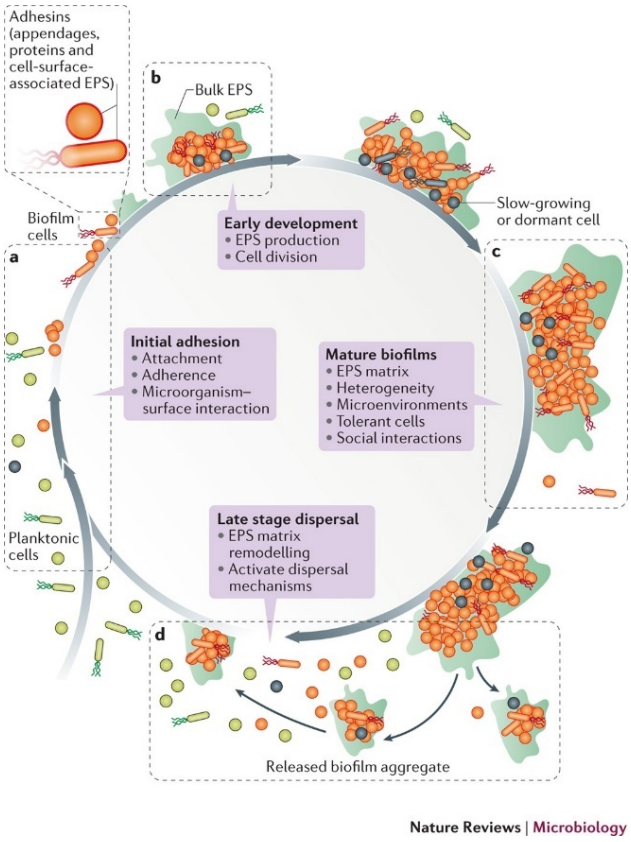

Figure 1.1. Biofilm formation lifecycle.[1]

The growth of bacteria on surface can be controlled at various stages of biofilm formation. For example, the initial stage of bacteria adhesion can be prevented by preventing the bacteria to adhere on surface. Initial stage of biofilm development can be prevented by preventing the cell division or EPS production. Disruption or degradation of biofilm can be achieved by physical removal or using a condition such as high or low pH that can eliminate the biofilm. Biofilm dispersal can be achieved in early stage by remodeling EPS and promoting cell dispersal.

1.2 Interaction of bacteria with surfaces

Bacteria close to the surface experience two main interactions; Lifshitz van der Waals (LW), which is attractive in nature and electrical double layer (EL), which can be

either attractive or repulsive. Bacteria-surface interaction can be described by classical DLVO (Derjaguin, Landau, Verwey, Overbeek) theory of colloidal stability.[16] This theory has been extensively used to calculate interaction energy for bacteria-surface or bacteria-bacteria interaction as a function of separation distance. This theory assumes the interacting system inert. An extended DLVO (XDLVO) theory was introduced by Van Oss to include short-range Lewis acid-base interactions to account for hydrogen bonding. This polar interaction can be attractive or repulsive depending on hydrophilic and hydrophobic properties of the bacterium and the surface. According to XDLVO theory, the total interaction energy (G_{slb}^{DLVO}) for a bacterium (b) and surface (s) in an aqueous medium (l) is given by,

$$G_{slb}^{DLVO}(d) = G_{slb}^{LW}(d) + G_{slb}^{EL}(d) + G_{slb}^{AB}(d),$$

where G_{slb}^{LW} is the Lifshitz van der Waals energy, G_{slb}^{EL} is the electrical double layer energy, and G_{slb}^{AB} is the acid-base energy. When this interaction energy is negative, adhesion is favorable.

Adhesion of bacteria on liquid-liquid surface is relatively more complex due to the fact that bacteria may partially submerge in both phases, however, the thermodynamic principle of adhesion remains the same. In recent years, there have been many works on understanding bacteria adhesion and biofilm formation on oil-water interfaces.[17–20]

1.3 Factor affecting bacteria adhesion

The effect of solid surface properties on bacterial adhesion is widely studied. It has been shown that surface hydrophobicity, surface functional group, surface roughness, surface topology can affect the bacterial adhesion.[21–28] Surfaces with hydrophobic -C_9CH_3 showed higher adhesion of *E. coli* whereas surface with hydrophilic group -C_{15}

COOH showed lowest amount of bacterial adhesion.[21] Another study suggested that bacterial adhesion increases nonmonotonically with water contact angle of surface.[23] Bacterial adhesion was highest at water contact angle of 95° and it decreases at the water contact angle above 95°. Bacterial adhesion and antifouling properties of surface are also dependent on thickness of polymer layer and polymer dispersity of surface.[24] Adhesion and removal of bacteria can also be altered by salt-responsive polymer functionalized surface.[25] Surface roughness and topology can also help in preventing bacterial adhesion.[26,27]

Bacterial adhesion on oil-water interface at different condition is not well studied. In recent years, oil-spills in ocean have drawn a lot of focus on understanding the adhesion and biofilm formation to oil-water interface.[17,18,29–35] One of the most abundant bacteria in oil-spill region, *Alcanivorax borkumensis* has shown an improved growth of bacteria in presence of low concentration of dioctyl sulfosuccinate sodium salt (AOT).[17] It has also been shown that *A. borkumensis* grown under oil spill (hexadecane layer as a carbon source) showed three times more growth than grown in clean environmental condition (marine broth).[18] This bacteria species has shown better dispersion of oil droplets when used in conjunction with Corexit.[30] In another study, bacteria surface hydrophobicity measured by BATH assay and its adsorption on n-decane was compared for *P. aeruginosa*, *S. aureus*, and *S. epidermidis*.[32] *P. aeruginosa* showed the highest value of BATH whereas other two species showed nearly zero hydrophobicity. Hydrophilic *S. aureus* did not grow a biofilm. Despite showing nearly zero hydrophobicity *S. epidermidis* adsorbed on oil-water interface and formed biofilm due to secreted biosurfactants.

1.4 Objective and organization of dissertation

The objective of this research to understand how surfactant chemistries and its concentration, and bacteria motility affect bacterial adhesion on oil/water interfaces. We also explored the bacteria-driven droplet motion and surfactant induced bacteria aggregation. Together, this work contributes a broader field of understanding biofilm, biodegradation, and microactuators.

In the first part of this research, we developed microfluidic techniques to make dodecane in water emulsions stabilized with different surfactants at various concentrations. We functionalized inner wall of glass capillaries (imaging chamber) with polyethyleneglycol-APTES to prevent adhesion of bacteria and oil droplets to walls. We found that bacteria adhere to smallest droplet to the greatest value and smallest droplet shows faster adhesion. A large percentage of adhering bacteria align along with the droplet surface. Interfacial cell densities decrease with increase in surfactant concentration for all five surfactants. Decrease in interfacial cell density is more monotonic for anionic surfactants. In addition, electrostatic repulsion due to surface charge of bacteria and droplets also plays role in bacterial adhesion. This study shows that although use of surfactant would provide more available surface of bacteria to adhere by breaking larger oil droplets into smaller droplets, a higher concentration of surfactant may lead to lower adhesion.

In the second part of this thesis, we explored the motion, in particular rotational motion, of oil droplets driven by motile bacteria at oil interface. We found that oil droplets rotate in clockwise direction when viewed from liquid side due to hydrodynamic

interaction of adhered bacteria to wall. Angular speed of droplets are inversely proportional to its diameter. The speed of droplet rotation decreases with increase in surfactant concentration due to fewer number of adhered cells, and due to the less-strongly adhered cells at interface. The speed of droplets rotation is also varied among different bacteria species due to varied interfacial affinities.

In the third part of this project, we explored the effect of bacteria motility on adhesion to hexadecane droplets. For this, we chemically modified (using CCCP), and mechanically modified (shearing flagella) the bacteria to make them nonmotile. Both motile and nonmotile bacterial adhesion followed first-order Langmuir adsorption kinetics. Interfacial cell density of motile bacteria on droplet reaches the equilibrium value much faster compared to the nonmotile bacteria. Motile bacteria adhere nearly six times more compared to nonmotile bacteria. Interfacial cell density decreases with increase in DOSS concentration for both nonmotile and nonmotile bacteria. At highest DOSS concentration interfacial cell density of nonmotile bacteria is nearly zero whereas it is nonzero for motile bacteria. This study suggests that motility may enhance the bacteria adhesion, and therefore can enhance biofilm formation and subsequent biodegradation.

In the final part of this thesis, we explored the condition of bacteria aggregation. We found that *Marinobacter hydrocarbonoclasticus* form aggregates when both DOSS concentration and Ca^{2+} are present in suspension. The size of aggregates and number density of aggregates increase with increase in DOSS concentration. An increase in calcium chloride concentration further increased the aggregation. Motile *H. titanicae* show slightly higher aggregation compared to nonmotile *H. titanicae*. This result may

have wider implication in understanding why bacteria aggregate at various environmental conditions important in bioremediation and pathogenesis.

Chapter 2: Adhesion of *Marinobacter hydrocarbonoclasticus* to Surfactant-Decorated Dodecane Droplets

2.1 Introduction

Dispersed hydrocarbons are widely found in marine environments, emerging naturally from oil seeps and as an unintended consequence of petroleum extraction and transportation processes.[36] Thus, many marine bacteria can degrade hydrocarbons.[9,11,37–41] Indeed, the surprisingly rapid disappearance in the 2010 Deepwater Horizon spill is thought to be due to bacterial biodegradation.[42–44] The efficacy of biodegradation depends, in part, on the bioavailability of dispersed oil to bacteria. In a typical oil spill scenario, dispersants such as COREXIT 9500EC that contain one or more surfactants[45] are applied near the wellhead and on the water surface[46] to speed biodegradation.[47–50] Dispersants decrease the interfacial tension between the oil and water phases, reducing the Gibbs free energy[51,52] and leading to smaller droplets. Dispersants thus increase the surface area per unit volume and hence the bioavailability of the oil.[11] Because bacterial adhesion to the oil/water interface can promote biodegradation, it is important to understand how surfactants affect adhesion of bacteria at these interfaces.[53–56]

From a thermodynamic perspective, the surface energies of bacteria and the two phases determine the extent of adhesion to oil/water interfaces.[57–59] Briefly, bacteria adhere to the oil/water interface when the sum of the surface energies is lower with the bacterium at the oil-water interfaces than it is with the bacterium entirely in the aqueous phase.[60,61] Surfactants reduce the surface energy of liquid/liquid and bacteria/liquid interfaces, depending on the length and branching of the hydrocarbon chain and on the partitioning of surfactant molecules between the bulk phase and the interface.[62,63] The

curvature of the interface between oil droplets and water alters the volume available to surfactant tails and thus modifies the free energy of adsorption in the presence of surfactants,[64] complicating predictions of the adsorption of bacteria to curved oil/water interfaces.

Here, we investigate the effect of interfacial properties on adhesion of hydrocarbon-degrading *Marinobacter hydrocarbonoclasticus* at oil/water interfaces. Using co-flow microfluidic devices, we prepare monodispersed dodecane/water emulsions with drop sizes of 20 – 60 μm, stabilized with various surfactants. Using confocal microscopy and bacteria-tracking algorithms, we first quantify the number of bacteria adhering at the oil/water interface over time for drops stabilized by dioctyl sodium sulfosuccinate (DOSS), a component of the COREXIT dispersant used in oil spill remediation and used in a variety of emulsification applications. Adhesion of bacteria follows first-order Langmuir kinetics, with a time constant that increases with drop size. Surprisingly, the areal coverage of bacteria on small 20 μm droplets is larger than that on larger droplets. We subsequently examine the long-time adsorption bacteria on interfaces stabilized by various surfactants, comparing DOSS to two other anionic sodium sulfosuccinates [dibutyl sodium sulfosuccinate (DBSS), dicyclohexyl sodium sulfosuccinate (DCHSS)] as well as to two other surfactants [cationic cetyltrimethylammonium bromide (CTAB), non-ionic Tween 20)]. For all surfactants, increasing the surfactant concentration at a fixed droplet size reduces the interfacial tension and bacterial adhesion. The type and charge of surfactant also affect the extent of equilibrium adsorption, with fewer bacteria adhering to anionic (DOSS, DCHSS) interfaces than to CTAB or Tween 20-decorated interfaces at high normalized surfactant

concentrations. Our results suggest that the use of surfactants may have competing effects on bacterial adhesion: the increase in adhesion due to a decrease in droplet size contrasts with the reduction in adhesion due to the lower oil/water interfacial tension.

2.2 Materials and Methods

2.2.1 Chemicals

Hydrogen peroxide 30% (Macron), sulfuric acid 98% (EMD Millipore), potassium hydroxide (Sigma-Aldrich), methanol (Sigma-Aldrich), acetic acid (EMD Millipore), 3-aminopropyl trimethoxysilane (APTES, Gelest), biotin-mPEG (5,000 Da, ThermoFisher), biotin-PEG-SVA-5000 (5,000 Da, ThermoFisher), sodium bicarbonate (Sigma-Aldrich), dodecane (>99%, Sigma), dioctyl sodium sulfosuccinate (DOSS, ≥97%, Sigma-Aldrich), dibutyl sodium sulfosuccinate (DBSS, as received, Aldrich), dicyclohexyl sodium sulfosuccinate (DCHSS, ≥98%, Sigma-Aldrich), cetyltrimethylammonium bromide (CTAB, ≥99%, Sigma-Aldrich), Tween 20 (ThermoFisher), Zobell marine broth 2216 (HiMedia lab), sodium pyruvate (Amresco), SYTO9 (ThermoFisher), Nile red (Sigma-Aldrich), sodium chloride (Macron), diiodomethane (Sigma-Aldrich), ethylene glycol (Sigma-Aldrich), acetone (BDH), and ethanol (100%, Decon Labs) were used as received. The chemical structures of the five surfactants are shown in Figure 2.1.

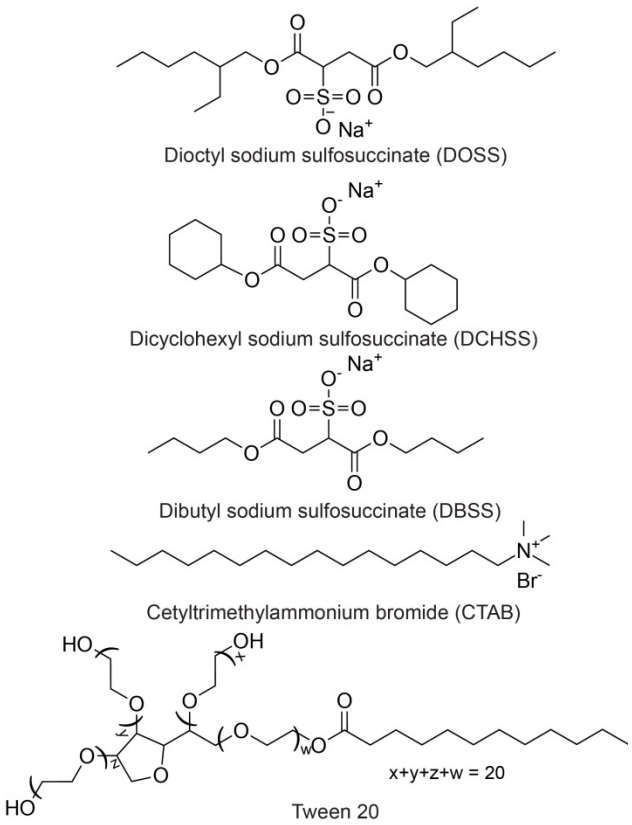

Figure 2.1. Molecular structure of surfactants used in this study.

2.2.2 Co-flow microfluidic device fabrication

To prepare aqueous emulsions of dodecane with controlled droplet size, we fabricated co-flow glass capillary microfluidic devices. The device consisted of two coaxially aligned glass capillaries,[65,66] as shown in Figure 2.2(a). The square outer capillary (Vitrocom) had an outer diameter of 1 mm, an inner diameter of 0.90 mm, and a length of 50 mm. The circular inner capillary (Vitrocom) had an outer diameter of 0.87 mm and an inner diameter of 0.70 mm. A dual-stage glass micropipette puller (PC-10, Narishige) was used to generate tapered inner capillaries with a taper length of ~5 mm and an opening diameter of 5 μm. The outer capillary was also pulled to create a constriction of inner diameter 120 – 150 μm and length 10 mm near its midpoint. The inner capillary was inserted within the outer capillary and aligned coaxially near the

constriction at the midpoint of the outer capillary. The inlet and outlet were coupled to 18 gauge blunt needles (BD) by using UV adhesive (NOA 68T, Norland), with a glass slide (75 mm × 50 mm, Corning) as a supporting base. Tygon tubing (0.03" ID, Cole palmer) was used for all inlet and outlet connections.

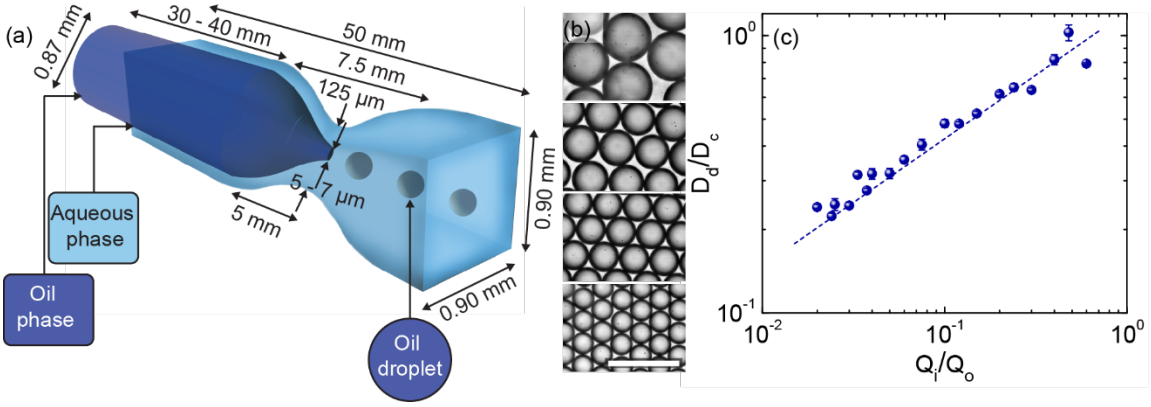

Figure 2.2. (a) Schematic of the glass-based co-flow microfluidic device used to prepare monodisperse dodecane-in-water emulsions. (b) Brightfield micrographs of monodisperse dodecane-in-water emulsions, stabilized by DOSS at 35 ppm, with drop diameters of 72, 50, 40, and 31 µm, obtained at outer fluid flow rates of 3000, 1500, 1000, and 500 µL min^{-1}, respectively. Scale bar is 100 µm. (c) Normalized droplet size (D_d/D_c) as a function of inner to outer fluid flow rate (Q_i/Q_o). Drop size (D_d) is normalized by the inner diameter of the outer capillary (D_c) measured near the tip location of the inner capillary. Dashed line indicates the fit to eq 2.1 [ref[67]]. Error bars indicate the standard deviation of droplet diameters in a single micrograph, confirming that the emulsions are monodisperse.

2.2.3 Preparation of oil-in-water emulsions

Monodisperse emulsions of dodecane in MilliQ water (18.2 MΩ · cm) were prepared using the co-flow microfluidic devices.[65] Dodecane droplets were stabilized in water using one of five surfactants: dioctyl sodium sulfosuccinate (DOSS, at concentrations of 2 – 360 ppm in the aqueous phase), dibutyl sodium sulfosuccinate (DBSS, 1300 – 130,000 ppm in the aqueous phase), dicyclohexyl sodium sulfosuccinate

(DCHSS, 290 – 29,000 ppm in the aqueous phase), cetyltrimethylammonium bromide (CTAB, 2 – 80 ppm in the aqueous phase), or Tween 20 (1.5 – 150 ppm in the aqueous phase). The inner oil phase and outer aqueous phase were dispensed through two gas-tight Luer lock syringes (Hamilton; 2.5 mL inner, 100 mL outer) at constant flow rates by using two syringe pumps: NE-1002X New Era for inner fluid, and Fusion 200 Chemix for outer fluid. The device was operated at outer flow rates of 50 – 2000 μL min^{-1} and inner flow rates of 5 – 25 μL min^{-1}. As-prepared emulsions were stored at 4° C in dark and used within one week.

2.2.4 Preparation of glass capillaries for imaging

Thin rectangular borosilicate capillaries (0.1 mm height × 1 mm width × 50 mm length, 0.07 mm wall thickness, Vitrocom) were used as sample chambers in imaging experiments. To minimize adhesion of bacteria and prevent wetting of oil droplets, the inner capillary surface was functionalized with polyethylene glycol (PEG) brushes. To prepare the surface for functionalization, capillaries were cleaned with water and acetone, and subsequently treated with 1M KOH solution and with piranha solution; subsequently, the cleaned capillary was functionalized with 3-aminopropyl trimethoxysilane (APTES) and then with PEG (5,000 Da).[68] The water contact angle measured on PEGylated glass slide was 32 ± 2° for three replicates.

2.2.5 Bacteria strain

Marinobacter hydrocarbonoclasticus is an extremely halotolerant marine bacterium that is able to degrade both cyclic and non-cyclic alkanes,[69] and increases in abundance in both the marine environment[70] and in beach sands[4] after an oil spill. *M.*

hydrocarbonoclasticus (ATCC 49840) was obtained from Dr. Douglas Bartlett (Scripps Institute of Oceanography, UCSD). The strain was stored in Zobell marine broth 2216 (Difco)/50% glycerol at -70° C. *M. hydrocarbonoclasticus*, 2 – 3 μm in length and 0.3 – 0.6 μm in diameter, is motile in synthetic medium supplemented with NaCl at concentrations of 0.6 M – 1.0 M;[69] we confirmed visually, using optical microscopy, that this strain was not motile in the conditions of this study.

2.2.6 Growth conditions

M. hydrocarbonoclasticus was streaked from a frozen stock on a marine broth plate (37.4 g L^{-1} marine broth, 10 g L^{-1} sodium pyruvate, 15 g L^{-1} agar) and incubated at 30 °C for 48 h. A single colony selected from the plate was inoculated into 20 mL of culture media (37.4 g L^{-1} marine broth and 10 g L^{-1} pyruvate) and incubated for 20 h in an orbital incubator shaker (New Brunswick Scientific) at 200 rpm and 30 °C. Finally, a subculture was prepared by inoculating 75 μL of the principal culture into 20 mL of culture media and grown to late exponential phase in an orbital incubator shaker at 30 °C and 200 rpm for 20 h.

2.2.7 Zeta potential and surface energy

For surface characterization, *M. hydrocarbonoclasticus* cells were grown to late exponential phase. 20 mL of bacteria samples were centrifuged at 5000g for 10 minutes in a Sorvall ST 16 Centrifuge (Thermo Fisher Scientific). The supernatant solution was removed and the pellet was twice resuspended in 20 mL MilliQ water and centrifuged for cleaning. After cleaning, the pellet was resuspended in MilliQ water. The final optical

density (OD) was adjusted to 0.04 (Laxco DSM-Micro Cell Density Meter, 600 nm) with MilliQ water.

The zeta potential of the bacteria, measured using a Nicomp 380 ζ-potential analyzer, was −45 ± 3 mV (Table 2.1). The zeta potential of the bacteria did not markedly change in the presence of surfactants (Table 2.2). For measurements of the surface energy, the resuspended bacteria sample (OD 1.0) in MilliQ water was filtered through cellulose acetate membrane filters (pore diameter 0.45 μm, Advantec) under vacuum (100 mm Hg below atmospheric pressure) using a GEM 8890 vacuum pump (Welch).[60,71,72] The filters were attached to glass slides (75 mm × 50 mm) using dental wax (Electron Microscopy Sciences) to ensure that the surface remained flat. The contact angles for three liquids (MilliQ water, ethylene glycol, and diiodomethane) were measured on the lawns using a Dataphysics OCA 15EC goniometer. The surface energy of the *M. hydrocarbonoclasticus* bacteria, 23 ± 1 mN m^{-1}, was calculated from inbuilt software using the method of Wu.[73,74] Contact angles and surface energy data are provided in Table 2.3.

Table 2.1. Zeta potential of *M. hydrocarbonoclasticus* in DI water, determined from three independent bacterial cultures.

Culture	**ζ [mV]**
1	-49 ± 2
2	-42 ± 3
3	-45 ± 1

Table 2.2. Zeta potential of bacteria suspensions in DI water at various surfactant concentrations. Error within each sample indicates the standard deviation in measurement in a single culture. The low value of the zeta potential at [CTAB] = 1.00 CMC is a signal of the reduced viability of the cells under these conditions.

C [CMC]	Zeta potential [mV]		
	DOSS	**CTAB**	**Tween 20**
0.00	-50 ± 3		
0.01	-54 ± 2	-54 ± 2	-55 ± 2
0.10	-47 ± 1	-51 ± 2	-55 ± 2
1.00	-50 ± 1	-23 ± 2	-52 ± 2

Table 2.3. Static water contact angle and surface energy of *M. hydrocarbonoclasticus*. Each sample is from an independent bacteria lawn prepared from an independent culture. Errors reported for each sample indicate the standard deviation of the contact angle measurements for five different sessile drops on each lawn.

Culture	**W [°]**	**DIM [°]**	**EG [°]**	**SE [mN m^{-1}]**	**ζ [mV]**
1	88 ± 2	90 ± 3	98 ± 5	22	-49 ± 2
2	85 ± 2	87 ± 1	93 ± 1	24	-42 ± 3
3	85 ± 2	83 ± 2	103 ± 3	22	-45 ± 1

2.2.8 Interfacial tension

To determine the interfacial tension as a function of surfactant concentration, solutions of the various surfactants (DOSS, DCHSS, DBSS, CTAB, Tween 20) were prepared in 5 g L^{-1} NaCl in MilliQ water. Approximately 3 mL of surfactant solution was taken into a cuvette. Dodecane was dispensed through a U-shaped needle into a surfactant solution-filled cuvette and a video (25 fps) was captured of the drop shape using a Dataphysics OCA15EC goniometer. At least three replicates were examined for each concentration. The interfacial tension was determined from the radius of curvature of the drop using the Young-Laplace equation.[75,76] CMC of DOSS in SSW was determined using this method (Figure 2.3).

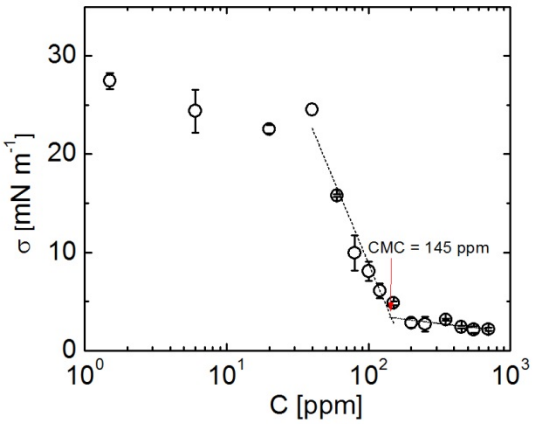

Figure 2.3. Interfacial tension σ between dodecane and water as a function of surfactant concentration in synthetic seawater for determination of the critical of the critical micelle concentration (CMC) for DOSS. The crossover between the two different regimes determine the CMC.

2.2.9 Determination of the critical micelle concentration (CMC) using fluorescence method

Surfactant solutions at various concentrations were prepared in MilliQ water with 5 g L^{-1} NaCl. Nile red (excitation/emission maxima ~552/636 nm, Sigma-Aldrich) was added to each surfactant solution at a concentration of 0.1 mg mL^{-1} and each solution was vigorously vortexed for 5 – 10 minutes to solubilize the dye with micelles present in the solution.[77] The solution was vortexed for 1 minute every hour. After 3 hours, 200 µL of each solution were pipetted into a 96-well plate (Nunc MicroWell 96-Well Optical-Bottom Plates with Polymer Base) and the fluorescence intensities were measured using a SpectraMax Gemini EM Microplate Spectrofluorometer. The intersection of the lines fit to the fluorescence intensity at low and at high surfactant concentration yielded the CMC value of the surfactant in presence of 5 g L^{-1} NaCl in water (Figure 2.4).

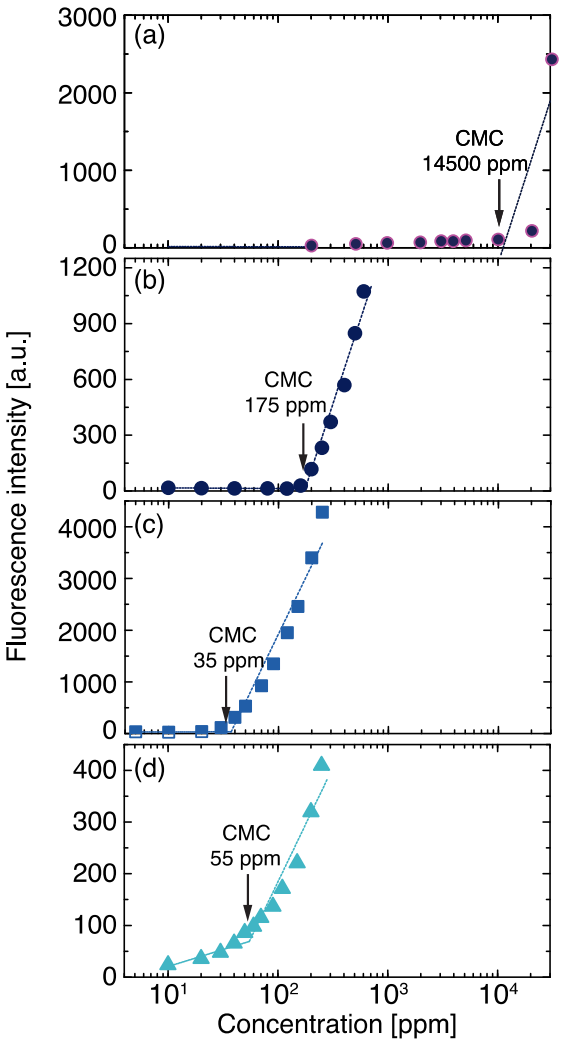

Figure 2.4. Fluorescence intensity as a function of surfactant concentration in 5 g L^{-1} NaCl, for determination of the critical micelle concentration (CMC) using the fluorescence method. (a) DCHSS, (b) DOSS, (c) CTAB, and (d) Tween 20. The crossover between the two different regimes determines the CMC.

2.2.10 Imaging of cells near dodecane-water interfaces

For imaging experiments, cells were harvested at late exponential phase. For fluorescence imaging, 140 µL of the cell suspension were mixed with 860 µL of saline solution (10 g L^{-1} NaCl) or 860 µL of synthetic sea water (g L^{-1}, in distilled water : Tris (hydroxymethyl amino methane), 12.1 ; KCl, 0.75; $CaC1_2$, 1.5 ; NH_4Cl, 3.47 ; $MgSO_4$. 7H20, 6.16 ; $MgCl_2$. 6H20, 5.08; NaCl, 11.7, pH 7.5 with 10 M HCl. 2 mL and 4 mL of

aqueous solutions of iron sulfate (0.1% w/v) and sodium phosphate (lo%, w/v), respectively, were added to SSW immediately before use.) containing the fluorescent stain SYTO9 (1 μL per 1 mL of cell suspension) and incubated at room temperature in the dark for 5 – 10 minutes. 200 μL of the dodecane/water emulsion was added into a 1.5 mL Eppendorf tube containing 200 μL of the stained cell suspension. Importantly, to preserve the droplet size the resultant oil/water emulsion was not strongly mixed. 6.5 μL of this suspension, which had a final NaCl concentration of 5 g L^{-1}, was injected into a glass microfluidic channel and both ends of the channel were sealed with vacuum grease. Experiments were run in the limit of very low concentration of emulsion droplets (volume fraction $\phi = 0.003 – 0.01$), so that the bacteria were at excess.

Bacteria were imaged in 3-D over time as they attached to the oil/water interface using a VT-Infinity (Visitech, Sunderland, UK) confocal microscope. The confocal scanhead was mounted on an inverted microscope (Leica Microsystems DM4000) equipped with a 40x oil-immersion lens (HCX PL APO, NA 1.25 − 0.75). An excitation wavelength of 488 nm was used to excite the SYTO9 stain. To generate a 3-D image stack, we acquired sequential 2-D images over 40, 60, 70, and 80 μm (spacing $\Delta z = 0.31$ μm) for oil droplets of diameter 20, 40, 50, or 60 μm, respectively. 3-D stacks were acquired at times t = 5, 15, 30, 60, 90, 120, 150, and 180 min after the cell suspension was added to the emulsion and loaded into the capillary. Each experiment was reproduced with at least three independent cultures.

To assess the long-time adhesion of bacteria to oil/water interfaces as a function of the surfactant concentration, emulsions containing dodecane droplets of diameter 20 or 50 μm were added into cell suspensions and loaded into capillaries. The loaded

capillaries were incubated at room temperature in dark for at least 90 minutes to reach equilibrium (as determined from the time experiments), and z-stack images were acquired for three different droplets in each sample. This experiment was replicated three times at each surfactant concentration for droplets of diameter 20 μm and 50 μm for DOSS (2, 6, 20, 60, and 180 ppm), DBSS (670 and 67,000 ppm), DCHSS (145 and 14,500 ppm), CTAB (1, 2, 5, 15, and 40 ppm), and Tween 20 (1, 2, 7, 22, and 74 ppm). The centroid and orientation of each cell near the oil/water interface were determined using a MATLAB algorithm based on least-square fitting of backbone of cells in 3D.[78,79] We counted only those cells on the lower hemisphere of the drop to avoid any noisy data associated with cells interacting with the top surface of the microcapillary channel. We confirmed that bacteria in all experiments except CTAB at 1.0 CMC remained viable by streaking post-experiment cells onto agar plates and observing growth.

2.3 Results and Discussion

2.3.1 Monodisperse emulsion droplets using microfluidics

We generate monodisperse emulsions of dodecane in DI water using a co-flow capillary microfluidic device (Figure 2.2(a)). The device is operated in the jetting regime, in which a thin jet of liquid is formed at the inner capillary tip and is eventually broken into droplets by the Rayleigh – Plateau instability.[80,81] The jet diameter and the droplet diameter depend on the viscous drag of outer fluid, which can be varied through the flow rate of the outer fluid. We thus tune the diameter of dodecane droplets from 20 μm to 300 μm in water by varying the outer fluid flow rate from 500 to 3000 μL min^{-1} (Figure

2.2(b)). These droplet diameters are typical of those measured in the presence of dispersants in the Deepwater Horizon Spill in 2010.[82]

The droplet diameter D_d, normalized by the diameter of the outer capillary (D_c) at the location of the tip of the inner capillary tip (diameter D_i), increases as a power law with the ratio of the inner and outer fluid flow rates (Q_i/Q_o) with slope ~ 0.5 (Figure 2.2(c)). The normalized drop diameter changes with the normalized flow rate as predicted for the jetting regime,[67]

$$\frac{Q_i}{Q_o} = \frac{\eta_o}{\eta_i}\frac{x^4}{(1-x^2)^2} + \frac{2x^2}{(1-x^2)} \quad (2.1)$$

where $x = D_d/D_c$, Q_i and Q_o are the fluid flow rates of the inner and outer fluids, and η_i and η_o are the viscosities of the inner and outer fluids. This equation was derived in ref 34 by solving the Navier-Stokes equations assuming no-slip boundary conditions, a continuous shear stress at the interface, and an interfacial pressure difference given by the Laplace equation. The power-law behavior arises in our experiments because the first term on the right-hand side of eq 2.1 is negligible and $1 - x^2 \approx 1$.

2.3.2 Time dependent adsorption of bacteria at interfaces

Confocal imaging reveals that the adhesion of *M. hydrocarbonoclasticus* bacteria to DOSS-stabilized dodecane droplets (in solutions of final salt concentration 5 g L^{-1} NaCl) depends on droplet size and time (Figure 2.5). Using tracking algorithms, we quantify the number of bacteria on the interface of dodecane droplets of diameter 20, 40, and 60 μm. For all droplet sizes, the number of *M. hydrocarbonoclasticus* bacteria adhered at a dodecane/water interface initially increases with time and then saturates on longer time scales (Figure 2.6(a)). No significant change in the number of adhered cells is observed

after 3 hours. Because *M. hydrocarbonoclasticus* bacteria are not motile under these experimental conditions, the transport of cells to the interface is driven by diffusion; on long time scales cells become depleted near the oil/water interface, leading to a plateau in adsorption.

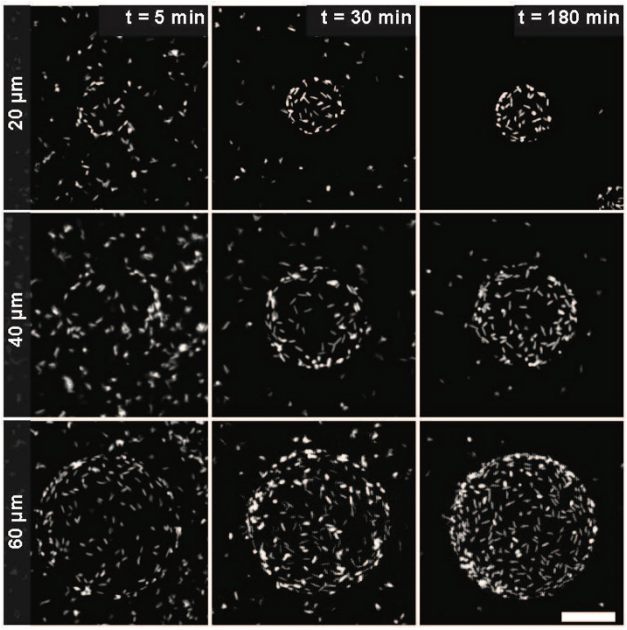

Figure 2.5. 2-D projections of 3-D confocal micrographs of bacteria adhering at dodecane/water interfaces for droplets of diameter 20, 40, and 60 µm at 5, 30, and 180 min after inoculation of bacteria into the o/w emulsion. Scale bar is 20 µm. In all experiments DOSS (18 ppm final concentration) is added to the aqueous phase to stabilize the dodecane droplets in saline solution (final salt concentration 5 g L^{-1} NaCl).

This scenario suggests that the number of bacteria on the dodecane/water interface at time t, $N(t)$, can be modeled using a Langmuir first-order kinetics model,[83–85]

$$N(t) = N_\infty - (N_\infty - N_0)e^{-t/\tau} \quad (2.2)$$

where N_0 and N_∞ are the number of cells that initially (at the earliest time point, as soon as possible after bacteria are inoculated into the oil/water emulsion) and finally (as $t \rightarrow \infty$) adhere, respectively, and τ is the characteristic time for the interface to saturate. The time constants τ extracted from fits to eq 2.2 increase linearly with droplet diameter,

indicating that bacteria adhere more rapidly to smaller droplets (Figure 2.6(b)). This linear dependence on droplet diameter is consistent with a kinetic model for the time required, in irreversible Langmuir adsorption, to reach a fractional coverage within a factor h of the equilibrium value on a sphere,[86] $t_h = -\frac{RK\gamma_s \ln h}{D(1+KC_0)^2}$, where K is an affinity constant, R is the radius of the droplet, D is diffusivity of cells, C_0 is cell concentration, and γ_s is the number of adsorption sites per unit surface area. The applicability of this model requires that bacteria are in excess, that the droplet is homogenous, and that K and γ_s are constant across the different drop sizes, which are reasonable assumptions for our experiments.

The good fit of the data to eq. 1 confirms that the dynamics of adhesion for non-motile bacteria obey first-order Langmuir kinetics. The value of N_∞ increases with the droplet radius, as expected because the droplet surface area also increases. We therefore normalize by the droplet hemisphere surface area to obtain the interfacial areal density of bacteria $\rho_s(t) = N(t)/\,2\pi R^2$. The areal density is greatest for the smallest 20 μm droplets but is constant (within measurement error) for the two larger droplets (Figure 2.6c). This result suggests that decreasing the oil drop size may provide at least two mechanisms to increase accessibility to bacteria: by increasing the surface area per volume available for adhesion, and by enhancing cell adhesion on smaller droplets. Similarly, volumetric density, number of cells normalized with the volume of the droplet, is the highest for the smallest droplets (Figure 2.7).

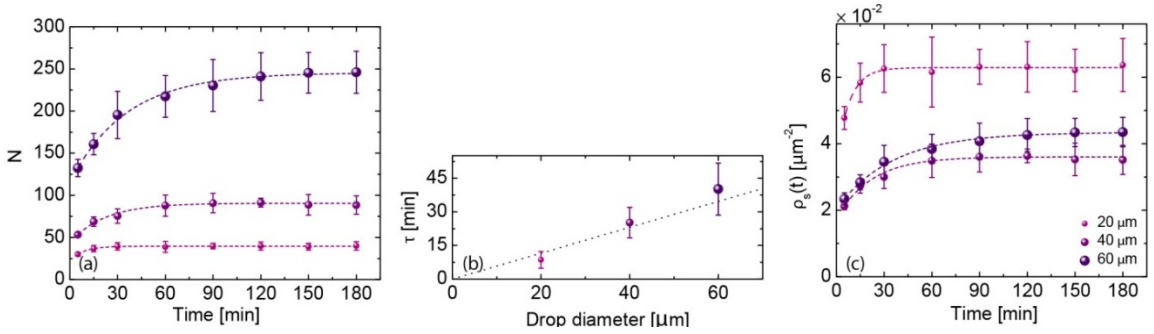

Figure 2.6. (a) Number of bacteria at the dodecane/water interface N(t) as a function of time for droplets of diameter 20, 40, and 60 μm. (b) Number of cells per unit surface area ρ_s (t) as a function of time for 20, 40, and 60 μm dodecane droplets. In all experiments DOSS (18 ppm final concentration) is added to the aqueous phase to stabilize the dodecane droplets in saline solution (final salt concentration 5 g L^{-1} NaCl). Error bars represent standard deviation from three independent cultures. Dashed lines in (a,b) represent fits to the first-order Langmuir kinetics model (eq. 1).

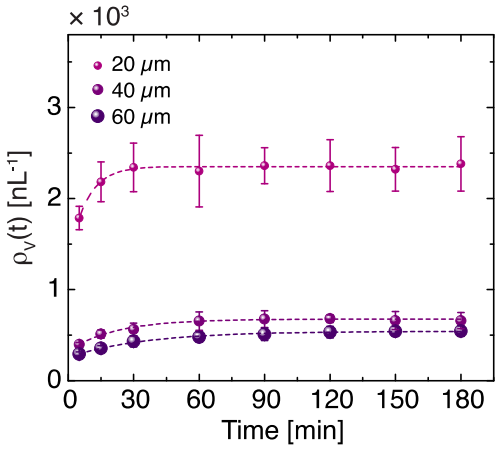

Figure 2.7. Number of bacteria at the dodecane/water interface normalized by the volume of the droplet $\rho_V(t)$ as a function of time for varying drop sizes. Error bars represent standard deviation from three independent cultures.

We next examine the orientation of bacteria on the oil/water interface, defined as the angle between the bacterial body and the local surface normal. For all droplet sizes, the majority of adherent cells are oriented at an angle > 60° to the surface normal (Figure 2.8) and align roughly parallel to the interface. The parallel orientation of the cells provides one route to minimize the energy cost due to interfacial tension.[87,88] A

significant fraction of cells, however, orient at lower angles with respect to the surface normal. Although bacteria with relatively hydrophobic surface regions can uniformly orient perpendicular to fluid/fluid interfaces,[89] the distribution of orientations suggests contributions from additional factors.

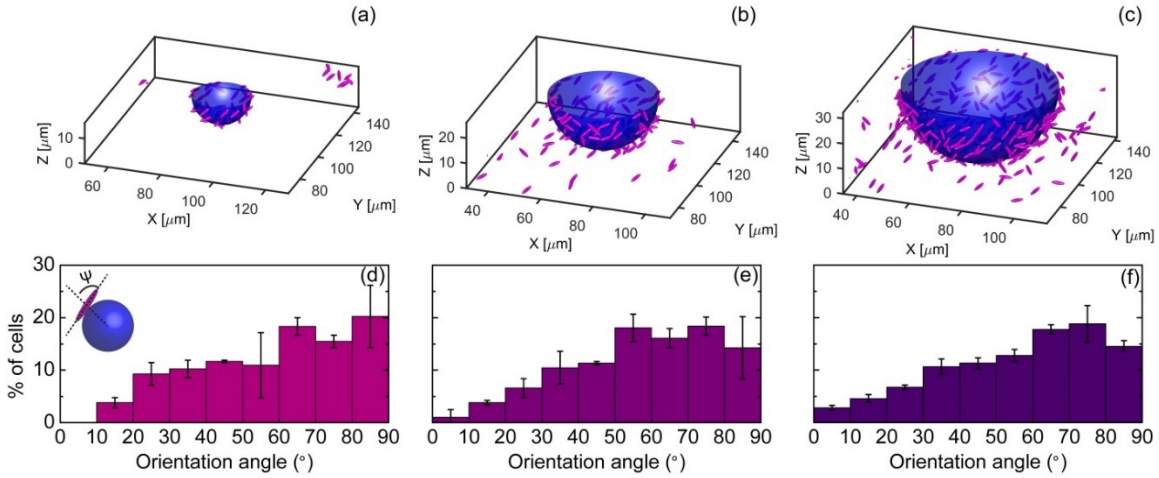

Figure 2.8. (a–c) Representative 3-D renderings of the location and orientation of bacteria around dodecane droplets in saline solution (final salt concentration 5 g L^{-1} NaCl) of diameter (a) 20, (b) 40, and (c) 60 μm. (d–f) Distribution of the orientation angle ψ at which bacteria adhere to the interface for dodecane droplets of diameter (d) 20, (e) 40, and (f) 60 μm. ψ is defined by the angle between the cell backbone and the normal on the droplet that passes through the cell centroid, as indicated in the inset to Figure 2.8(d).

2.3.3 Thermodynamic analysis: energy cost for bacterial adhesion to oil/water interfaces

In the following equations,[90] the total surface area of bacteria is A_b; the surface area of bacteria in the oil phase is A_{bo}; the area of oil/water interface removed by the adsorbed bacterium is A_{ow}; the area of the oil/water interface before adhesion is A_s; and the bacteria-water, bacteria-oil, and oil-water interfacial tensions are σ_{bw}, σ_{bo}, and σ_{ow}, respectively. The energy of the system before adhesion is given by,

$$E_{\mathrm{i}} = A_b\sigma_{bw} + A_s\sigma_{ow}, \tag{2.3}$$

and the energy of the system after adhesion is given by,

$$E_{\mathrm{f}} = (A_b - A_{bo})\sigma_{bw} + A_{bo}\sigma_{bo} + (A_s - A_{ow})\sigma_{ow}. \quad (2.4)$$

Thus, the energy cost of adhesion is given by,

$$\Delta E = E_{\mathrm{f}} - E_{\mathrm{i}}, \quad (2.5)$$

which leads to,

$$\Delta E = (A_b - A_{bo})\sigma_{bw} + A_{bo}\sigma_{bo} + (A_s - A_{ow})\sigma_{ow} - A_b\sigma_{bw} - A_s\sigma_{ow}, \quad (2.6)$$

or,

$$\Delta E = A_{bo}(\sigma_{bo} - \sigma_{bw}) - A_{ow}\sigma_{ow}. \quad (2.7)$$

From the Young – Laplace equation, the relationship between the three interfacial tensions and the wetting angle at the three phase line between the oil, water and bacterium is given by,

$$\sigma_{bo} = \sigma_{bw} + \sigma_{ow}\cos\theta_c. \quad (2.8)$$

From equation (2.7) and (2.8), the thermodynamic cost of adhesion can be written as,

$$\Delta E = -\sigma_{ow}(A_{ow} - A_{bo}\cos\theta_c) \quad (2.9)$$

where θ_c is the water contact angle in oil of the adsorbed bacterium (Figure 2.9).[90,91]

We note that these equations are derived for a planar interface. It has been suggested[2] that they remain valid for curved interfaces so long as the particle radius is much smaller than the emulsion droplet radius; this assumption holds for our study, where the diameter of the oil droplets (minimum 20 μm) is at least a factor of six greater than the bacterium length (2 – 3 μm). Because the bacterium is curved $A_{bo} > A_{ow}$,

which sets a lower limit on the contact angle required for the bacterium to adhere to the oil.

Here, we assume that the only change that occurs upon addition of surfactants is a decrease in the oil/water interfacial tension (σ_{ow}). Chemically isotropic but geometrically anisotropic colloidal particles, such as ellipsoids[92,93] or cylinders,[94] typically align along an interface and thereby maximize the oil/water interfacial area displaced by the particles. The fact that many bacteria do not orient parallel to the interface suggests that the assumptions underlying the thermodynamic model do not all hold. Indeed, particles with chemical and/or topographic[95,96] surface heterogeneity can exhibit a broad distribution of contact angles[97] and adsorb in metastable configurations.[98–101] While our results suggest that bacteria preferentially adsorb in the thermodynamically-favored configuration, the broad distribution of orientations likely reflects their surface heterogeneity.

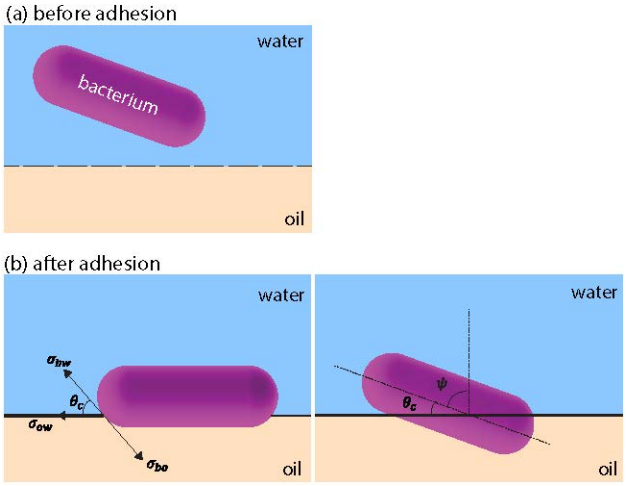

Figure 2.9. Schematic illustration of bacteria adsorbed (a) before adhesion in water and (b) after adhesion for planar or tilted orientations at an oil/water interface.

2.3.4. Effect of surfactant chemistry and concentration on adhesion of bacteria at dodecane/water interface

The adhesion dynamics reported in Figure 2.6 follow first-order Langmuir kinetics, with the extent of adhesion differing between the smallest and the larger drops. We next examine the equilibrium adhesion of *M. hydrocarbonoclasticus* bacteria on curved dodecane/water interfaces. For a series of three commercially-available anionic sodium sulfosuccinates [dibutyl sodium sulfosuccinate (C-4, DBSS), dicyclohexyl sodium sulfosuccinate (cyclo C-6, DCHSS), and DOSS (C-8)], we quantify the number of cells adhered on long time scales to surfactant-decorated dodecane/water interfaces at low ($C/\mathrm{CMC} \approx 0.01$) and high ($C/\mathrm{CMC} \approx 1$) surfactant concentrations, where CMC indicates the critical micelle concentration determined through fluorimetry (data not shown). The areal density of bacteria on the dodecane/water interface of a 20 μm droplet stabilized by each of the three sulfosuccinates is the same within experimental error (Figure 2.10(a)).

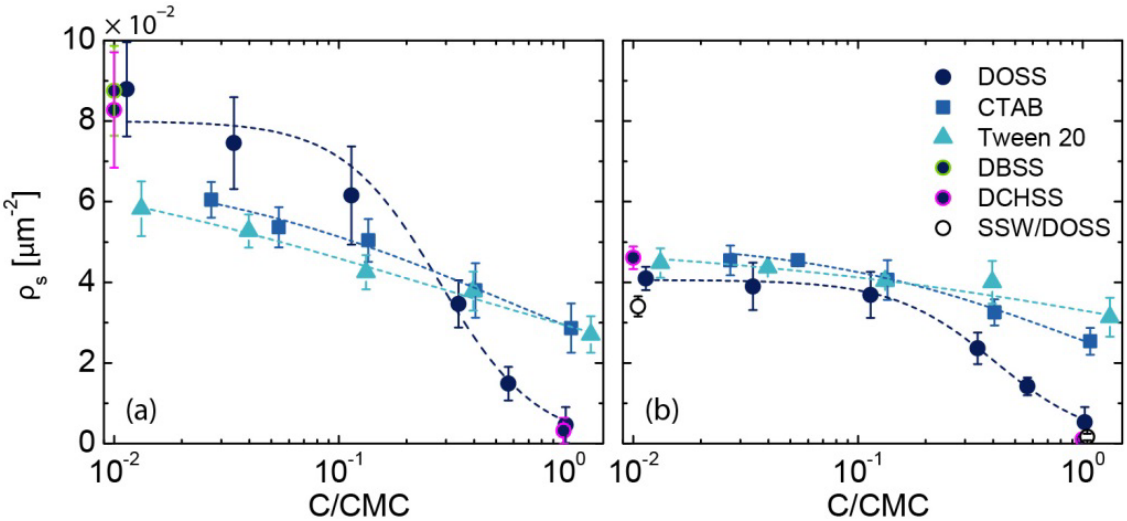

Figure 2.10. Areal density ρ_s of cells adhering at the dodecane/water (closed) or dodecane/synthetic sea water (open) interface as a function of normalized surfactant concentration C/cmc for drops of diameter (a) 20 or (b) 50 μm. Error bars represent the standard deviation calculated from three independent cultures.

Next, we quantify the packing efficiency via the surface excess Γ, defined as the number of moles of surfactant molecules per unit interfacial area, and the surface area occupied by a surfactant molecule.[102–106] The surface excess is calculated at the CMC from the dependence of the IFT on the surfactant concentration (Figure 2.11) via

$$\Gamma = -\frac{1}{nRT}\left(\frac{\partial\sigma}{\partial \ln C}\right)_{T,P} \tag{2.10}$$

where σ is the IFT of dodecane/water, C is the surfactant concentration, R is the gas constant, T is the temperature, and n = 1 when electrolyte is present. We assume that the surfactant activity coefficient is equal to one. The surface coverage per surfactant molecule is then given by $A_a = \frac{1}{N_A\Gamma}$. The interfacial tension σ initially decreases sharply with an increase in the surfactant concentration, as more surfactant molecules adsorb at the dodecane/water interface; above the critical micelle concentration (CMC), the interfacial tension decreases slowly as the surfactant concentration is further increased (Figure 2.11). For a similar normalized surfactant concentration, σ for DCHSS is much higher than that of DOSS. Furthermore, σ for DOSS falls to near-zero at its CMC but remains finite up to (at least) 3CMC for DCHSS. The surface area per DOSS molecule (A_a) 78 ± 2 Å^2, is in good agreement with literature values[107] and is larger than that for DCHSS, 54 ± 2 Å^2 (Table 2.4). Because the areal density of bacteria is identical for the three sodium sulfosuccinates, despite distinct values of the interfacial tension and surface area per molecule, we conclude that the electrostatic repulsion of the negatively-charged bacteria from the negatively-charged surfactants affects bacterial adhesion to these surfactant-decorated dodecane/water interfaces. Moreover, this effect is likely partly

kinetic (i.e., through the double-layer force) because adhesion cannot be predicted solely from the interfacial tension (i.e., thermodynamics).

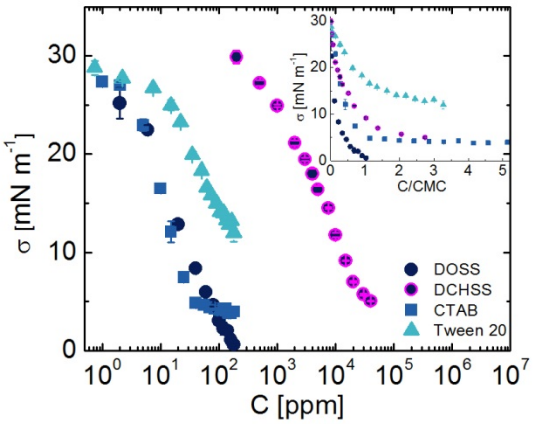

Figure 2.11. Interfacial tension σ between dodecane and water containing 5 g L^{-1} sodium chloride in the presence of various surfactants.

Table 2.4. Surface coverage per molecule at CMC of different surfactants.

Surfactant	Γ [10 $^{-6}$ mole m^{-2}]	A_a [Å^2]
DOSS	2.12 ± 0.05	78 ± 2
Tween 20	2.34 ± 0.09	71 ± 3
CTAB	2.74 ± 0.24	61 ± 5
DCHSS	3.26 ± 0.07	54 ± 2

We next compare results on bacterial adhesion from DOSS to those obtained for two other common surfactants used in bacterial studies,[17] non-ionic Tween 20 and cationic CTAB. The areal density of bacteria on the oil/water interface decreases for each surfactant as its concentration is increased (Figure 2.10). This trend holds both for larger 50 µm droplets, for which the final number of adhered bacteria scales with the interfacial surface area, and for small 20 µm droplets, which exhibit anomalously high adhesion. The areal densities (and hence number) of bacteria adhered to drops stabilized by CTAB and by Tween 20 are similar for a given droplet diameter, and are larger than the number of bacteria adhered to DOSS-decorated dodecane/water interfaces near CMC.

We again compare the IFT of surfactant-decorated dodecane/water interfaces and the surface area per molecule as a function of surfactant concentration. The high-concentration values of σ are markedly different for CTAB and Tween 20 compared to DOSS: σ for CTAB and Tween 20 remains nonzero even at surfactant concentrations of up to 180 ppm, whereas σ for DOSS decreases to near zero at its CMC value. Indeed, the areal density of bacteria adhering at droplet interfaces decreases concomitant with σ for all surfactants (Figure 2.12). These results are consistent with earlier studies reporting a decrease in adhesion of bacteria on solid surfaces as the surface tension is decreased,[57,108,109] such that the free energy of adhesion becomes less negative.[60,110] For 50 μm droplets, the areal density of adhered bacteria nearly collapses onto a universal curve with σ for DOSS, CTAB, and Tween 20; for 20 μm droplets, however, the number of bacteria does not cleanly collapse with σ. This result, like that in Figure 2.6, is consistent with droplet-size-dependent adhesion of bacteria.

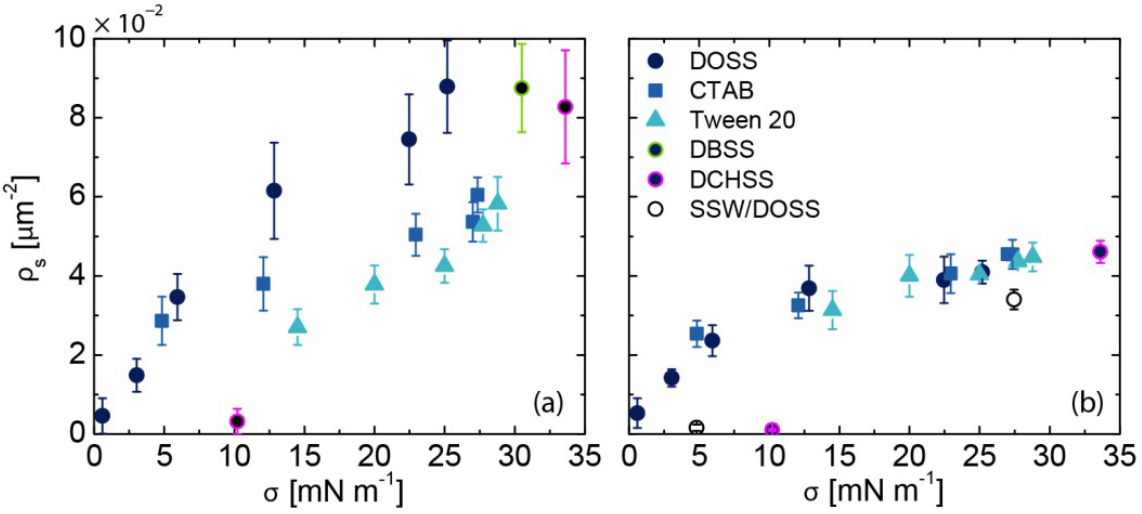

Figure 2.12. Areal density ρ_s of bacteria at the dodecane/water (closed) or dodecane/synthetic sea water (open) interface as a function of the IFT σ for droplet diameters of (a) 20 or (b) 50 μm. Error bars represent the standard deviation from three independent bacteria cultures.

Finally, we compare the surface excess and surface area per molecule for the different surfactants. DOSS has the highest surface area per molecule of the four surfactants examined; the surface area per molecule increases in the order DCHSS < CTAB < Tween 20 < DOSS. The high surface area per molecule of DOSS is due to its two branched linear chains, which increases its emulsification efficiency.[107,111] The efficiency of coverage is further enhanced due to counterions in solution that occupy the space between the head groups.[111] At the CMC, however, bacterial adhesion onto a 20 μm droplet increases in the order DCHSS ≈ DOSS < CTAB ≈ Tween 20, indicating that the surface area of the surfactant molecule does not strongly affect bacterial adhesion.

Together, the results presented in Figures 2.10 – 2.12 suggest that both interfacial tension and electrostatic interactions affect the adhesion of *M. hydrocarbonoclasticus* to dodecane/water interfaces in saline solution. The areal density of bacteria on 50 μm droplets increases with interfacial tension across the range of surfactants test (Figure 2.12(b)). Pronounced differences between the areal densities on smaller 20 μm droplets stabilized by various surfactants, however, indicate that non-thermodynamic factors also contribute to adhesion. To understand the origin of these differences, we measured the zeta potential of surfactant-stabilized emulsions (DOSS, CTAB, Tween 20) containing droplets of 20 or 50 μm. The magnitude of the zeta potential was greater for the smaller 20 μm droplets than for the 50 μm droplets (Table 2.5), consistent with (albeit not proof positive) of an enhanced role for electrostatic interactions in the adhesion of bacteria to these droplets. Likewise, comparison of adhesion on DCHSS- and CTAB-decorated 20 μm droplets suggests contributions from electrostatics. The interfacial tension of droplets stabilized by 1 CMC DCHSS [14500 ppm] and 1 CMC CTAB [35 ppm] are similar, as

are the surface areas per molecule (Table 2.4), but significantly fewer (negatively-charged) bacteria adhere to the anionic, DCHSS-stabilized dodecane/water interface than to the cationic CTAB-stabilized dodecane/water interface.

Table 2.5. Zeta potential of uniform emulsion droplets of 20 and 50 μm in MilliQ water for various surfactants at three concentrations. Errors are the standard deviation of 10 runs obtained from measurements on a single sample.

C [CMC]	DOSS		CTAB		Tween 20	
	20 μm	**50 μm**	**20 μm**	**50 μm**	**20 μm**	**50 μm**
0.01	-79 ± 2	-59 ± 5	70 ± 2	35 ± 4	-12 ± 1	-7 ± 1
0.1	-77 ± 3	-68 ± 3	77 ± 2	54 ± 7	-21 ± 1	-21 ± 1
1.0	-118 ± 2	-100 ± 4	95 ± 3	76 ± 3	-33 ± 1	-55 ± 1

2.4 Conclusion

We examined the effect of droplet size and surfactant type and concentration on bacterial adhesion at dodecane/water interfaces. Bacteria adhere in slightly greatly areal densities on small droplets of diameter 20 μm, and reach equilibrium coverage more slowly as the droplet size is increased. Bacteria preferentially align parallel to the local oil/water interface, in agreement with expectations from thermodynamics to maximize the displaced interfacial area, but the distribution of angular orientations suggest that bacteria can become kinetically trapped in non-equilibrium orientations. At equilibrium, bacteria adhere more to droplets stabilized by lower concentrations of surfactants. This result is consistent with an increase in the free energy of adhesion due to the decrease in the oil/water interfacial tension (neglecting any changes in bacteria/oil or bacteria/water interfacial tensions). Comparison of adhesion to droplets of various sizes decorated by different surfactants suggests that electrostatics also play a role in determining the number of adhered bacteria, especially for smaller 20 μm droplets.

Overall, these results indicate that surfactants may have contrasting effects on bacterial adhesion to dodecane/water interfaces: for a constant volume of emulsified oil, increasing the surfactant concentration increases the surface area available for bacteria to adhere, but lowers bacterial adhesion energy due to the decrease in interfacial tension. Furthermore, the surface density of adhered bacteria and its dependence on the interfacial tension are different for the smallest 20 μm droplets, consistent with an additional role for electrostatics. These effects should be considered for optimal (i.e., minimal) application of surfactants or dispersants early in an oil spill scenario. On longer time scales, however, oil-metabolizing bacteria may be able to grow on the oil/water interface[112] and further modify the interfacial tension, further complicating predictions of the extent of biodegradation by oil-metabolizing bacteria. In addition, some strains of *M. hydrocarbonoclasticus* are able to produce biosurfactants that likely aid attachment to the oil/water interface.[113] Finally, the adhesion of non-motile bacteria to a dodecane/water interface under quiescent conditions studied here represents a simplification of conditions encountered during marine biodegradation: crude oil contains a mixture of aromatic and non-aromatic hydrocarbons; other hydrocarbon-degrading species involved in biodegradation are motile; and even gentle flow alters the behavior of microorganisms.[114] Both flow and motility are likely to modify the interactions of bacteria as they become confined near oil/water interfaces.[115] Very recent experiments suggest that bacterial attachment may be quite different in clean environmental conditions (featuring dissolved organic carbon) and in an oil spill scenario (featuring only hydrocarbons as the carbon source).[18] Future studies examining the effects of growth, bacterial exudates, motility,

flow, and organic matter on interfacial adhesion are expected to provide additional insight into the processes influencing biodegradation.

The results reported here have broader implications for technological processes in which bacteria interact with oil/water interfaces. Microfluidically-produced droplets of water in oil, as one example, are increasingly used as controlled microscale reactors for pathogen detection, antibiotic susceptibility, and biotechnological selection, among other emerging applications.[116] Likewise, interactions with hydrocarbon/water interfaces are important for treatment of wastewater.[117] The methods applied here to hydrocarbon-degrading bacteria can be used to optimize and tune the interactions of other bacteria strains with interfaces in these technologically relevant settings.

Chapter 3: Rotating oil droplets driven by motile bacteria at interfaces

3.1 Introduction

Active fluids[118] that contain biological motors[119–122] offer an intriguing route to actuation on the microscale. As one example, bacteria convert chemical energy into mechanical energy.[123] Numerous and diverse in species, they are inexpensive biological power sources. Using bacteria to rotate microscopic gears, as mixers or propellers,[124] or transport particles, for drug delivery,[125–127] requires fundamental understanding of how bacterial motility couples to object motion.

Small numbers of adherent bacteria can rotate and/or translate solid objects of size of order 10–100 μm, up to one hundred times greater than their body dimensions and up to one million times greater in mass.[128–135] The speed and persistence of motion in such systems, however, are often limited by the lack of coherence in the orientation of cells and their flagella.[128,130] These limitations can be overcome by coupling the motion of collectively moving bacteria to asymmetric rotors, which break symmetry to provide a consistent direction of rotation.[136–139] Swimming *Escherichia coli* bacteria at concentrations of order 10^{10} bacteria mL^{-1} produced a maximum angular speed of 4 rpm,[138] and swarming dense *Vibrio alginolyticus* bacteria produced a maximum angular speed of 7 rpm.[140] Carefully-designed 3-D microrotors, designed to capture up to 15 swimming cells within microchambers at the rotor edge, rotated at speeds of up to 20 rpm.[139] Rotors in these examples, however, were required to be chiral to exploit the breaking of detailed balance in active baths[141] and generate directional motion.

By contrast, the use of active fluids to move non-rigid liquid droplets, for which surface tension imposes a spherically symmetric shape, remains understudied. It is well

established that emulsions can be made to move through addition of surfactants, which generate interfacial Marangoni stresses that drive self-sustaining motion.[142–152] Symmetry is broken through the spatial gradient of surfactants on the droplet surface.[142,147] Rotational torque can be generated by coupling the surfactant-induced surface flows to nematic order in a confined liquid crystal.[153] Fewer studies, however, have investigated droplet motion driven by active fluids. Molecular motors confined with microtubules inside droplets can generate internal vortex formation.[154] Likewise, bacteria confined within droplets can generate internal vortices.[155] These studies do not directly investigate motion of the drop itself. Bundles of active microtubules that adsorb to the internal oil–water interface can drive droplet translation.[121] Nonetheless, examples of droplet motion driven by external active fluids, including bacteria, remain infrequent.

Here, we show that active, adherent flagellated bacteria can drive rotation of spherical liquid droplets near a liquid–solid interface. We characterize adhesion of bacteria using confocal microscopy and analyze droplet motion using brightfield microscopy and particle tracking. Symmetry-breaking hydrodynamic interactions of bacteria with the nearby liquid–solid interface lead to clockwise rotation of the droplets when viewed from the liquid side. The rotation rate scales approximately inversely with the droplet radius, consistent with a physical picture in which bacteria randomly attached at the droplet surface drive the rotation. The speed of rotation can be tuned by changing the number of adherent bacteria, through variations in cell concentration, bacterial species, or surfactant concentration. By showing how active bacteria can be used to drive the directional rotation of non-chiral, spherically symmetric droplets, this study opens a route to manipulate fluid droplets in an active bath.

3.2 Materials and methods

3.2.1 Chemicals

Dodecane (≥99%, Sigma-Aldrich), hexadecane (≥99%, Sigma-Aldrich), 1 μm FluoSpheres sulfate microspheres (ThermoFisher), potassium nitrate (≥99%, EMD), Zobell marine broth 2216 (HiMedia Lab), sodium pyruvate (Amresco), SYTO9 (ThermoFisher), ethylene glycol (Sigma-Aldrich), and diiodomethane (Sigma-Aldrich) were used as received.

3.2.2 Bacteria strains

We used two motile bacteria isolated from the Gulf of Mexico during the Deepwater Horizon oil spill, obtained from Dr Romy Chakraborty and Dr Gary Anderson (Lawrence Berkeley National Laboratory) *via* Dr Douglas Bartlett (Scripps Institute of Oceanography, UCSD). Bead 10BA (isolated from 1509 m) is related to *Halomonas titanicae*. *H. titanicae* is a moderately halophilic, Gram-negative marine bacterium. These bacteria are rod-shaped, roughly 0.5 – 0.8 μm in diameter and 1.5 – 6 μm in length, and swim using their peritrichous flagella.[156]

Bead B37B (isolated from 150 m) is related to *Shewanella haliotis* strain DW01. *S. haliotis* is Gram-negative, rod-shaped, and 0.5 – 0.7 μm in diameter and 2.0 – 4.3 μm in length.[157] *Shewanella* species typically swim using a single polar flagellum.[158,159] The two Gulf bacteria are hereafter referred to by their closest species name.

In addition to the Gulf isolates, we also examined one model motile bacterium. *Escherichia coli* MC1061, provided by Dr Patrick Cirino (University of Houston), is Gram-negative, rod-shaped, and 0.7 – 0.9 μm in diameter and 2.0 – 3.0 μm in length and swims by bundling its peritrichous flagella.

3.2.3 Growth conditions

H. titanicae and *S. haliotis* were streaked from a frozen stock on a marine agar plate (37.4 g L^{-1} marine broth, 10 g L^{-1} sodium pyruvate, 15 g L^{-1} agar) and incubated at 30 °C for 40 h. A single colony selected from these plates was inoculated into 20 mL of culture medium (37.4 g L^{-1} marine broth and 10 g L^{-1} pyruvate) and incubated for 20 h in an orbital incubator shaker (New Brunswick Scientific) at 200 rpm and 30 °C. Finally, a subculture was prepared by inoculating 60 μL of the principal culture into 20 mL of culture medium and grown to late exponential phase in an orbital incubator shaker at 30 °C and 200 rpm for 20 h. *E. coli* was streaked on a Luria-Bertani agar plate and cultured in Luria-Bertani medium at 37 °C and 250 rpm for 12 h.

3.2.4 Preparation of glass capillaries for imaging

Thin rectangular borosilicate capillaries (0.1 mm height, 1 mm width, 50 mm length, 0.07 mm wall thickness, Vitrocom) were used as sample chambers in imaging experiments. To minimize adhesion of bacteria and prevent wetting of oil drops, the capillaries were made hydrophilic by plasma treatment (Harrick plasma cleaner PDC-32G) using oxygen plasma for 2 minutes. The plasma-treated surface was fully wetted by water when the water contact angle was measured using a DataPhysics OCA 15EC contact angle goniometer. This hydrophilic surface prevented adhesion of cells and droplets on the inner surface of the glass capillary. The plasma-treated capillaries were immediately filled with the droplet-cell suspension for imaging to minimize any change in surface hydrophilicity during the experiment.

3.2.5 Zeta potential and surface energy

Cells were grown to late exponential phase for surface characterization. 20 mL of each bacteria suspension was centrifuged at 5000*g* for 10 minutes in a Sorvall ST 16 Centrifuge (Thermo Fisher Scientific). The resultant pellet was resuspended in 20 mL MilliQ water and centrifuged again. The process was repeated one more time and the final pellet was resuspended in MilliQ water. The final optical density at 600 nm (OD_{600nm}) was adjusted to 0.04 (Laxco DSM-Micro Cell Density Meter) with MilliQ water.[59]

The zeta potentials of the bacteria suspensions and particle suspension were measured using a Nicomp 380 ζ-potential analyzer (Table 3.1). For measurements of the surface energy, the bacteria suspension (OD 1.0 in MilliQ water) was filtered through cellulose acetate membrane filters (pore diameter 0.45 μm, Advantec) under vacuum at 100 mm Hg below atmospheric pressure using a GEM 8890 vacuum pump (Welch).[72] The contact angles for three liquids (MilliQ water, ethylene glycol and diiodomethane) were measured on the lawns using a Dataphysics OCA 15EC goniometer. The surface energy of the bacteria was calculated from inbuilt software using the method of Wu.[73,74] Contact angle and surface energy data are provided in Table 3.2.

Table 3.1. Zeta potential of PS particles and different bacteria strains used in this study. Standard deviations are calculated based on three different samples.

Sample	Mobility [m.u.]	Zeta potential [mV]
Sulfate-modified PS particles	-3.0 ± 0.1	-39 ± 2
Halomonas titanicae	-3.6 ± 0.3	-46 ± 3
Shewanella haliotis	-2.7 ± 0.4	-34 ± 5
Escherichia coli	-3.0 ± 0.1	-39 ± 2

Table 3.2. Contact angle and surface energy of bacteria. Standard deviations are calculated based on at least two bacteria lawns. The surface energy of bacteria lawn is calculated from method of Wu.

Bacteria species	Water [°]	DM [°]	EG [°]	SE [mN m^{-1}]
Halomonas titanicae	23 ± 4	57 ± 5	29 ± 4	64 ± 1
Shewanella haliotis	14 ± 2	45 ± 4	26 ± 4	66 ± 1
Escherichia coli	19 ± 2	60 ± 6	17 ± 2	66 ± 1

3.2.6 Brightfield imaging assay for drop rotation

For imaging experiments, cells were harvested at late exponential phase. 10 mL of the cell suspension was centrifuged at 2000*g* for 10 min to remove the medium and the pellet was resuspended in 10 g L^{-1} of potassium nitrate solution prepared in MilliQ water. Separately, emulsions of dodecane in potassium nitrate solution were made by shaking 20 µL of dodecane or hexadecane in 300 – 400 µL of KNO_3 solution. To these emulsions, 25 µL of PS particles (0.04% v/v) were added and the suspension shaken again. Using this technique, we obtained drops of diameter 10 – 100 µm (Figure 3.1). The PS particles were added to aid in the determination of the angular position of the drop over time. We selected the particle concentration such that only 1 – 4 particles attached to the dodecane/water interface. We confirmed that the PS particles attached to the droplet/water interface using confocal microscopy (Figure 3.2).

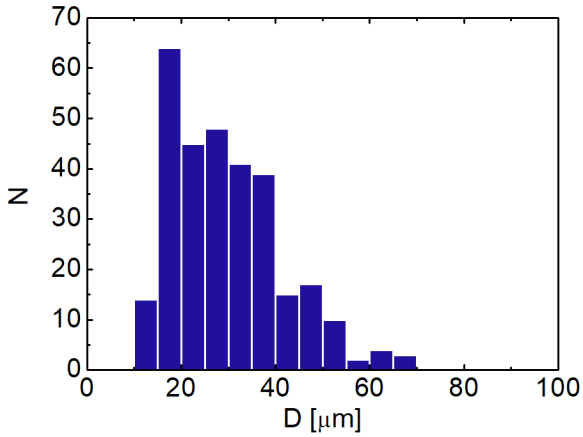

Figure 3.1. Distribution of the diameter of dodecane droplets prepared by shaking 20 μL of dodecane in 500 μL of water (10 g L^{-1} KNO_3). The sample was introduced into an imaging chamber immediately after because droplets were not stable without added surfactant.

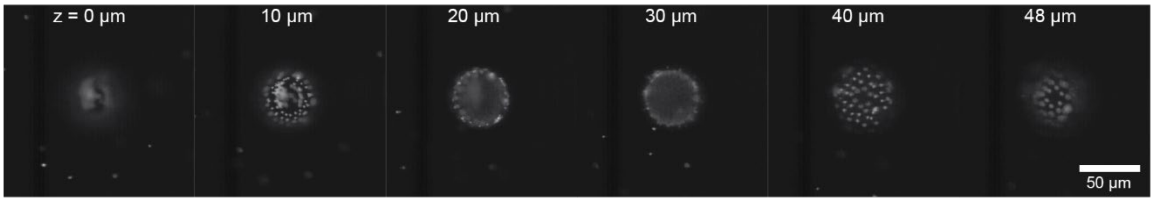

Figure 3.2. Micrograph of polystyrene (PS) particles attached to the dodecane-water interface.The label in each panel indicates the distance of focal plane from the bottom surface of the droplet. The outer aqueous phase is 10 g L^{-1} potassium nitrate in water.

The final suspension was prepared by adding 100 – 200 μL of cell suspension to an Eppendorf tube. Through this protocol, we generated bacterial suspensions with optical densities of 0.3 – 3, corresponding to number concentrations of 8.1×10^8 cells mL^{-1} to 8.1×10^9 cells mL^{-1} for *H. titanicae*; optical density of 1.0, corresponding to number concentration of 2.7×10^9 cells mL^{-1}, for *E. coli*; and optical density of 0.31, corresponding to number concentration of 2.7×10^9 cells mL^{-1}, *S. haliotis*. The OD was adjusted to obtain the same number density for comparisons between different species. These concentrations are lower than those typically required to obtain collective swimming ($\sim 10^{10}$ cells mL^{-1} (ref. 105)).

Finally, 6.7 μL of the emulsion-bacteria suspension was injected into a glass microfluidic channel and both ends of the channel were sealed with vacuum grease. The droplets, whose density was lower than that of water, were preferentially located at the top wall of the capillary, within one micron of the surface. Occasionally, a droplet remained near the bottom surface due to an interaction with the substrate.

We used a brightfield inverted microscope (Leica Microsystems DM4000) equipped with a 40X objective lens (HCX PL APO, NA 1.25 – 0.75) to image rotating droplets. Images of droplets located at least 400 μm away from the side walls of the capillaries, to avoid any interference from the lateral walls, were acquired for up to ten minutes after injection to ensure that the capillary surface remained hydrophilic throughout the measurement; we note that droplet rotation persisted for more than two hours (Figure 3.3). Images were captured at a rate of 5 frames s^{-1} for 60 s using a digital camera (Olympus DP21). To analyze the drop rotation, we tracked the positions of the PS particles attached to the droplet interface using algorithms written in Matlab. We determined the angular speed of individual droplets from the slope of total rotation as a function of time over at least 20 s.

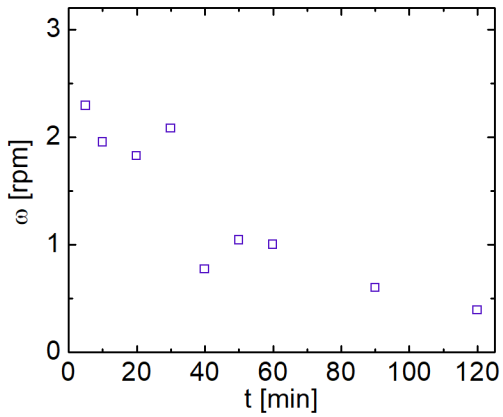

Figure 3.3. Angular speed of a 40 μm dodecane droplet as a function of time. The droplet rotated for more than 2 h, but its angular speed decreased markedly after 30 min. The angular speed was measured for the same droplet over time and each point of the plot is for one droplet. The optical density of cells suspension was 1.0 (2.7×10^9 cells mL^{-1}). The aqueous phase is water (10 g L^{-1} potassium nitrate) without added surfactant.

3.2.7 Confocal imaging assay for cell adhesion

Bacterial suspensions for confocal imaging were prepared similarly to those for the rotation assay, except that PS particles were not added and cells were stained with SYTO9 (ThermoFisher) following our standard protocol.[160] Cells were imaged in 3-D by acquiring sequential 2-D images separated by a vertical step $\Delta z = 0.31$ μm using a VT-Infinity (Visitech, Sunderland, UK) confocal microscope equipped with the aforementioned 40× lens. Each image stack, containing 193 images, was merged into a single 2-D image to obtain a visual representation of cell density on droplet surface. We acquired five *z*-stacks of droplets for three independent cultures for each OD. We enumerated the number of cells adhered on each droplet manually using ImageJ software.

3.3 Results and discussion

3.3.1 Droplet rotation by *H. titanicae*

Dodecane droplets in a concentrated suspension of *H. titanicae* bacteria rotate clockwise over time, as shown for a droplet of diameter 40 μm located near the top surface of the capillary in Figure 3.4(a). The optical density OD_{600nm} of the suspension was 1.0, corresponding to a number density of 2.7×10^9 cells mL^{-1}. The droplet rotates steadily over 10 s. Bacteria appear to strongly adhere to the surface of the oil droplets and do not swim when attached, as indicated by their lack of relative rearrangement on the interface over time. Conversely, a droplet of similar diameter does not rotate when placed in a bacterial suspension of lower concentration (optical density $OD_{600nm} = 0.03$) (Figure 3.4(b)). We varied the concentration of bacteria across three orders of magnitude in optical density, which also altered the cell concentration on the droplet surface (Figure 3.5), and the droplet diameter by a factor of five. Generally, droplets do not rotate when the concentration of bacteria is below $OD_{600nm} \approx 10^{-1}$ except for the smallest droplets examined (Figure 3.4(c)). We therefore conclude that rotation is driven by activity of the bacteria.

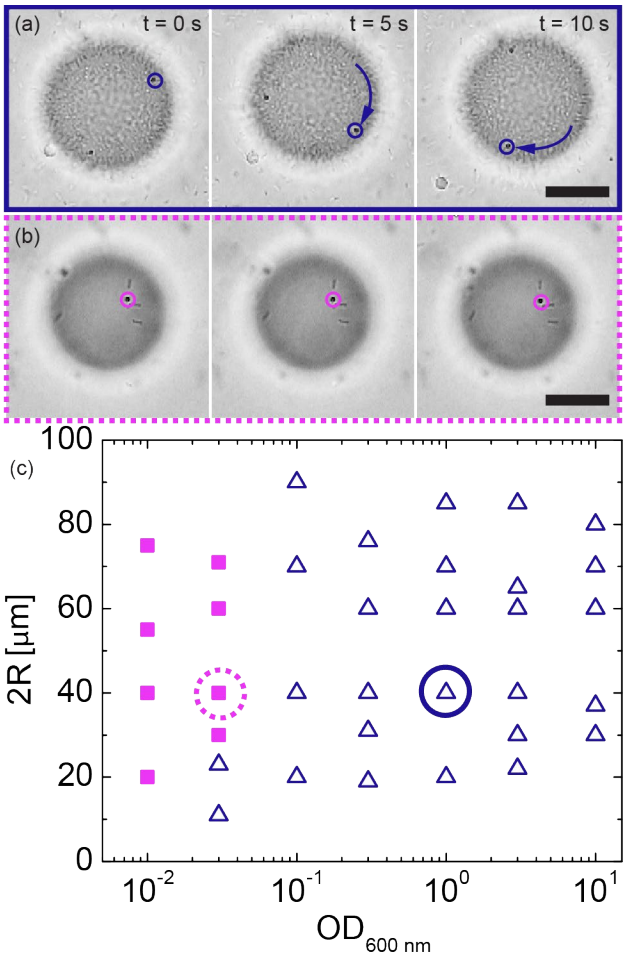

Fig. 3.4. (a and b) Micrographs of droplets at 0, 5 and 10 s in suspensions of *H. titanicae* at OD_{600nm} of (a) 1.0 and (b) 0.03. Arrows indicate the net rotation between images. The scale bar is 20 μm. (c) State diagram for rotation of dodecane droplets in *H. titanicae* suspensions containing 10 g L^{-1} potassium nitrate as a function of drop diameter $2R$ and bacterial optical density (OD_{600nm}). A state point was considered to be non-rotating if all droplets moved less than 2° in 30 s ($n \geq 10$ droplets for each state point). Squares and triangles respectively indicate non-rotating and rotating droplets.

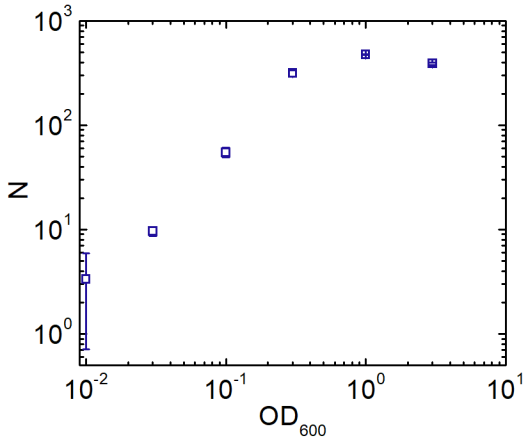

Figure 3.5. Number of cells (*H. titanicae*) adhered on 40 μm dodecane droplets as a function of optical density. The aqueous phase is water (10 gL^{-1} potassium nitrate) without added surfactant. Each data point is an average for three droplets from a single sample.

These experiments are carried out in a microchannel of height 100 μm. Although most (low-density) oil droplets are located near the top of the microchannel, a few droplets remain near the bottom channel surface. Droplets near each surface rotate in a consistent direction: clockwise near the top surface and counter-clockwise near the bottom surface, as shown for representative droplets and schematically in Figure 3.6. This rotation is due to hydrodynamic interaction of the bacteria flagella with the solid wall. A bacterium located above a wall swims in a clockwise direction, due to these hydrodynamic interactions.[161,162] Bacteria adhering to a droplet experience similar hydrodynamic interactions. Because the cells are adhered to the interface, the torque generated by their flagella is transferred to the droplets, driving the droplet to rotate in a consistent direction. This mechanism is similar to that proposed for the directional bias in rotation of a planar square driven by adherent bacteria[133] and of clusters of bacteria.[163]

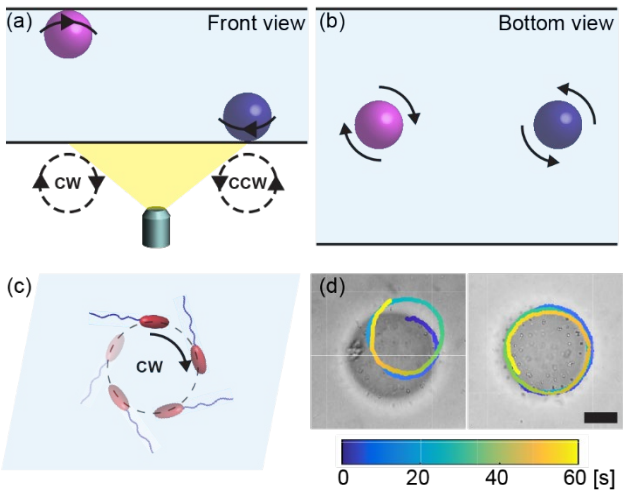

Fig. 3.6. (a and b) Schematic illustrating the direction of rotation of droplets located near the top and bottom surfaces as viewed from the (a) front and (b) bottom. (c) Schematic illustrating the clockwise trajectory of a bacterium located near a solid surface, viewed from above (liquid side). (d) Clockwise (left) and counter-clockwise (right) rotation of droplets as revealed from the trajectories of PS particles, overlaid onto micrographs of the droplets of at the start of the movie. The scale bar is 20 μm.

3.3.2 Angular speed of rotation

To characterize the effect of bacterial activity on droplet rotation, we add PS microparticles to suspensions of *H. titanicae* bacteria and dodedecane droplets (20–95 μm diameter) in aqueous solutions of KNO_3. The PS particles strongly adhere to the dodecane-water interface but do not attach to the negatively-charged cells, so that their motion can be tracked over time (Figure 3.7). We also track the motion of the droplet centroid, which was calculated from the average position of the oil–water interface at a given time. From the trajectory of the droplet centroid, we calculate the droplet mean-square displacement (MSD) as a function of time (Figure 3.8). The MSD for droplets of similar size varies markedly (Figure 3.9). This variation likely results from differences in the interactions of droplets with the nearby wall and is not discussed further.

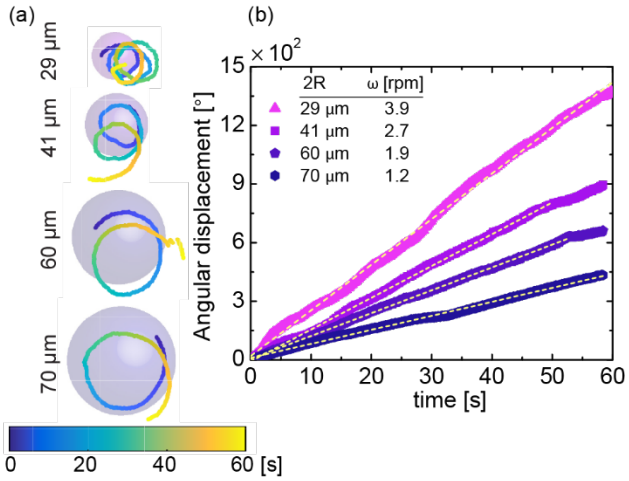

Figure 3.7. (a) Representative trajectories of PS particles adhered on the surface of dodecane droplets of diameter 29, 41, 60, or 70 µm suspended in 10 g L^{-1} potassium nitrate in water. Color indicates time; the underlaid circles indicate the initial position and diameter $2R$ of droplets. (b) Net rotation of droplets shown in (a) as a function of time. The corresponding speed of rotation, in rotations per minute (rpm), is provided in the inset. The OD_{600nm} of the cell suspension prior to mixing of the oil droplets was 1.0.

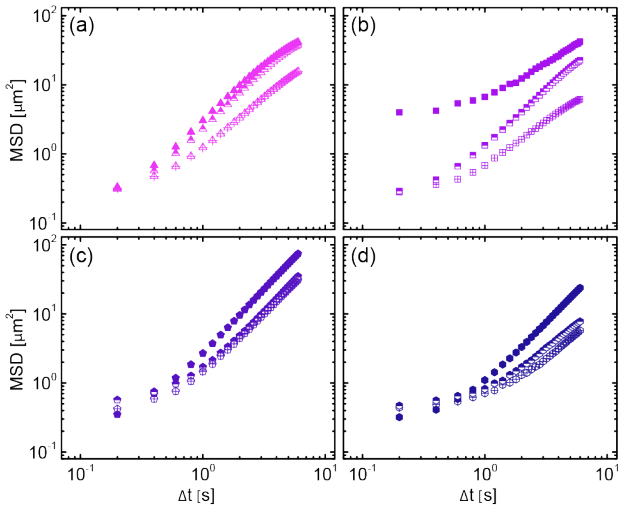

Figure 3.8. Mean-square displacement (MSD) of the droplet centroid as a function of time or droplets of diameter (a) 30 ± 1 µm, (b) 40 ± 1 µm, (c) 60 ± 1 µm, and (d) 70 ± 1 µm.

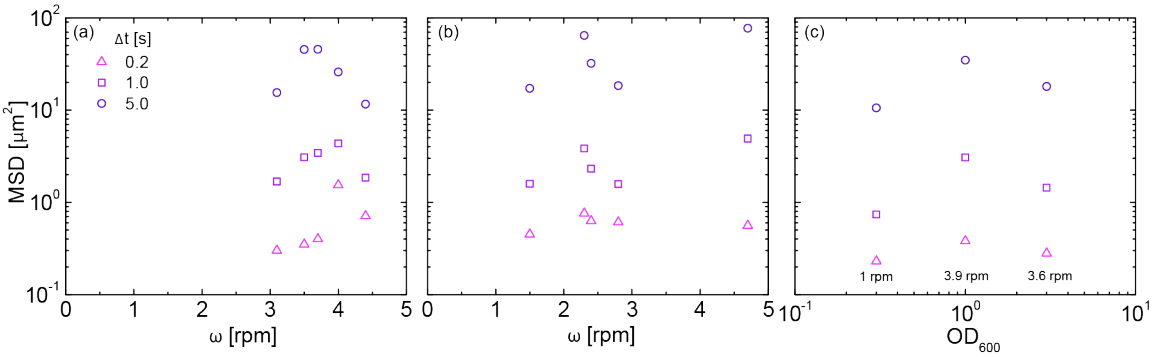

Figure 3.9. Mean-square displacement (MSD) as a function of angular speed (a and b) and optical densities (c) for droplets of diameter (a) 40 μm, (b) 65 μm, and (c) 30 μm.

The angular displacement of droplets increases linearly with time (Figure 3.7(b)). We extract the angular speed ω from a linear fit of the angular displacement as a function of time. The maximum speed of rotation observed here, 7.5 rpm for 20 μm diameter droplets, is comparable to speeds measured for microscale objects rotated by free-swimming, trapped, or adherent bacteria. For example, collectively-swimming bacteria drove rotation of a hexagonal microrotor of side length 10 μm at 2 rpm,[136] and of microgears of diameter 24 and 48 μm at 7.1 rpm[140] and 4 rpm,[138] respectively. Swimming bacteria trapped within microcavities on a micromotor of diameter 15.2 μm rotated at 20 rpm.[139] Finally, bacteria adhered to a square of side length 60 μm drove rotation at 1.3 rpm.[133]

The angular speed ω decreases as the droplet size is increased (Figure 3.10 & 3.11). A similar decrease in ω with increasing R is also observed for bacteria on hexadecane droplets (Figure 3.12). The change in angular speed reflects two factors: the number of adherent bacteria, which in our earlier work depended on drop size,[160] and the drag force on a rotating droplet, which increases with the drop diameter.[164,165] We systematically explore these effects, starting with the concentration of bacteria in suspension. The

angular speed ω of droplets of similar diameter increases less than linearly with the optical density (Figure 3.11). As the optical density is varied by one order of magnitude, ω varies by a factor of 2 to 3 depending on the droplet diameter. Because the standard deviation of ω is large, this variation may fall within statistical errors for certain droplet diameters (*e.g.*, 30 μm).

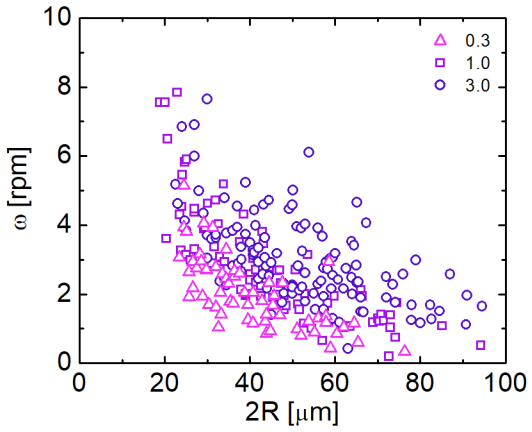

Figure 3.10. Angular speed of dodecane droplets as a function of droplet diameter for OD of 0.3, 1.0, and 3.0. The aqueous phase is water (10 g L^{-1} potassium nitrate) with no added surfactant.

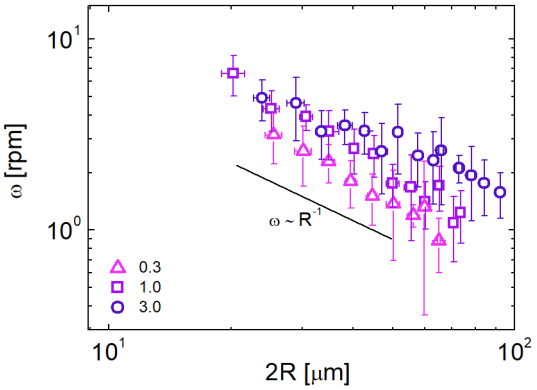

Fig. 3.11 Angular speed of dodecane droplets in 10 g L^{-1} potassium nitrate in MilliQ water as a function of droplet diameter 2*R*. Symbols indicate different concentrations of bacteria, with OD 0.3 (triangles), 1.0 (squares), or 3.0 (circles). Data points indicate the average and standard deviation over $n = 3$ to 18 droplets whose diameters fell within 4 μm. The solid line indicates a power-law with exponent −1. The R^2 values of the fits are 0.95, 0.93, and 0.84 for ODs of 0.30, 1.0, and 3.0, respectively.

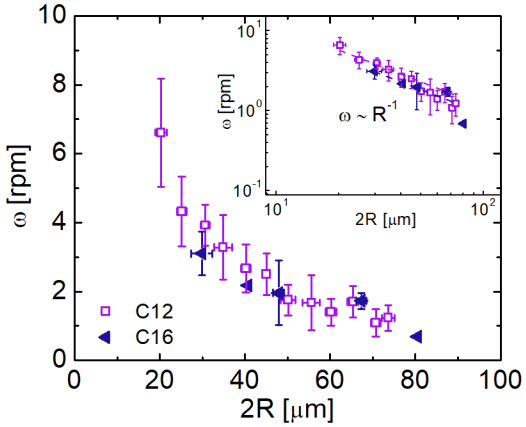

Fig. 3.12. Angular speed as a function of drop diameter for dodecane and hexadecane droplets. Optical density of *H. titanicae* suspension is 1.0. The aqueous phase is water (10 g L^{-1} potassium nitrate) with no added surfactant.

The optical density is a measure of the concentration of bacteria in suspension, but does not necessarily proportionally scale with the number of bacteria at the oil–water interface.[160] To relate the number of bacteria at the interface to the optical density, we count the number of bacteria directly adhered to the interface in 3-D confocal micrographs (Figure 3.13). The number of cells on the droplet surface increases by 30 ± 3% (n = 15) as the OD_{600nm} is increased from 0.3 to 3.0. Assuming that attached bacteria are randomly oriented on the surface, the net propulsive force exerted by N bacteria is expected to scale as $N^{1/2}$.[128–130,163] We find, however, that the percentage increase in $N^{1/2}$ (14 ± 1%, n = 15) is lower than the percentage increase in angular speed (77 ± 47%, n > 10). (The large errors on the angular speed likely reflect differences in the interactions between droplets and the nearby capillary surface, which also affect the MSD.) This result suggests that cells in suspension begin to contribute to droplet rotation as the concentration is increased.

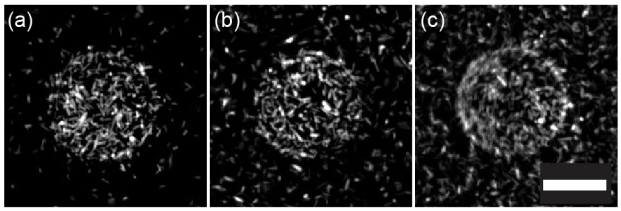

Fig. 3.13. 2-D projection of 3-D images of *H. titanicae* cells on 30 μm dodecane drop interfaces at optical densities of (a) 0.3, (b) 1.0, and (c) 3.0 captured using confocal microscopy. The number of attached cells is 284 ± 16, 363 ± 20, and 368 ± 23 for OD of 0.3 (n = 15 droplets), 1.0 (n = 15 droplets), and 3.0 (n = 15 droplets), respectively. The scale bar is 20 μm.

As a first step towards understanding how bacteria drive droplet rotation, we consider droplet rotation propelled by cells attached to the droplet surface. The torque counteracting frictional rotational drag[164,165] on a droplet is given by $T_{\text{drag}} = 8\pi\mu R^3\omega$, where R is the radius of the droplet and μ is the solution viscosity. This rotational drag is balanced by the net torque exerted by attached bacteria. For N randomly-oriented bacteria, the net torque scales as $T_{\text{net}} = F_a N^{1/2} R$, where F_a is the propulsive force from one bacterium. In our earlier experiments the number of adherent cells scaled approximately with the droplet surface area, such that $N^{1/2} \propto R$.[160] Equating these two expressions suggests that $\omega \propto R^{-1}$. Our data at the two lowest OD values (0.30 and 1.0) are consistent with this scaling (Figure 3.11), as indicated by R^2 values of 0.95 and 0.93 for a fit to $\omega \sim R^{-1}$. At higher OD = 3.0, however, ω decreases less rapidly than R^{-1}, as confirmed by the R^2 value of 0.84, indicating that droplets rotate slightly faster than expected from their size. This result suggests that collective swimming effects may become important at number densities approaching 10^{10} cells mL^{-1} for *H. titanicae*.

The scaling expression $\omega \propto R^{-1}$ approximates a bacterium as a force monopole. Because swimming bacteria must exert zero total force on the fluid, a bacterium should be approximated to lowest order as a force dipole.[166,167] A correction to the net torque, derived in ref. 132, was obtained by considering the propulsive force exerted by a

flagellum, which generates an additional drag force that acts on a rotating object. The torque exerted by a bacterium, accounting for this dipole correction, is given by $T_{\text{net}} \propto N^{1/2}R[1 - R(l^2 + R^2)^{-1/2}]$, where l is the length of a flagellum.[163] The dipole torque model, however, less accurately captures the droplet size dependence of ω than does the monopole torque model (Figure 3.14), likely because the droplet size remains comparable to the flagellum length $l \approx 10$ μm. The viscous drag due to a nearby wall leads to a numerical correction but to lowest order does not alter the R-scaling of the net torque at low Reynolds number;[168] this correction is of order 15% for a droplet of radius 15 μm that is located 1 μm from the wall.[169]

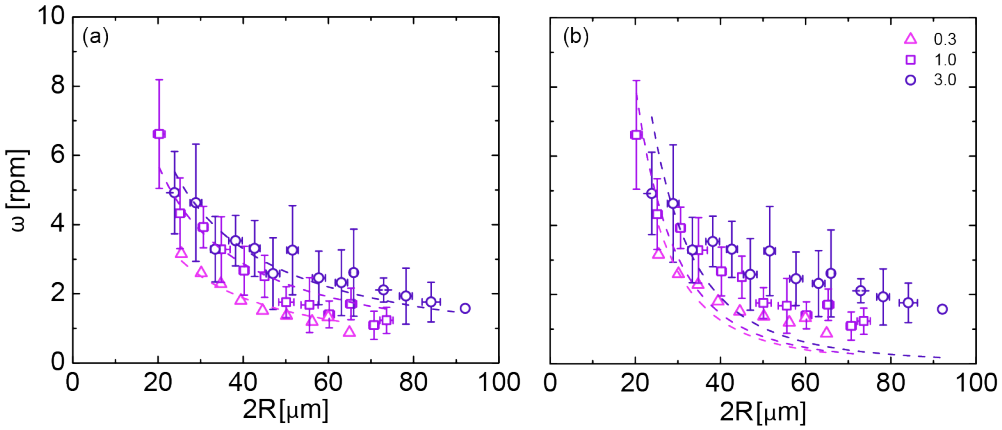

Fig. 3.14. Angular velocity as a function of droplet diameter with (a) monopole and (b) dipole model.

3.3.3 Tuning rotation through interfacial tension

The results presented in Figure 3.3 – 3.14 reveal that the rotation of droplets is driven by adherent bacteria. This result suggests that modifying the interaction between bacteria and the interface will alter the rotation behavior. To test this idea, we examine the effect of the oil–water interfacial tension on drop rotation. We use an anionic surfactant, dioctyl sodium sulfosuccinate (DOSS), to modify the interfacial tension between dodecane and water. We previously showed that increasing the surfactant concentration decreased the

interfacial tension of dodecane–water (Figure 3.15), which increased the free energy of adhesion and thereby reduced adhesion of cells to droplets.[160] Thus, changing the concentration of DOSS is expected to alter bacteria-driven rotation of droplets.

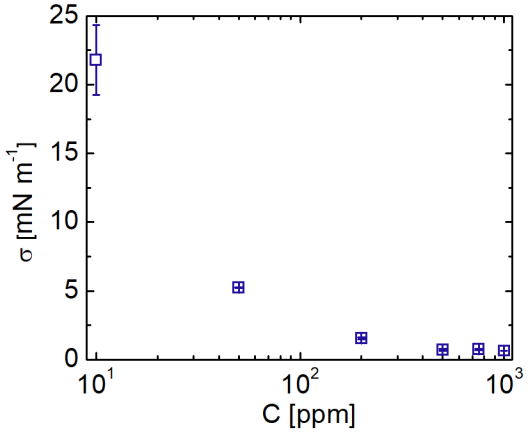

Figure 3.15. Dodecane-water interfacial tension σ as a function of dioctyl sodium sulfosuccinate (DOSS) concentration. Water contains 10 g L^{-1} of potassium nitrate.

We observe droplet rotation driven by *H. titanicae* for DOSS concentrations in the range 0 – 3500 ppm (Figure 3.16). The angular speed of droplets appears to decrease with increasing surfactant concentration above 100 ppm. Because the interfacial tension decreases as the concentration of DOSS is increased, the PS particles do not strongly adhere to the droplet interface, as indicated by changes in their relative positions on the interface over time. The bacteria also appear to rearrange relative to others over time, suggesting that they are able to swim while attached to the DOSS-decorated interfaces. Thus, the movement of the PS particles does not quantitatively capture the droplet angular speed. Indeed, at high DOSS concentration the PS particles move much faster than the droplet, so that the droplet angular speed cannot be accurately measured. Two mechanisms may contribute to the apparent decrease in droplet angular speed as the surfactant concentration is increased. First, fewer cells adhere to the interface due to the

lower interfacial tension,[160] thereby reducing the total torque. A similar mechanism was shown in ref. 102, in which adding surfactants removed the cells attached to a microgear that drove its motion. Second, adding surfactant also reduces the strength of adhesion of cells at the droplet interface. In support of this idea, cells swim more at the interface as the surfactant concentration is increased. We propose that less-strongly adhered cells transmit force less efficiently to the droplet, again reducing the net torque.

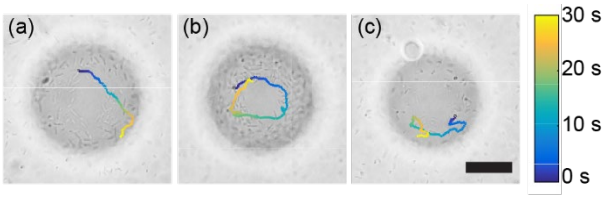

Figure 3.16. PS particle trajectories on rotating droplets as a function of DOSS concentration: (a) 50 ppm, (b) 200 ppm, and (c) 500 ppm. The scale bar is 20 μm.

3.3.4 Tuning rotation through interfacial affinity

Finally, we characterize droplet rotation for three species of motile bacteria, monotrichous *S. haliotis* and peritrichous *E. coli* and *H. titanicae*. All three bacteria readily swim in the aqueous salt solution, with average near-surface speeds of 13 ± 2, 10 ± 3, and 10 ± 4 μm s^{-1} for *E. coli*, *S. haliotis*, and *H. titanicae*, respectively. The swimming speed is approximately constant despite different numbers of flagella in the three species, consistent with experimental observations[170] and a theoretical model.[171] The surface energies of the three strains are 66, 66, and 64 mN m^{-1} for *E. coli*, *S. haliotis*, and *H. titanicae*, respectively. The angular speed of 40 μm droplets, determined from the trajectories of PS particles adhered to the oil–water interface (Figure 3.17(a–c)), increases from 0.1 rpm for *E. coli* to 2.5 rpm for *H. titanicae* (Figure 3.17(a)).

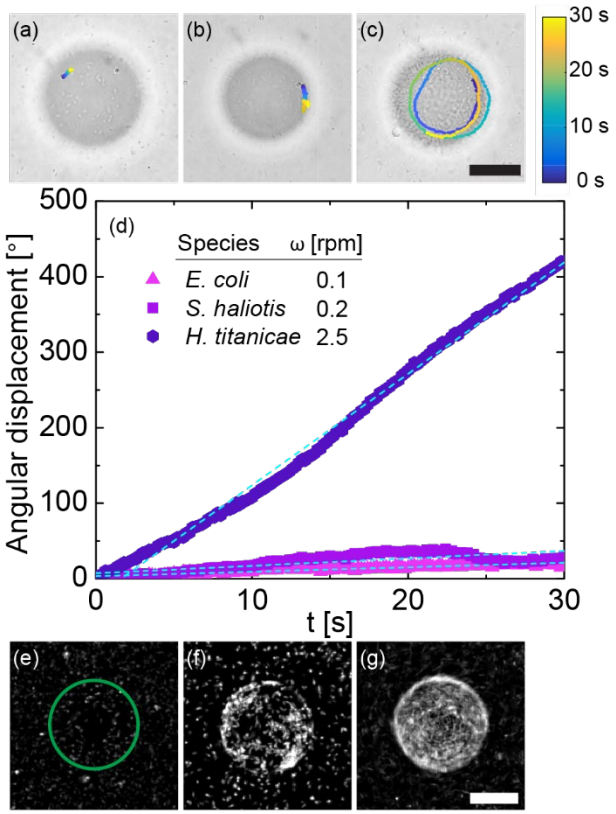

Figure 3.17. Trajectories of a PS particle on the interface of a dodecane droplets of diameter 40 μm in the presence of (a) *E. coli*, (b) *S. haliotis*, and (c) *H. titanicae* bacteria at cell concentration =2.7 × 10^9 cells mL^{-1}. (d) Angular displacement as a function of time for the three species. The inset table provides the rotation rate, determined from the slope. (e–g) 2-D projections of 3-D images, obtained using confocal microscopy, for (e) *E. coli*, (f) *S. haliotis*, and (g) *H. titanicae*. The scale bars in (c) and (g) are 20 μm.

Confocal micrographs reveal that very few *E. coli* adhere to the oil–water interface (Figure 3.17e). Thus, the slow rotation for this species is likely due to the low number of bacteria propelling the droplet. Although *S. haliotis* bacteria adhere at the interface in slightly lower numbers as compared to *H. titanicae* (Figure 3.17(f and g), droplets propelled by *S. haliotis* rotate twelve times slower than those driven by *H. titanicae*. Increasing the concentration of *S. haliotis* increases the droplet rotation speed (Figure 3.18). Movies of *S. haliotis* indicate that these bacteria are more motile at the interface than *H. titanicae*. We therefore speculate that the relatively slow rotation of *S. haliotis*-driven droplets results from the weaker interfacial adhesion.

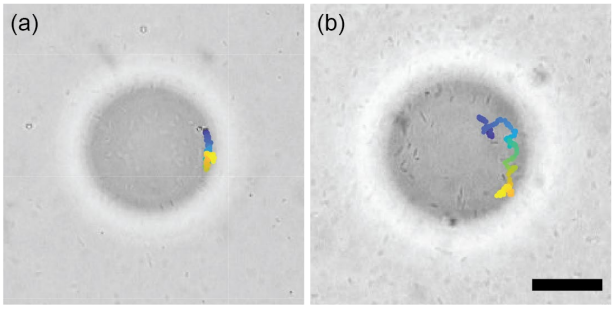

Figure. 3.18. PS particle trajectories on rotating droplets for *S. haliotis* concentrations of (a) 2.7×10^9 cells mL^{-1} and (b) 8.7×10^9 cells mL^{-1}. Droplet in (a) rotated at 0.2 rpm whereas droplet in (b) rotated at 0.5 rpm. Scale bar is 20 µm.

3.4 Conclusions

We examined the effect of droplet diameter, cell concentration, oil–water interfacial tension, and bacteria species on the directional rotation of droplets near a liquid–solid interface. Droplets begin to rotate when the concentration of bacteria is increased above a certain optical density. Variation in droplet rotational speed reflects differences in the number of bacteria adhered at the droplet interface. The angular speed of droplets decreases with increasing droplet diameter, consistent with a physical picture in which rotation of flagella of randomly-oriented bacteria generates a torque on the droplets. The speed of rotation can be tuned through the number of bacteria adhered to the interface, by varying surfactant concentration or bacterial species.

The clockwise rotation, as viewed from the liquid side, is driven by the hydrodynamic interactions of flagella with the nearby surface. This mechanism, arising from interactions of bacteria confined near a surface,[115] enables directional rotation of a symmetric object to be generated from active suspensions, in contrast to symmetry-breaking through object chirality[136–139] or non-uniform bacterial adhesion.[130,172] Bacteria-driven droplet rotation may provide a route to enhance mixing and thereby promote mass

transport in multiphase microbial reactors[173] or drive cells to agglomerate at the droplet surface through hydrodynamic interactions.[174,175] Thus the ability to actively drive droplet rotation may be useful in a variety of practical settings involving microbes.

In addition, active particles can exhibit a wide range of interesting collective behaviors. For example, self-propelled droplets can form clusters that collectively translate and rotate when confined.[176,177] Whether droplets driven by adhered bacteria exhibit collective motion at high densities is an open question for future study.

Chapter 4: Bacterial motility enhances adhesion to oil droplets

4.1 Introduction

Adhesion of bacteria at the interface between two liquids can alter the rate of biodegradation of hydrocarbons[39,42,43,178] during marine oil spills and the efficacy of bioprocess engineering operations that involve multiple immiscible fluid phases.[179,180] Adhesion of bacteria on solid or liquid surfaces can depend on physicochemical properties of the surfaces (e.g., surface functionality and topography) and liquids (e.g., surfactant concentration, ionic strength, pH, and concentration of the carbon source) as well as cell surface hydrophobicity (which, in turn, depends on adhesin and polysaccharide expression).[160,181–184] These properties affect the electrostatic and van der Waals forces that control the thermodynamics of adhesion for micron-size bacteria at interfaces. Many bacteria, however, are active and motile, moving randomly and in response to chemical[115,185–189] or physical (e.g., gravity,[190] viscosity,[191] flow[192]) gradients. Thus, motility may also affect adhesion to liquid-liquid interfaces.

Bacteria motility is known to enhance adhesion of bacteria to solid surfaces.[193–201] For example, the fractional surface coverage by motile *Pseudomonas aeruginosa* PAO1 bacteria is up to 2.5 times greater than that of a nonmotile mutant, depending on the ionic strength and Reynolds number.[199] This result suggests that motility enabled bacteria to attach to surface sites that were otherwise inaccessible; in the picture of Ref. 168, swimming provided a kinetic "force" that competed with the electrostatic and hydrodynamic forces controlling attachment of nonmotile cells.[199] Similarly, approximately five to ten times more motile *Escherichia coli* bacteria adhered on a nanostructured biocidal surface compared to mutants that lacked rotating flagella or the

receptors required for chemotaxis.[201] Motility may increase the frequency at which bacteria collide with the surface, as suggested by the positive correlation between attachment rate and swimming speed for motile *Alcaligenes* and *Alteromonas* spp.[196] As a final example, motile and nonmotile *E. coli* bacteria were located on average at different distances above the surface, affecting the interactions which acted upon the bacteria and hence their surface attachment.[197] Motility is less studied near liquid-liquid interfaces, such as the oil-water interfaces encountered in an oil spill scenario. Recent studies reveal that *P. aeruginosa* bacteria display a variety of motility behaviors near a planar oil-water interface,[29,135,202] and that bacterial motility can provide sufficient energy to move dispersed oil droplets.[203,204] How bacterial motility affects adhesion to oil-water interfaces, however, remains incompletely understood.

Here, we show that bacteria motility enhances adhesion of the marine bacterium *Halomonas titanicae* on hexadecane droplets suspended in artificial seawater. Using confocal microscopy and single cell tracking algorithms, we quantified the number of cells adhering to hexadecane droplets over time. To render cells, we added a proton decoupler, carbonyl cyanide m-chlorophenyl hydrazine (CCCP), or applied mechanical shear to remove the flagella. Both motile and nonmotile cells exhibited first-order Langmuir kinetics for adhesion. The time constant extracted from the Langmuir fit was smaller for motile bacteria. Furthermore, the long-time density of bacteria on the droplet was greater for motile bacteria. Increasing the concentration of an anionic surfactant, diocytl sodium sulfosuccinate (DOSS), reduced the oil-water interfacial tension, causing fewer cells to attach to the interface. The long-time density of motile bacteria on the oil-water interface was greater than that of the nonmotile bacteria over a wide range of

DOSS concentrations. Our results suggest that motility can lead to faster and greater adhesion of bacteria, which may advantage bacteria during biodegradation and other processes that involve access to a dispersed fluid phase.

4.2 Materials and methods

4.2.1 Chemicals

Zobell marine broth 2216 (HiMedia lab), sodium pyruvate (Amresco), nutrient agar (Difco), hexadecane (≥ 99%, Sigma-Aldrich), dioctyl sodium sulfosuccinate (DOSS, ≥97%, Sigma-Aldrich), SYTO9 (ThermoFisher), carbonyl cyanide 3-chlorophenylhydrazone (CCCP, ≥ 97%, Sigma-Aldrich), sodium chloride (≥ 99%, BDH), magnesium chloride hexahydrate (≥ 99%, Alfa Aesar), magnesium sulfate heptahydrate (≥ 99.5%, Sigma-Aldrich), calcium chloride dihydrate (Sigma-Aldrich), potassium chloride (≥ 99%, BDH), potassium nitrate (≥ 99%, EMD), dipotassium phosphate (≥ 98%, Sigma-Aldrich), ethylene glycol (≥ 99.8%, Sigma-Aldrich), and diiodomethane (≥ 99%, Sigma-Aldrich) were used as received.

4.2.2 Bacteria strains and growth conditions

We studied two species of marine bacteria. The Bead 10BA strain is closely related to *Halomonas titanicae*. It was isolated from samples collected at 1509 m during the Deepwater Horizon oil spill in the Gulf of Mexico by Dr. Romy Chakraborty and Dr. Gary Anderson (Lawrence Berkeley National Laboratory) and recieved from Dr. Douglas Bartlett (Scripps Institute of Oceanography, UCSD). Hereafter, it is referred to by its closest species name, H. titanicae. H. titanicae is moderately halophilic, Gram-negative, and rod-shaped, with diameter of 0.5 – 0.8 μm and length of 1.5 – 6 μm. These bacteria swim using their peritrichous flagella.[156] *Marinobacter hydrocarbonoclasticus* (ATCC

49840) was obtained from Dr. Bartlett. *M. hydrocarbonoclasticus* is halotolerant, Gram-negative, and rod-shaped, with length of 2 – 3 μm and diameter of 0.3 – 0.6 μm.[69] It is nonmotile under the conditions of our experiments. Marine agar plates (38.7 g L^{-1} marine broth, 10 g L^{-1} sodium pyruvate, 15 g L^{-1} agar) were streaked from frozen stocks of these bacteria and incubated at 30 °C for 40 h. To initiate the principle culture, 20 mL of culture medium (38.7 g L^{-1} marine broth and 10 g L^{-1} pyruvate) was inoculated from a single colony of bacteria and incubated for 20 h in an orbital incubator shaker (New Brunswick Scientific) at 200 rpm and 30 °C. To prepare subcultures, 20 mL of culture medium was inoculated with 65 μL of the principal culture and grown to late exponential phase in an orbital incubator shaker at 30 °C and 200 rpm for 20 h.

4.2.3 Zeta potential

For zeta potential measurements, bacteria cells were grown to late exponential phase. First, 20 mL of each bacteria suspension was centrifuged at 5000 *g* for 10 minutes in a Sorvall ST 16 Centrifuge (ThermoFisher Scientific). The pellet was resuspended in 20 mL MilliQ water and centrifuged again. After repeating this process one more time, the pellet was resuspended in MilliQ water. The resultant suspension was diluted to an optical density at 600 nm ($OD_{600\ nm}$) of 0.04 – 0.06 (Laxco DSM-Micro Cell Density Meter) with MilliQ water. The zeta potentials of suspensions were measured using a Nicomp 380 zeta-potential analyzer (Table 4.1).[59]

4.2.4 Contact angle and surface energy

Bacteria suspensions for surface measurements were prepared in a similar manner as those for zeta potential measurements, except that the final OD was adjusted to 1.0. Each bacteria suspension was filtered through cellulose acetate membrane filters (pore

diameter 0.45 μm, Advantec) under vacuum at 100 mm Hg below atmospheric pressure using a GEM 8890 vacuum pump (Welch) to create a bacterial lawn.[24,72] Contact angles were measured for three liquids (MilliQ water, ethylene glycol and diiodomethane) on the lawns using a Dataphysics OCA 15EC goniometer. The surface energy of the bacteria was calculated using the method of Wu.[73,74]

Table 4.1 Contact angle, surface energy (SE), and zeta potential (ζ) of *H. titanicae* (HT) and *M. hydrocarbonoclasticus* (MH) without CCCP (-) and incubated for with one hour incubation in 5 μM CCCP at room temperature (+). Standard deviations are calculated from two independent bacteria cultures.

Bacteria sp.	CCCP	Water [°]	DIM [°]	EG [°]	SE [mN m^{-1}]	ζ [mV]
HT	-	23 ± 4	57 ± 5	29 ± 4	64 ± 1	-51 ± 2
	+	25 ± 2	64 ± 7	27 ± 4	63 ± 1	-47 ± 7
MH	-	86 ± 3	87 ± 4	98 ± 5	23 ± 1	-45 ± 4
	+	56 ± 7	101 ± 8	71 ± 1	42 ± 1	-39 ± 4

4.2.5 Interfacial tension

The interfacial tension of hexadecane/water was measured as a function of DOSS concentration via the pendant drop method using a Dataphysics OCA 15EC goniometer. The outer phase was artificial seawater (ASW: 0.33 M NaCl, 0.06 M $MgCl_2$, 0.03 M $MgSO_4$, 0.016 M $CaCl_2$, 0.007 M KCl, 0.019 M KNO_3, and 0.0007 M HK_2PO_4)[18,112] with DOSS (1 – 500 ppm) and the inner phase was hexadecane.

4.2.6 Imaging chamber for confocal microscopy

Two types of chambers were prepared for imaging experiments. For nonmotile cells, a glass slide and a glass cover slip were exposed to oxygen plasma for 2 min. A PDMS layer of thickness 1 – 1.5 mm on a 100 mm silicon wafer was prepared by spincoating at 100 rpm for 30 seconds using a spin coater (Brewer Science CEE 200CB). A 15 × 20 mm^2 rectangle of PDMS was cut from the layer and a well of 3 – 4 × 6 – 8

mm^2 was created to contain the bacteria sample. The PDMS rectangle was placed onto a plasma-cleaned glass slide right after the plasma treatment and covered with a plasma-cleaned glass cover slip (Fig. 4.1). A similar chamber was prepared for motile cells, except that the top cover slip was replaced with a cellulose dialysis tubing patch (12 – 14 kDa cutoff, Carolina Biological) attached with vacuum grease. For motile cell experiments, NaCl solution was introduced through the membrane to reduce cell motility during imaging.

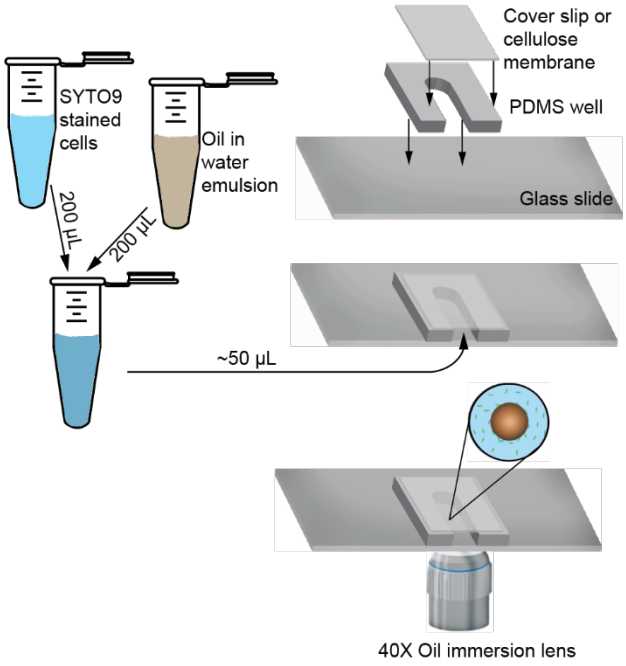

Figure 4.1. Schematic diagram of experimental steps and imaging setup.

4.2.7 Turning off motility

Many bacteria can swim using one or more flagella, which are driven by electrochemical gradients of protons or sodium ions across the cytoplasmic membranes.[187] Carbonyl cyanide 3-chlorophenylhydrazone (CCCP) was introduced to cell suspensions to inhibit cell motility. CCCP is a protonphore that collapses the proton motive force (PMF) across the cytoplasmic membrane, and thereby halts cell motility.[205] A solution of CCCP of concentration 5 mM was added to bacterial suspensions at an

appropriate volume to obtain a final concentration of 5 μM and incubated for about 3 minutes. Using a brightfield microscope, we confirmed that nearly all cells stopped swimming after 3 minutes of incubation time.

We also mechanically sheared off the flagella by rapidly agitating 50 mL of a washed cell suspension at OD 0.4 using a blender (Oster 6642) in liquify mode at high for 15 sec. This process temporarily renders cells nonmotile by removing flagella.[206] Sheared cells on average did not recover motility over 2 h (Figure 4.2). Sheared cells were stained and imaged using the protocol for nonmotile cells described in the following subsection.

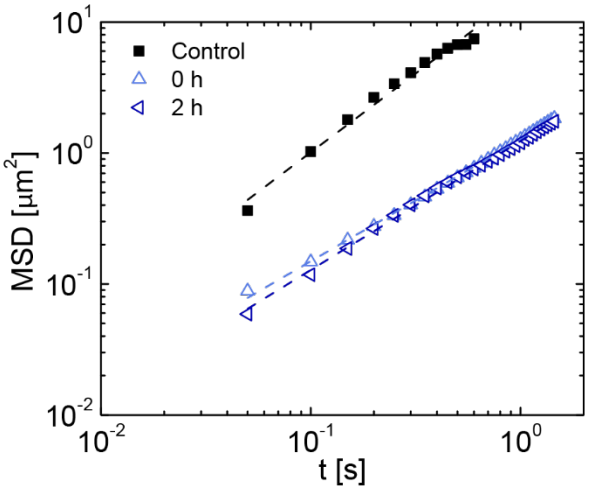

Figure 4.2. MSD of *H. titanicae* without mechanically shearing (control), immediately after mechanically shearing (0 h), and two hours after mechanically shearing (2 h). Optical density of cells suspension was 0.2 and DOSS concentration was 2 ppm.

4.2.8 Imaging cells adhering on hexadecane droplets

From a suspension of cells grown to late exponential phase, 20 mL was centrifuged at 2000 *g* for 10 minutes. After the supernatant was discarded, the resultant pellet was suspended in 2x ASW by gentle shaking and the OD was adjusted to 0.4.

SYTO 9 (1 μL) was added to 1 mL of this cell suspension and incubated at room temperature in the dark for 2 – 5 minutes.

For nonmotile bacteria experiments, 1 μL of 5 mM CCCP was added along with 1 μL of SYTO9 to 1 mL of cell suspension, which resulted in a final CCCP concentration of 5 μM. Hexadecane-in-water emulsions were prepared by manually shaking 10 μL of hexadecane in 1 mL of MilliQ water containing DOSS (4, 40, 100, 200, 300, and 400 ppm) in a 1.5 mL Eppendorf tube. From the cell suspension, 200 μL was transferred into a 1.5 mL Eppendorf tube, to which 200 μL of emulsion was subsequently added. This protocol resulted in a final CCCP concentration of 2.5 μM. The resulting suspension (OD = 0.2, 5.4×10^8 cells mL^{-1}) was introduced in an imaging chamber and sealed using vacuum grease.

Because *H. titanicae* bacteria remained motile at the droplet surface after adhesion, we halted the motility by addition of NaCl to enable quantification of cells. Although cells adhered on the droplet could move along the surface, they did not appear to detach. A modified protocol was adopted for imaging suspensions containing motile cells. For these experiments, 10 μL of NaCl solution (350 g L^{-1} NaCl in MilliQ water) was introduced into a suspension of motile cells through the membrane that formed the top boundary of the imaging chamber. Sodium chloride diffused through the membrane into the cell-and-emulsion suspension and the cells stopped swimming in 1 – 3 minutes due to the high NaCl content. Suspensions were imaged within 15 min after introduction of NaCl. The cessation of swimming motion facilitated imaging and quantification because cells exhibited minimal displacement during the 3-D scanning.

Bacteria were imaged in 3-D over time using a VT-Infinity (Visitech, Sunderland, UK) confocal scanhead. The confocal scanhead was mounted on an inverted microscope (Leica Microsystems DM4000) bearing a 40X oil-immersion lens (HCX PL APO, NA 1.25 – 0.75). Stacks of two-dimensional images separated by a height $\Delta z = 0.31$ μm were acquired at times t = 5, 10, 20, 30, 60, 90, and 120 min after the cell suspension was added to the emulsion. For imaging motile bacteria, 350 g L^{-1} NaCl was introduced at 5, 10, 20, 30, 60, 90, and 120 min after the bacteria suspension was mixed with the emulsion. Subsequently, z-stacks were acquired after cell motility was arrested (between 1 and 3 min) after introduction of NaCl. Each experiment was repeated with at least four independent cultures. For equilibrium adhesion experiments, 3-D images were acquired 1 hour after the emulsion was introduced into the cell suspension. Cells at the oil-water interface were enumerated using both particle tracking algorithms written on MATLAB[160] and through manual counting using ImageJ. The cell density was calculated by dividing the number of cells adhered on the top hemisphere of a droplet by the surface area of the hemisphere.

4.3 Results and discussion

4.3.1 Bacterial adhesion on hexadecane droplets over time

Using confocal microscopy and single-cell tracking, we analyzed the adhesion of *Halomonas titanicae* bacteria over time on 20 μm hexadecane droplets stabilized by DOSS and suspended in ASW. We assessed the effects of motility on adhesion by comparing results from suspensions in the absence and presence of CCCP, which arrests cell motility by collapsing the PMF.[205] Examination of confocal micrographs reveals that the number of bacteria adhered on hexadecane droplets changes over time (Figure 4.3).

The density of cells at the oil-water interface ρ_s , calculated from the 3-D images, initially increases with time and is approximately constant after 60 minutes for both motile and nonmotile bacteria (Figure 4.4). The interfacial cell density for motile bacteria is higher than that of both the chemically modified and mechanically sheared nonmotile bacteria. Although $\rho_s(t)$ is slightly greater for the mechanically sheared bacteria than the chemically modified bacteria on all time scales, the difference is within the measurement error. The time-dependent densities of both motile and nonmotile bacteria follow a Langmuir first-order kinetic model, $\rho_s(t) = \rho_{s,\infty} - (\rho_{s,\infty} - \rho_{s,0})e^{\frac{-t}{\tau}}$, where $\rho_{s,0}$ is the density of cells at the interface at t = 0 min, $\rho_{s,\infty}$ is the cell density at long time ($t \rightarrow \infty$), and τ is the characteristic time constant of adhesion. The time constants extracted from the fits are 4 ± 1 min, 12 ± 1, and 16 ± 3 min for motile, nonmotile (CCCP), and nonmotile (mechanically-sheared) bacteria, respectively; the time constant of nonmotile *H. titanicae* is close to the time constant (9 ± 4 min) determined in our previous study of adhesion of nonmotile *Marinobacter hydrocarbonoclasticus* on 20 µm droplets.

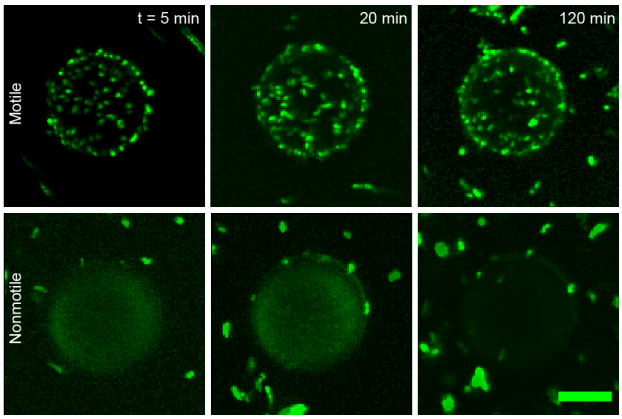

Figure 4.3. 2D projections of 3D confocal images of cells adhered on 20 µm hexadecane droplets for motile bacteria (top panel), and nonmotile bacteria (bottom panel) at *t* = 5 (first column), 20 (second column), and 120 min (third column). DOSS concentration is 2 ppm. Scale bar is 10 µm.

This result indicates that motility enhances the rate of adhesion at the oil-water interface but does not affect the order of the kinetics. A variety of colloidal adsorption processes also follow Langmuir kinetics.[83,207,208] Likewise, first-order Langmuir-type kinetics have been applied to model the adhesion of *S. epidermidis* on silicone,[83] of *Actinomyces viscosus* on silica beads,[207] and of *S. epidermidis* on titanium alloy.[208]

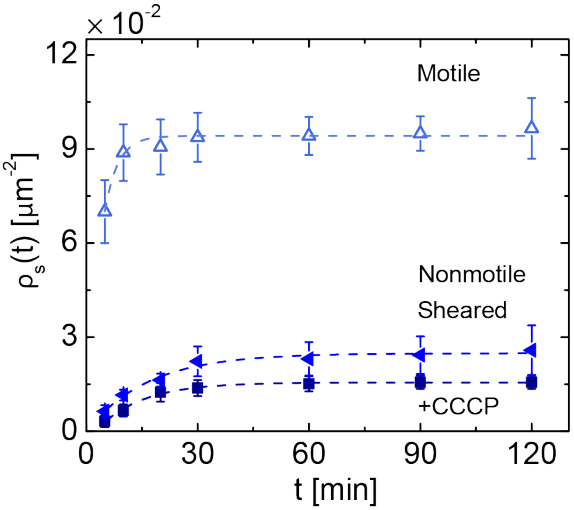

Figure 4.4. Interfacial density $\rho_s(t)$ of cells adhered on 20 μm hexadecane droplets as a function of time for motile (-CCCP, open triangles), chemically nonmotile (+CCCP, solid squares), and mechanically nonmotile (sheared, solid left triangles). The DOSS concentration in suspension was 2 ppm. Dashed lines represent first-order Langmuir adsorption fits. Error bars represent the standard deviation calculated from at least 30 droplets (at least 6 droplets for at least 5 independent bacterial cultures).

4.3.2 Long-time adhesion

In addition to reducing the time needed to reach steady-state adsorption, motility also affects the long-time cell density $\rho_{s,\infty} = \rho_s(t \to \infty)$. In our experiments, $\rho_{s,\infty}$ of motile bacteria is approximately six times greater than that of nonmotile *H. titanicae* bacteria (Figure 4.5). Our finding is consistent with earlier studies showing that bacteria motility enhances adhesion of bacteria on solid surfaces.[196,199–201] By contrast, the long-time interfacial density of a bacterium that is nonmotile under these experimental conditions, *M. hydrocarbonoclasticus* is not altered by addition of CCCP. Its interfacial

density is slightly greater than that of the nonmotile *H. titanicae*, consistent with the idea that the chemical structure of the bacterium surface affects interfacial adhesion.

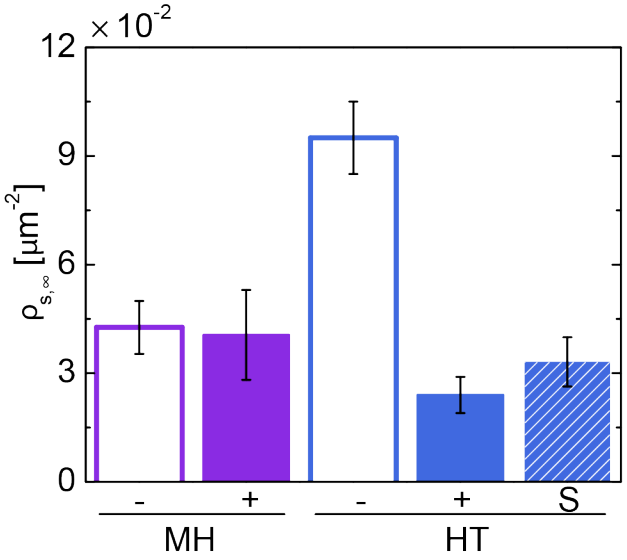

Figure 4.5. Effect of motility on adhesion of bacteria to 20 μm hexadecane droplets. Outer phase is ASW. MH and HT respectively indicate *M. hydrocarbonoclasticus* and *H. titanicae*. `+' and `-' respectively indicate the presence or absence of 5 μM of CCCP, which arrests cell motility. Sample S represents data acquired for nonmotile *H. titanicae* prepared by mechanically shearing off the flagella. Data acquired for nonmotile *M. hydrocarbonoclasticus* suggest that CCCP does not affect the bacterial adhesion through modification of cell or emulsion surfaces. The optical density was 0.2, which corresponds to 5.4×10^8 cells mL^{-1} for *H. titanicae* and 3.5×10^8 cells mL^{-1} for *M. hydrocarbonoclasticus*.

Motility in our experiments is arrested through the addition of CCCP, which may affect the interfacial properties of cells or droplets. To confirm that the difference in $\rho_{s,\infty}$ is due to bacterial motility, we characterized the interfacial properties of bacteria and droplets. The zeta potentials (Table 4.2) of a bacterium that is nonmotile under these experimental conditions, *M. hydrocarbonoclasticus*, are the same with or without CCCP, within experimental error, although the surface energy is somewhat greater with CCCP. Furthermore, CCCP does not change the interfacial properties of oil-in-water emulsions, as indicated by the near-constant values of interfacial tension and zeta potential measured for these emulsions (Figure 4.7(a) and Table 4.2). Finally, the surface properties (surface

energy and zeta potential) of *H. titanicae* remain unchanged in presence and in absence of CCCP. Together, our results suggest that CCCP alters adhesion through arrest of bacterial motility and not by changing the surface properties of droplets or cells. This result suggests that motility is the dominant factor controlling the difference in adhesion.

Table 4.2. Zeta potential of hexadecane droplets in Milli-Q water at various DOSS concentrations. Emulsion droplets were prepared by shaking hexadecane in water (O/W = 1:1000). The standard deviations are calculated from three independent emulsion suspensions.

[DOSS] [ppm]	**ζ [mV] -CCCP**	**+CCCP**
1	-56 ± 4	-73 ± 2
2	-67 ± 3	-72 ± 1
3	-71 ± 4	-70 ± 10
4	-79 ± 2	-85 ± 3
5	-90 ± 7	-88 ± 6
6	-88 ± 15	-93 ± 3

Bacterial adhesion is often considered to be a two-step process. First, a bacterium must diffuse from bulk of liquid suspension to close to the droplet surface. Second, the bacterium must displace the water layer at the interface to access the surface and subsequently adhere on it.[209] The first of these processes is dominated by bacterial transport; the second is additionally affected by the thermodynamics of colloidal adhesion at a liquid-liquid interface.[57,109,160] From thermodynamics, the number of cells adsorbed on a liquid-liquid interface depends on the free energy of adhesion, which depends on the three-phase contact angle and the surface energy of each phase.[210] To determine how motility may affect these processes, we estimate the transport-controlled interfacial cell density for nonmotile and motile bacteria. We assume that bacteria can be modeled as spheres of diameter 1 μm. The diffusivity is then given by the Stokes-Einstein equation, $D_{nm} = \frac{k_B T}{6\pi\eta R_H}$, where, R_H is the hydrodynamic radius. For a prolate

ellipsoid, $R_H = \sqrt{a^2 - b^2} / \ln\left(\left[a + \sqrt{a^2 - b^2}\right]/b\right)$, where a and b are the major and minor axis lengths, respectively.[211] Taking the room temperature as T = 298 K, the viscosity of the medium as that of water, η = 0.89 cP, and the major and minor axes of a bacterium as a = 2 μm and b = 0.6 μm, respectively, we estimate R_H ~ 1 μm and D_{nm} ~ 0.25 $\mu m^2\ s^{-1}$. In our experiments, bacteria are much smaller than the oil droplets (20 – 35 μm). Finally, we assume that the adsorption of bacteria is nearly irreversible and that the bulk cell concentration does not deplete over time. With these assumptions and conditions, the density of cells on the droplet surface is given by $\rho_s(t) = 2C_0\sqrt{\frac{D_{nm}\, t}{\pi}}$.[102,212] This functional form, scaling as $t^{0.5}$, represents the short-time limit of Fick's second law of diffusion. We note that the long-time limit of Fick's second law recovers the exponential function used to fit our data in Figure 2.[213] Similar short-time and long-time functional dependences can be recovered more generally from a statistical rate theory treatment,[213,214] which also leads to a $t^{0.5}$ dependence on short time[214] and an exponential form of the general kinetic equation on long time scales.[213] We choose the characteristic time scale of adsorption to be 3τ, where τ is the time constant obtained from adsorption kinetics; at this time scale, the surface density is expected to reach 95% of its long-time limit. For an initial bulk cell concentration of 5.4×10^8 cells mL^{-1} the interfacial density of nonmotile cells is predicted to be 0.014 cells μm^{-2}. This value is in reasonable agreement with the experimentally-measured interfacial density, which for nonmotile *H. titanicae* cells is 0.024 ± 0.005$ cells μm^{-2}

Motility increases the effective diffusivity of bacteria.[215–217] We observe experimentally that peritrichously flagellated *H. titanicae* swim using a run-and-tumble mechanism. The diffusivity of a motile bacterium that undergoes runs and tumbles is

given by $D_m = \frac{v^2\tau_{run}}{3(1-\alpha)}$, where v is the mean swimming speed, τ_{run} is the mean duration of straight runs, and α is the mean value of the cosine of the angle between successive runs.[218] For successive runs that are uncorrelated in direction, α = 0 and $D_m = \frac{v^2\tau_{run}}{3}$. In our previous study,[203] the average swimming speed of *H. titanicae* was 10 μm s^{-1}, yielding D_m = 33 μm^2 s^{-1}. We again take the characteristic time scale to be 3τ= 9 min. Therefore, the density of motile cells $\rho_s(t) = 2C_0\sqrt{\frac{D_m\, t}{\pi}}$ is predicted to be 0.081 cells μm^{-2}. The gradual decrease in motility over 1 − 3 min after addition of NaCl may affect the interfacial cell density measurement on shorter time scales. Using $\rho_s(t) = 2C_0\sqrt{\frac{D\, t}{\pi}}$,[102,212] we estimate that the interfacial density is at most 10% and 26% greater than at t = 6 min and t = 8 min, respectively, compared to that at t =5 min. This value is close to the experimentally obtained value of 0.095 ± 0.010 cells μm^{-2}. The reasonable agreement between the predicted and measured densities suggests that motility can increase adhesion by increasing the flux towards the interface. We note, however, that our adhesion curves approximately attain a plateau and do not follow $t^{0.5}$ scaling[102] on long times. This finding suggests that the accessible surface for adhesion becomes saturated after the initial increase; in this context, motility allows the effective packing density to be increased.[199] Droplets incubated with *H. titanicae* bacteria at room temperature for 48 hours did not change in size.

4.3.3 Effect of doss concentration on adhesion of bacteria to hexadecane droplets

We applied our imaging method to investigate the effect of surfactant concentration on adhesion of motile and nonmotile *H. titanicae* to hexadecane droplets (Figure 4.6). We chose as the surfactant DOSS, a major component of the Corexit

dispersant used in oil spill response.[45] Confocal micrographs revealed that the number of cells adhered to the oil-water interface decreases as the surfactant concentration is increased (Figure 4.6) Earlier studies have reported conflicting trends for bacterial adhesion at oil-water interfaces in the presence of surfactants.[219–221] A microbial adhesion to hydrocarbon (MATH) assay showed that *Sphingomonas spp.* GY2B adhesion to oil phase decreases with increases in rhamnolipid concentration.[221] In contrast, *Klebsiella oxytoca* PYR-1 cell adhesion to oil phase increases concomitant with Tween 20 and Tween 40 concentration up to the critical micelle concentration (CMC).[220]

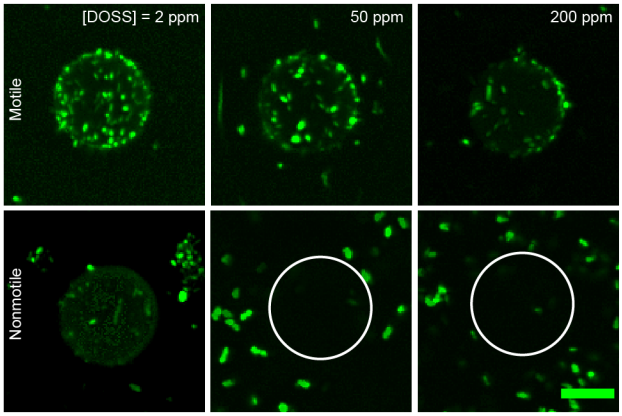

Figure 4.6. 2D projections of 3D confocal images of cells adhered on 20 μm hexadecane droplets for motile bacteria (top panel), and nonmotile bacteria (bottom panel) for [DOSS] = 2 (first column), 50 (second column), and 200 ppm (third column). Scale bar is 10 μm. White circle represents the location of droplet for clarity.

To understand the effects of surfactant concentration on interfacial adhesion, we first measured the interfacial tension of hexadecane in ASW with and without CCCP in the absence of bacteria. The interfacial tension σ is approximately constant at low DOSS concentrations and decreases to near zero at high concentrations of DOSS (Figure 4.7(a)). We determine the critical micelle concentration (CMC) of each DOSS/ASW system (with and without CCCP) from the intercept of linear fits of σ as a function of [DOSS] at low and high concentrations (Figure 4.7(a)). Addition of CCCP does not markedly alter

σ, and the critical micelle concentration (CMC) is 101 ppm in absence of CCCP and 105 ppm in presence of CCCP. The surface concentrations of DOSS in absence and in presence of CCCP are 3.2×10^{-6} and 2.2×10^{-6} mol m^{-2}, respectively. These are close to the values reported in the literature for the surface concentration of DOSS, which range from 1.6×10^{-6} to 2.2×10^{-6} mol m^{-2} (depending on the concentration of ammonium chloride) for hexadecane in artificial sea water.[222]

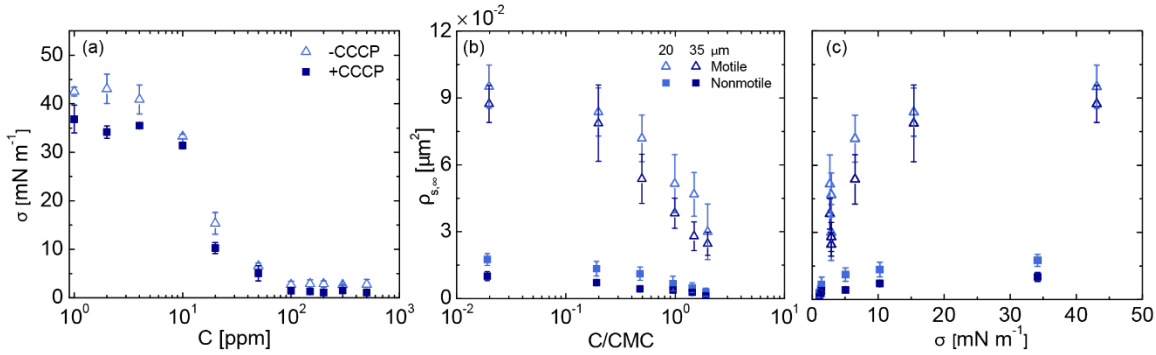

Figure 4.7. (a) Interfacial tension of hexadecane/ASW in absence and in presence of 2.5 μM CCCP as a function of DOSS concentration measured using pendant drop method. (b) and (c) Long-time interfacial density $\rho_{s,\infty}$ of cells adhered on hexadecane droplets as a function of (a) normalized surfactant concentration C/cmc, and (b) hexadecane/water interfacial tension. Error bars represent the standard deviation calculated from at least 40 observations (at least 10 droplets from minimum four independent bacterial cultures).

The density of cells at the oil-water interface decreases as the surfactant concentration is increased (Figure 4.7(b)). The interfacial density of nonmotile cells is nearly zero above the CMC. By contrast, $\rho_{s,\infty}$ of motile cells above the CMC is nonzero. Interestingly, $\rho_{s,\infty}$ for C/CMC > 1 is greater than that of nonmotile cells even at the lowest DOSS concentration (2 ppm). We were able to obtain sufficient statistics for droplets of two diameters: 20 μm and 35 μm, both of which fall on the low end of the droplet sizes measured during the Deepwater Horizon oil spill.[82] For motile cells, $\rho_{s,\infty}$ for the two droplet diameters is not distinguishable within experimental errors (Figure

4.7(b)). For nonmotile cells, $\rho_{s,\infty}$ is slightly greater for 20 μm droplets than for 35 μm droplets. This result is consistent with our previous work on adhesion of nonmotile *M. hydrocarbonoclasticus* to dodecane, in which the highest long-time cell density was obtained on the smallest droplets.[160] The decrease in surface concentration with increasing DOSS concentration is slightly more pronounced for nonmotile bacteria. The percentage decreases in $\rho_{s,\infty}$ from low (2 ppm) to high DOSS concentration (200 ppm) are 84%, and 68% for nonmotile bacteria and motile bacteria, respectively, on 20 μm, and 88% and 72% for nonmotile and motile bacteria, respectively, on 35 μm droplets.

The initial adhesion of bacteria is primarily controlled by the interfacial tension and surface energy.[57,110,223,224] Thus, we examined the cell density as a function of the hexadecane-ASW interfacial tension measured in the absence of bacteria σ (Figure 4.7(c)). The interfacial densities of both motile and nonmotile cells increase with σ. This result is consistent with our previous study of the effects of surfactant concentration on adhesion of nonmotile *M. hydrocarbonoclasticus* on dodecane droplets.[160] Cell adhesion decreases with increase in surfactant concentration due to an increase in free energy of adhesion.[110,210] The free energy of adhesion increases because σ decreases as the surfactant concentration is increased.[57,109] When the interfacial tension is close to zero, $\rho_{s,\infty}$ is nearly zero for nonmotile bacteria but nonzero for motile bacteria. This intriguing result suggests that motility may help bacteria overcome the energy barrier to access and remove the water layer at oil/water interface and attach there. These results are consistent with our earlier work on adhesion of nonmotile bacteria to oil droplets, in which we posited that the interfacial cell density was primarily controlled by interfacial tension

with additional contributions from electrostatic interactions between surfactant-decorated oil droplets and bacteria.[160]

4.4 Conclusions

We investigated the effect of motility on adhesion of bacteria to DOSS-stabilized hexadecane droplets suspended in artificial seawater. The time evolution of the interfacial cell density follows first-order Langmuir kinetics for both motile and nonmotile bacteria. The time constant of adhesion of motile bacteria is smaller than that of nonmotile bacteria, indicating that motility speeds adhesion kinetics. On long time scales the interfacial density $\rho_{s,\infty}$ of both motile and nonmotile bacteria approaches a constant values, and is greater for motile bacteria. This result suggests that motility may enable bacteria to pack more efficiently on the droplet interface. Finally, increasing the concentration of surfactant leads to a decrease in the interfacial tension and a decrease in the $\rho_{s,\infty}$ for both motile and nonmotile cells. Although $\rho_{s,\infty}$ approaches zero for nonmotile cells at high surfactant concentration, it remains nonzero for motile cells for all concentrations examined. Thus, motility may aid bacteria to colonize interfaces with very low interfacial tension.

Our results reveal how bacteria motility may enhance adhesion to oil droplets: motile bacteria may (a) adhere at a faster rate and (b) arrange more densely on a surface, as compared to nonmotile bacteria. Because these processes may enhance colonization of dispersed oil, our results suggest that motility may benefit biodegradation during marine oil spills. More broadly, this study contributes to a body of literature[196,199,201] that suggests that bacteria motility may provide an advantage in initial attachment of bacteria to various surfaces.

Chapter 5: Surfactant-driven aggregation of bacteria in solution

5.1 Introduction

Aggregation of bacteria can play an important role in biofilm formation and biodegradation.[225–231] There are two most important phases of surface colonization; first, initial cell attachment, and second, multiplication and cell cluster formation.[232] Aggregation behavior is also seen in pathogenesis[233] caused by foodborne pathogens such as *E. coli*.[234] Aggregates of bacteria efficiently remove pollutants in wastewater treatment.[235] In other settings, bacterial aggregation may act as a protective mechanism against environmental stressors.[236,237] Thus, understanding the mechanisms that drive bacterial aggregation in complex fluid solutions has significant practical implications.

Many bacteria are known to form aggregates in the presence of polymers. Addition of synthetic polymers can drive aggregation via depletion[238–244] or by bridging[228,230,245–252] interactions. Addditionally, bacteria can themselves produce polymers such as extracellular DNA (eDNA) that promote aggregation.[253] Extracellular DNA generates attractive Lifshiftz-van der Waals and acid-base interactions between bacteria.[249,250] Polymers such as mucin, however, can inhibit aggregation of motile bacteria.[254] Surface structures such as pili,[255] flagella,[256,257] or curli[258–260] can also cause aggregation in bacteria.

Calcium ions are very common in water bodies and it is an essential component for maintenance of cell structure, motility, and cell differentiation. Because the polymers and surface structures that drive bacterial aggregation are often charged, ions in solution can also affect aggregation processes. For example, divalent Ca^{2+} can form bridges negatively charge eDNA on the cell surface to cause cell-cell aggregation via bridging

interaction.[230] Cations can shield the charges on cells, reducing electrostatic repulsion; typically, significantly higher concentrations of monovalent cations than divalent cations are required to destabilize micron-size bacteria; likewise, the separation distance between cells decreased as cation valency increased. Finally, surfactants have also been shown to affect bacterial aggregation. PAO1 formed aggregations upon addition of sodium dodecylsulfate (SDS), which disintegrated when DNase1 was added.[261] Nonetheless, how the presence of multiple additives affects bacterial aggregation remains incompletely understood.

Here, we investigated the effect of dioctyl sodium sulfosuccinate (DOSS), a surfactant used in oil spill response, and calcium chloride on aggregation of *Marinobacter hydrocarbonoclasticus* SP17 and *Halomonas titanicae* Bead 10BA. We used optical density measurements to measure the extent of aggregation by comparing the initial and final optical densities. We acquired images using fluorescence and confocal microscopy and quantified the size and number of aggregates in each image. Both DOSS and calcium chloride enhanced aggregation of bacteria. Percentage decrease in optical density, a measure of aggregation, increases with increase in DOSS concentration. The size and number of aggregates of *M. hydrocarbonoclasticus* increases with increase in DOSS concentration. An aggregation assay run with addition of DNase1 reveals that bacterial aggregation is not due to eDNA. A control experiment run on saline solution confirms that aggregation is not due to micelle formation. Motile *H. titanicae* showed slightly higher aggregation compared to sheared bacteria. Together, these results contribute to understanding aggregate formation under conditions that may be important for biodegradation of pollutants and pathogenesis.

5.2 Materials and Methods

5.2.1 Chemicals

Zobell marine broth 2216 (HiMedia lab), sodium pyruvate (Amresco), nutrient agar (Difco), dioctyl sodium sulfosuccinate (DOSS, ≥ 97%, Sigma-Aldrich), SYTO9 (ThermoFisher), sodium chloride (≥ 99%, BDH), magnesium chloride hexahydrate (≥ 99%, Alfa Aesar), mag- nesium sulfate heptahydrate (≥ 99.5%, Sigma-Aldrich), calcium chloride (Sigma-Aldrich), potassium chloride (≥ 99%, BDH), potassium nitrate (≥ 99%, EMD), dipotassium phosphate (≥ 98%, Sigma-Aldrich), tris(hydroxymethyl) amino methane (≥ 99.8%, Sigma-Aldrich), ammonium chloride (≥ 99.99%, Sigma-Aldrich), iron sulphate (≥ 99%, Sigma-Aldrich), DNase1 from bovine pancreas (Sigma-Aldrich), and sodium phosphate (≥ 99%, Sigma-Aldrich) were used as received.

5.2.2 Bacteria strains and growth conditions

M. hydrocarbonoclasticus SP17 and *H. titanicae* bead 10BA plates were prepared by streaking bacteria from a frozen stock onto marine agar plates.[263] The plates were incubated at 30 °C for 40 hours. Cultures were prepared by inoculating 20 mL of marine broth (37.4 g marine broth and 10 g sodium pyruvate in 1 L of MilliQ water) from a single colony of bacteria from the plate and incubated for 20 h in an orbital incubator shaker (New Brunswick Scientific) at 200 rpm and 30 °C.

5.2.3 Cell aggregation assay

A cell culture (20 mL) grown to late exponential phase was centrifuged at 4000 \textit{g} for 10 minutes in a Sorvall ST 16 Centrifuge (ThermoFisher Scientific). The supernatant was discarded and the cell pellet was resuspended in 5 mL of synthetic

seawater (SSW). SSW was prepared by dissolving 12.1 g tris(hydroxymethyl) amino methane, 0.75 g KCl, 1.5 g calcium chloride, 3.47 g ammonium chloride, 6.16 g magnesium sulfate heptahydrate, 5.08 g magnesium chloride hexahydrate, and 35 g sodium chloride in 1 L of MilliQ water. The pH of the solution was adjusted to 7.5 with 5 M HCl. We subsequently added 2 and 4 mL of aqueous solutions of iron sulfate (0.1% w/v) and sodium phosphate (10%, w/v), respectively. We prepared 3 mL of cell suspensions at an optical density (λ = 600 nm) of 0.6 with DOSS concentrations of 0, 10, 30, 60, 100, 200, 300, 400, 500, and 600 ppm in 15 mL centrifuge tubes. The initial (t =0, OD_i) and final optical densities (t = 2 h, OD_f) of upper layers were measured using a cell density meter (Laxco DSM-Micro). For time dependent aggregation measurement, the optical density of each sample was measured over time in triplicates. The decrease in optical density is usually attributed to aggregation between bacteria and is referred as percentage aggregation,[238,239,264] defined as % Aggregation $= 100 \times \frac{(OD_i - OD_f)}{OD_i}$.

To measure the effect of DNase1, cells suspensions of optical density 0.6 were prepared at DOSS concentrations of 0, 200, and 600 ppm; and DNase1 was added in suspensions so that the final DNase1 concentration in suspensions were 2 mg mL^{-1}. The optical density of upper layer of each suspension was measured at t = 0 and t = 2 h.

To compare the effect of motility, 20 mL of *H. titanicae* suspension was blended to shear off flagella using a blender (Oster 6642) in liquify mode at high for 30 sec. Subsequently, the suspension was centrifuge at 4000g for 10 minutes in a Sorvall ST 16 Centrifuge (ThermoFisher Scientific). The supernatant was discarded and the cell pellet was resuspended in 5 mL of synthetic seawater (SSW). Similarly, unblended suspension

was centrifuged and suspended in SSW to remove the growth medium. The OD of each suspension was adjusted to 0.6 using SSW. Samples of varied DOSS concentration were prepared as discussed before and optical densities were compared.

5.2.4 Imaging cells using microscopy

We image our samples to confirm the aggregation in cell suspensions and to directly quantify the aggregates. 500 µL sample of each sample were stained using 0.5 µL SYTO9 and incubated at room temperature for 2 minutes. Imaging samples were prepared using imaging spacer (Sigma-Aldrich) on glass cover slip and 20 µL of cell suspension was dispensed on to the chamber and covered with another cover slip. Bacteria were imaged using fluorescence microscope (Leica Microsystems DM4000) with 40X oil-immersion lens (HCX PL APO, NA 1.25 – 0.75). At least six images were acquired for each sample and the experiment was triplicated. Images are analyzed using imageJ open source software. A blob of size greater than 100 pixels area were considered as aggregates. The number and the size distribution of aggregates were extracted from each image.

5.2.5 Surface tension and critical micelle concentration

The surface tension of DOSS in SSW and 58 g L^{-1} NaCl were determined using pendant drop method. The surface tension of SSW and NaCl solution were measured as a function of DOSS concentration using a Dataphysics OCA 15EC goniometer. Subsequently, we determined the critical micelle concentrations (CMC) of DOSS in SSW and in NaCl as the concentrations at which the slopes at low and high DOSS concentrations intercepted (Fig. 5.1).

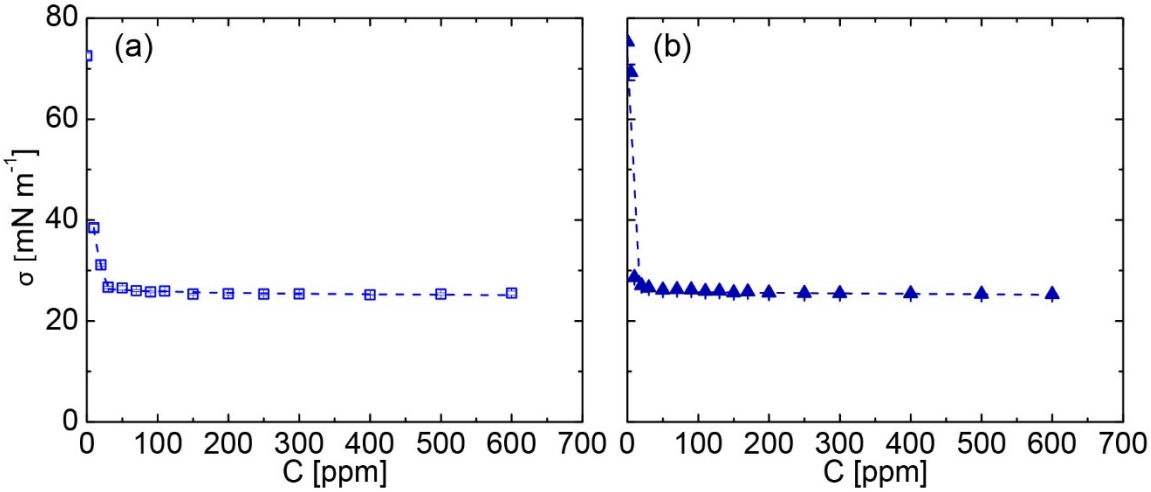

Figure 5.1. Surface tension of (a) synthetic seawater (SSW) and (b) NaCl (58 g L^{-1}) as a function of DOSS concentration. The CMC of DOSS is 30 ppm, and 18 ppm in SSW and NaCl, respectively, obtained from the intersection of slopes at high and low concentration of DOSS.

5.3 Results and Discussion

5.3.1 Cell aggregation as a function of time and DOSS concentration

We examined the change in stability of suspensions containing *M. hydrocarbonoclasticus*, calcium chloride, and the surfactant DOSS in synthetic sea water. Optical density measurements revealed that percentage aggregation of bacteria, defined as the percent decrease in optical density, increases linearly as a function of time (Fig. 5.2a), with a total increase of up to 27 ± 3% over 150 minutes for a suspension with cell concentration of 10^9 cells per mL. A similar decrease in optical density on short time scales has been previously observed for Yersinia adhesin YadA-expressing *E. coli* and was attributed to an increase in aggregation.[264] Measurements conducted at a fixed time of two hours after introduction of DOSS revealed that increasing the surfactant concentration leads to a more pronounced decrease in the optical density due to increase in aggregate size and sedimentation (Fig. 5.2b). Extracting additional information about

the aggregates from absorbance measurements, however, is tricky because the optical density is affected by both the size and number of aggregates.

In optical density measurements, the absorbance depends both on the number and size of scattering objects present in solution. According to the Beer-Lambert law, the absorbance is given by $A = \varepsilon c l$, where c is the concentration of particles, l is the optical path length, and ε is the molar absorbance coefficient.[265] The concentration c is directly proportional to the number of particles N in suspension, and the molar absorption coefficient depends on particle radius R. The molar extinction coefficient as a function of particle radius is given by $\varepsilon = \frac{A}{\sqrt{2\pi}\left(E_g + \frac{\pi h^2}{2\pi R^2}\right)} \frac{\mu R^2}{\pi h^2 \delta_R}$.[266] For smaller particles ε approaches to R^4, and for larger particles ε approaches to R^2. Therefore, $A \propto NR^2$ and because in a given system, NR^3 is constant therefore the absorbance decreases as aggregate size increases.

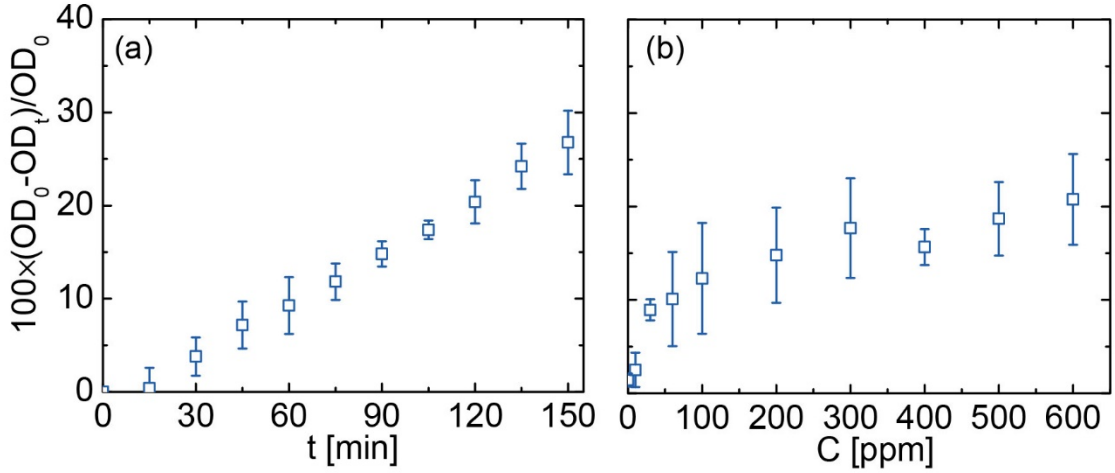

Figure 5.2. (a) Aggregation of *M. hydrocarbonoclasticus* measured as a percentage decrease in optical density as a function of time. DOSS concentration was 400 ppm, and the bacteria concentration was 10^9 cells per mL. (b) Aggregation of *M. hydrocarbonoclasticus* as a function of DOSS concentration. Error bars represent the standard deviation obtained from five independent cultures.

5.3.2 State diagram and characterization of aggregates

Next, we examined the effect of optical density and DOSS concentration of aggregation (Fig. 5.3). Confocal micrographs reveal that bacteria aggregates at higher DOSS concentration. To characterize the aggregation, we measured the number of aggregates as shown in the state diagram (Fig. 5.4). At a fixed OD, the number density ρ of aggregates generally increases as the DOSS concentration is increased. Further, aggregates form at lower concentrations of DOSS as the optical density is increased, due to the decrease in the average separation between cells. These results are qualitatively similar to those reported for polymer-driven aggregation of bacteria, for which aggregation increases with both bacteria and polymer concentration.[240] In depletion interacting system, as bacteria concentration was increased aggregation was achieved at relatively low polymer concentration whereas in bridging interaction systems, as bacteria concentration was increased aggregation was achieved at relatively higher polymer concentration.

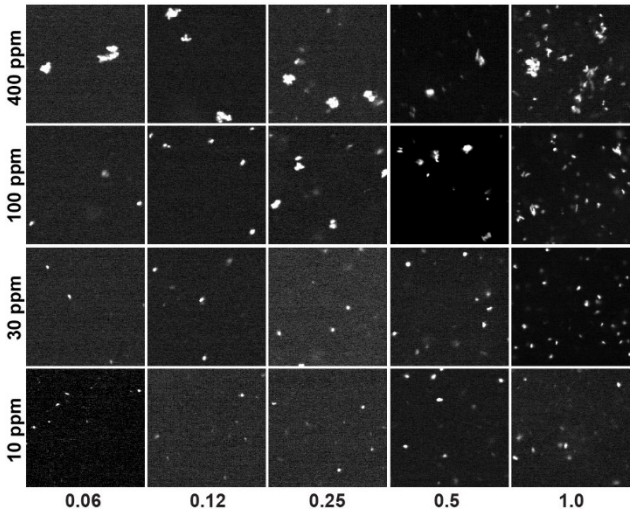

Figure 5.3. Confocal micrograph of *M. hydrocarbonocalsticu*s aggregation as a function of DOSS concentration (Y axis) and bacteria optical density (X axis). An OD of 1.0 is equivalent to 1.7×10^9 cells per mL. The scale is 20 μm.

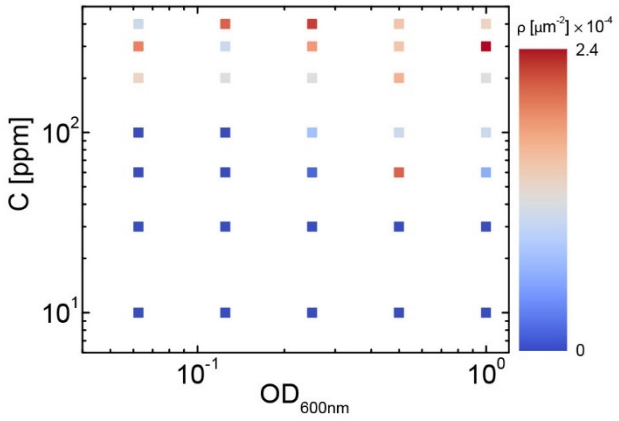

Figure 5.4. State diagram for *M. hydrocarbonoclasticus* aggregation as a function of DOSS concentration (C) and optical density (OD_{600}). The colorbar represents the variation in the aggregate number density.

The aggregate size also depends on OD and DOSS concentration (Fig. 5.5). Generally, increasing the DOSS concentration leads to a broader distribution of aggregation sizes. The average size of the aggregates also increases slightly as DOSS concentration is increased. Surprisingly, at the highest optical density and 400 ppm DOSS concentration the maximum size of aggregates is smaller compared to lower optical density sample at 400 ppm DOSS concentration. An increase in cell concentration reduces effective cell-cell distance and a higher DOSS concentration is likely causing an increased production of EPS which leads to higher aggregation. A large variation in size of aggregates has also been observed in systems of bacteria-polymer and bacteria-leukocytes.[239,267]

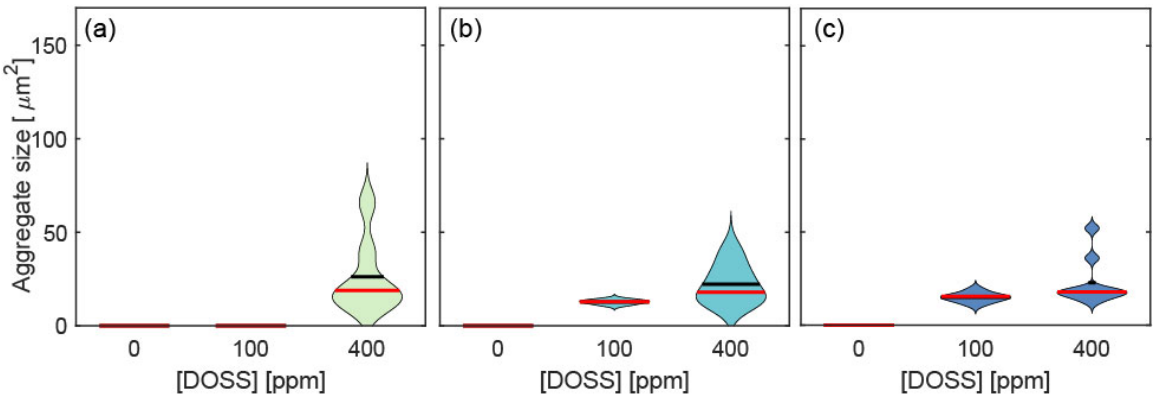

Figure 5.5. Aggregate size distribution as a function of DOSS concentration at optical density of (a) 0.06, (b) 0.25, and (c) 1.0. Black lines represent average size and red lines represent medians of size distributions.

5.3.3 Assays to test aggregation mechanisms

To understand the mechanisms driving aggregation of bacteria in the presence of DOSS, we first examined the effect of calcium chloride on aggregation of bacteria. Addition of divalent cation such as Ca^{2+} has shown increased aggregation of bacteria. No aggregation was observed when calcium chloride is not present in the suspension (Fig. 5.6a). Likewise, when the DOSS concentration is 0 or 30 ppm, bacteria do not aggregate even at the highest calcium chloride concentration of 3 g L^{-1}. Therefore, both DOSS and calcium chloride are essential for formation of bacteria aggregation. The number density of aggregates is increased as DOSS concentration is increased (Fig. 5.6a) or as calcium chloride concentration is increased (for DOSS concentrations of 100 and 400 ppm). Both the average and maximum sizes of aggregates increase as calcium chloride concentration is increased, for DOSS concentrations exceeding 100 ppm (Fig. 5.6a).

Because aggregation requires a sufficiently large concentration of DOSS, we wanted to determine whether micelles were involved in the aggregation process. Micelles can promote depletion-driven aggregation of colloidal droplets,[268] and the CMC of DOSS is below 30 ppm in both SSW and NaCl (Fig. 5.1). We therefore examined the

aggregation behavior of bacteria in 58 g L^{-1} NaCl as a function of DOSS (Fig. 5.1). The ionic strength of solution is 991 mM which is close to the ionic strength of SSW (990 mM). Bacteria do not aggregate in this solution even at the highest DOSS concentration of 600 ppm, well above the CMC concentration of DOSS. Thus, our results suggest that aggregation in this system is not solely due to depletion from DOSS micelles.

That aggregation requires calcium chloride is consistent with previous studies from other research groups that have shown the importance of divalent cations in aggregation and adhesion of bacteria. bacteria.[247,269–272] Ca^{2+} is known as important molecule in enhancing production of extracellular polymeric substances (EPS),[269,273] composed of proteins, enzymes, nucleic acids, lipids, polysaccharides, and other compounds such as humic acids.[274,275] Furthermore, divalent cations such as Ca^{2+} and Mg^{2+} can form crosslinks between extracellular material and bacteria.[228]

One component of EPS is extracellular DNA (eDNA). In an earlier study, Ca^{2+} acted as a crosslink between eDNA on bacteria surface..[230] Thus, to determine whether aggregation is due to eDNA, we examined the aggregation of *M. hydrocarbonoclasticus* in the presence of an enzyme, DNase1, that can break phosphodiester bonds by hydrolysis.[230] There was no significant change in aggregation of bacteria in presence and absence of DNase1 up to 600 ppm DOSS concentration (Fig 5.8). This result suggests that aggregation is not due to eDNA specifically. Instead, we suggest that it is likely due to bridging of other biopolymers in EPS by Ca^{2+} .Other studies have shown, for example, that Ca^{2+} can form bridges between bacterial alginate component of EPS, for example.[276] In another study of biofilm formation by *M. hydrocarbonoclasticus* at hexadecane-water interface has shown that protein is major component of biofilm matrix and addition of

proteinase K (PK) partially inhibited aggregation and biofilm formation on soild and liquid hydrocarbons.[277]

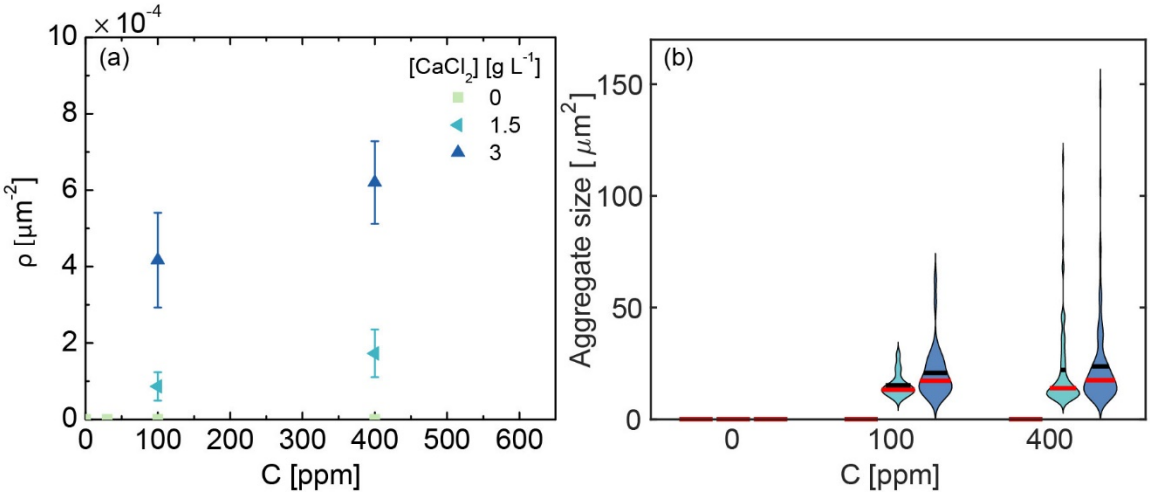

Figure 5.6. (a) Aggregate number density (ρ) and (b) aggregate size distribution as a function of DOSS concentration at 0, 1.5, and 3 g L^{-1} calcium chloride. bacteria concentration was 10^9 cells per mL.

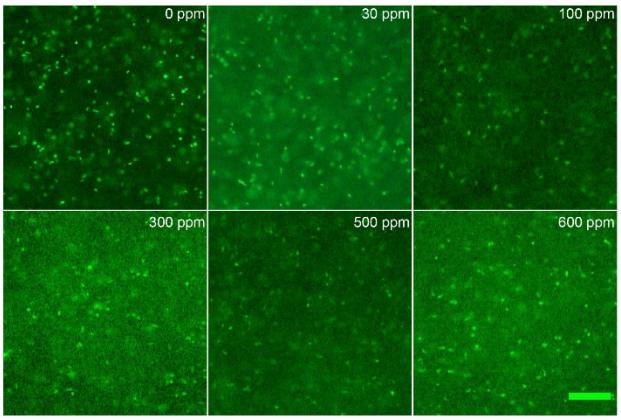

Figure 5.7. Fluorescence images of *M. hydrocarbonoclasticus* in NaCl (58 g L^{-1}) at different DOSS concentration. Bacteria concentration was 10^9 cells per mL. Scale bar is 20 μm.

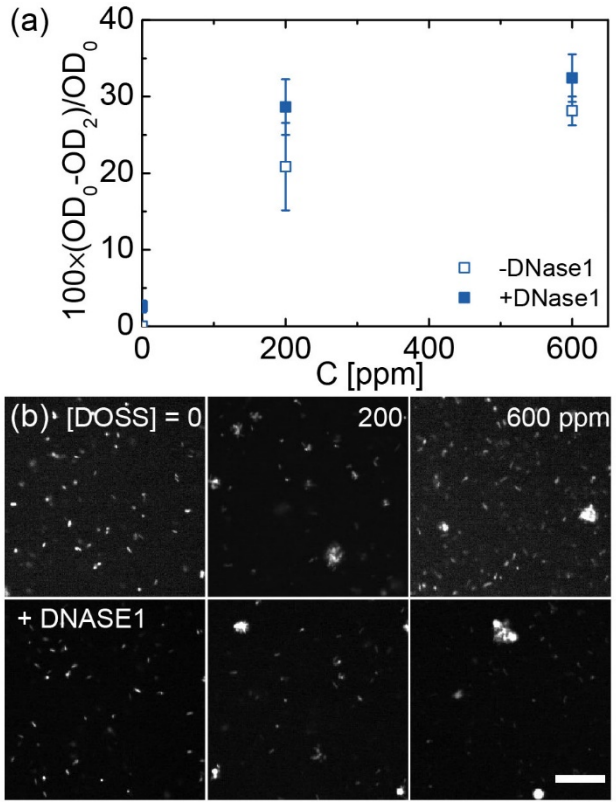

Figure 5.8. (a) Aggregation measured as percentage decrease in optical density as a function of DOSS concentration in absence and in presence of DNase11. Bacteria concentration was 10^9 cells per mL. (b) Confocal micrographs of aggregates in absence and presence of DNase1. Scale bar is 20 μm.

5.3.4 Effect of bacteria motility on aggregation

Finally, to examine the effect of motility on aggregation, we examined the aggregation behavior of *Halomonas titanicae*. This bacterium can be rendered nonmotile through mechanical shearing, which removes its flagella. Optical density measurements reveal that motile bacteria aggregate more readily than nonmotile unsheared bacteria (Fig. 5.9a). At a DOSS concentration of 600 ppm, where aggregation is most pronounced, motile and nonmotile bacteria respectively show a 40% and 30% decrease in OD. The number density of motile bacteria is slightly greater than that of nonmotile bacteria at intermediate DOSS concentration, whereas at high DOSS concentration the number density is within the error (Fig. 5.9b). The average size of aggregates is identical within

error for motile and nonmotile bacteria, but the distribution of aggregate sizes is much broader for motile bacteria. (Fig. 5.9c). These results suggest that motility may enhance bacteria aggregation. This result is consistent with another study that has shown that motility and chemotaxis enhance aggregation of *E. coli*.[278]

5.3 Conclusions

We investigated aggregation of *M. hydrocarbonoclasticus* and *H. titanicae* under conditions that mimic oil-spill remediation. Aggregation, measured as percentage decrease in optical density, increases linearly over time during first 150 min. Aggregation of *M. hydrocarbonoclasticus* increases with increase in DOSS concentration. Bacteria at lower OD aggregate at higher DOSS concentration compared to higher OD, however, a broader distribution of aggregate size was observed at lower OD. Microscopic assays reveal that the apparent increase in aggregation from the bulk assay reflects changes in both the number density and size of aggregates. Calcium chloride is essential for aggregation, and increasing its concentration increases both the number density and size of aggregates. Likewise, a sufficiently high concentration of DOSS is essential for aggregation. Addition of DNase1 did not alter aggregation behavior, indicating that aggregation is not solely dependent on eDNA. Finally, motile *H. titanicae* exhibit greater aggregation compared to nonmotile bacteria; the mean aggregate size of motile and nonmotile bacteria are identical, but the breadth of the size distribution is greater for motile bacteria.

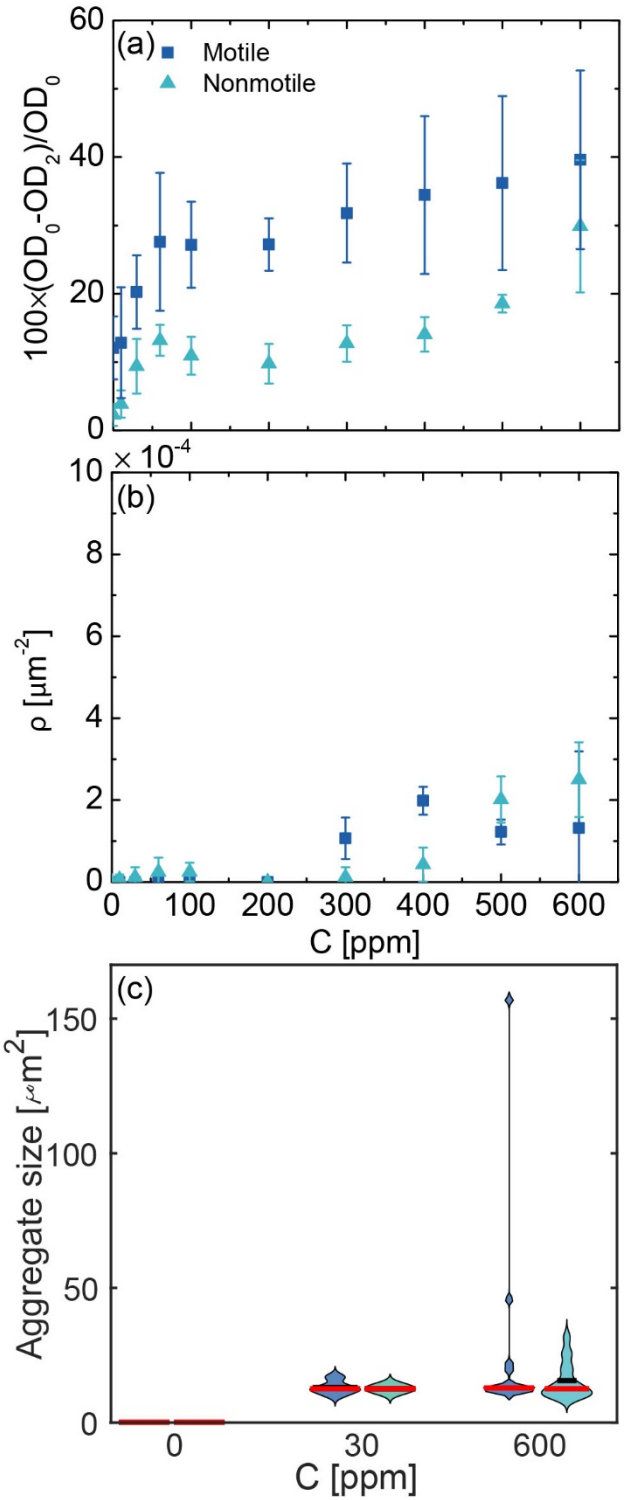

Figure 5.9. (a) Percentage decrease in optical density of motile and nonmotile *H. titanicae* as a function of DOSS concentration, (b) aggregate number density (ρ) as a function of DOSS concentration, and (c) aggregate size distribution (blue) as a function of DOSS concentration and calcium chloride concentration. Horizontal red lines represent medians and horizontal black lines represent means

of the distributions. Optical density of suspensions were 0.6 correspond to a concentration of 1.6×10^9 cells per mL. This experiment was replicated for at least three independent cultures.

Our results suggest that both DOSS and calcium chloride are essential for aggregation of bacteria. Neither DOSS micelles nor eDNA alone are responsible for aggregation in this system. Instead, aggregation is likely a result of a complex interaction between divalent cations, the DOSS surfactant, and a variety of EPS constituents secreted by bacteria. The aggregation formation is important in bioremediation processes and in wastewater treatment. Aggregation properties could be used as a sorting method for selection of adhering bacteria strains.[279,280]

Chapter 6: Summary and recommendations for future works

6.1 Summary

In this study, we developed a method to make oil in water emulsion using a glass-based microfluidics technique. We developed the design of experiments in imaging and various tracking methods to be able to quantify the cells on droplet surface. We investigated the effect of surfactant chemistry, surfactant concentration, bacteria motility, and droplets size on adhesion of bacteria on oil droplets. Broadly, we investigated the effect of surfactant on cell-cell interaction, and cell-substrate interactions.

In the first part of our research, we designed and fabricated glass-based coflow microfluidic device to produce dodecane in water emulsion stabilized with various surfactants (dioctyl sodium sulfosuccinate, dicyclohexyl sodium sulfosuccinate, dibutyl sodium sulfosuccinate, cetyltrimethylammonium bromide, Tween 20). We employed a confocal microscope to acquire 3D image of adhering cells on droplet surface. We used single-cell tracking algorithms to track location of each bacterium and its orientation. We investigated the effect of droplet size and surfactant type and concentration on bacterial adhesion at dodecane/water interfaces. Adhesion of nonmotile bacteria to oil droplet followed the first-order Langmuir adsorption kinetics. Bacteria interfacial density was highest for the smallest droplet and it reaches equilibrium faster than larger droplets. We found that bacteria preferentially align parallel to the local oil/water interface, in agreement with thermodynamics principle to maximize the displaced interfacial area and minimize energy, but the distribution of orientation angle suggests that bacteria can become kinetically trapped in nonequilibrium orientations. Equilibrium interfacial density of bacteria decreases with increasing the surfactant concentration. This result is

consistent with an increase in the free energy of adhesion because of the decrease in the oil/water interfacial tension as the surfactant concentration is increased. Adhesion results and zeta potential data for droplets suggest that electrostatic interactions also play a role in bacterial adhesion on droplets.

In the second part of our work, we explored the droplet rotation driven by adhering motile bacteria on the droplets. We found that droplets start to rotate in clockwise direction when certain number of motile bacteria adhered to the droplets. The angular speed of droplets decreases with increase in droplet diameter and with decrease in optical density of the cell suspension. The speed of rotation can be altered by changing the bacteria species which may alter the angular speed of droplets by means of having different adhesion density on the droplet or by weaker interfacial adhesion. The angular speed of oil droplets decreases with increase in surfactant concentration due to reduced cell density on surface and due to weaker interfacial adhesion. This droplet rotation may provide a route to enhance mixing in a bacteria suspension.

In the third part of our work, we investigated the effect of motility on adhesion of bacteria to DOSS-stabilized hexadecane droplets suspended in artificial seawater. The adhesion of nonmotile and motile bacteria follow first-order Langmuir kinetics with motile bacteria having lower time constant, indicating that bacterial motility speeds adhesion kinetics. Equilibrium interfacial density of motile bacteria is higher than nonmotile bacteria over a wide range of surfactant concentration which suggests that motility may enable bacteria to pack more efficiently on the droplet interface. The interfacial density of bacteria decreases with increase in surfactant concentration for both motile and nonmotile bacteria. In addition, the interfacial density of nonmotile bacteria

approaches zero at high surfactant concentration whereas, it remains nonzero for motile cells for all concentrations examined. Thus, motility may aid bacteria to colonize interfaces with very low interfacial tension. Our results suggest that improved adhesion due to motility may benefit biodegradation during marine oil spills.

In the final part of our research, we investigated the effect of dioctyl sodium sulfosuccinate and calcium chloride concentrations on aggregation of nonmotile *M. hydrocarbonoclasticus* SP17 and *Halomonas titanicae* Bead 10BA. We found that bacteria aggregation, measured as a percentage decrease in optical density, increased linearly over time for first 150 min. The aggregation of bacteria increases with increase in DOSS concentration. Analysis of confocal micrographs reveal that number of aggregate and size of aggregates increase with increase in DOSS concentration. We found that presence of Ca^{2+} is important in aggregation and aggregation is enhanced with increase in Ca^{2+} concentration. Motile *Halomonas titanicae* shows higher aggregation compared to nonmotile bacteria.

Our previous works drive the motivation to future work to study the velocity field created by bacteria-driven droplets, and effect of chemotaxis on bacterial adhesion on oil droplets.

6.2 Future Work

Based on the observations in our previous work of drop rotation and work on effect of bacteria motility on adhesion to droplets, the following recommendations are proposed for future work:

6.2.1 Flow field generated by the bacteria-driven oil droplets

In our previous work, we explored the bacteria-driven rotation of oil droplets in aqueous suspension. The oil droplets rotated in clockwise direction when viewed from the liquid side, due to symmetry-breaking hydrodynamic interaction of adhered bacteria with the interface. From the principle of fluid mechanics, the rotation of droplet generates a flow field around inside and outside of the droplets. The flow field would eventually vanish due to viscous dissipation and due to wall shear stress at the wall of the capillary channel. Therefore, the velocity vector will be the highest at the droplet interface and decrease monotonically with the distance from the droplet surface. The velocity would be highest on rotational plane of highest cross-sectional area of the droplet and would decrease as we move towards the rotational axis and away from the droplet.

Experimental evidence has suggested that the rotational field are indeed generated due to these bacteria-driven oil droplets. The existence of velocity field outside of the droplet was confirmed by circular trajectory of a small droplets and a particle (acting as tracer) around the droplet. In the Fig. 6.1, a small droplet outside the rotating droplet follows circular trajectory around a 40 μm dodecane droplets. It covers nearly ¾ of a complete revolution around the rotating droplet. However, the circular trajectory is noisy and changes its distance from the droplet surface due to swimming bacteria in the bulk solution, and likely also due to the hydrodynamic interaction with the rotating droplets. This complicates the estimation of velocity vector as a function of distance from the surface of the droplet (r) and as a function of distance along the rotational axis (z).

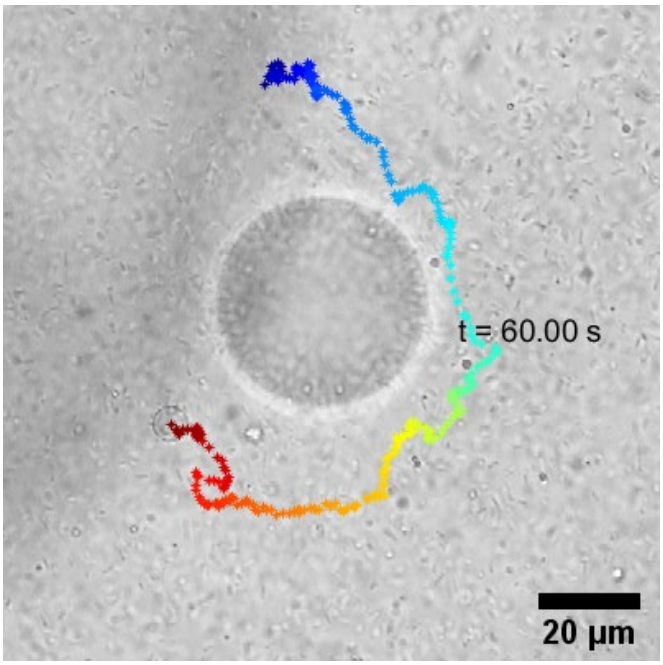

Figure 6.1. Clockwise circular trajectory of a smaller droplet (tracer) away from a rotating 40 µm dodecane droplet. The tracer travels roughly ¾ of the one complete revolution.

In future experiments, we recommend using lower concentration of cells in the suspension. This way we can minimize the noisy motion of tracers. If this method does not work then another possible solution to this problem is that to allow the cells to adhere to the droplets and remove the remaining cells in the bulk solution by diluting the suspension with a medium without cells or by size-dependent sorting technique using microfluidics. To trace the velocity field inside of the droplet, we can introduce hydrophobic particles to the emulsion so that few particles reside inside of the droplets. The rest of the experimental method, imaging method, and tracking method remain the same as mentioned in the drop rotation experiments. With these experiments, we aim to predict the velocity vector function $\phi(r,z)$ for droplets of different sizes and rotation speed.

Bacteria-driven droplet rotation may provide a route to enhanced mixing and thereby promote mass transport in multiphase microbial reactors or drive cells to

agglomerate at the droplet surface through hydrodynamic interactions. Thus, the ability to actively drive droplet rotation may be useful in a variety of practical settings involving microbes.

6.2.2 Transformation of *M. hydrocarbonoclasticus* to study the effect of chemotaxis in adhesion of bacteria on oil droplets

In our previous work, we examined the effect of bacteria motility on bacterial adhesion on oil droplets.[281] For this, motile *H. titanicae* Bead 10BA and non-motile *M. hydrocarbonoclasticus* SP17 were used to study the effect of motility on bacterial adhesion on hexadecane droplets. *H. titanicae* is chemotactic towards hexadecane, studied by Ford group at the University of Virginia. We made this bacteria species nonmotile by mechanically shearing off the flagella, and by blocking the proton transfer responsible for driving the flagella motor using CCCP. We want to investigate the effect of bacteria chemotaxis on adhesion of bacteria to oil droplets. For this, we attempted to transform the nonmotile *M. hydrocarbnoclasticus* bacteria into inducible motile bacteria. With inducible motile bacteria we can further compare the effect of motility on bacterial adhesion when bacteria were genetically modified. In addition, we want to delete the genes responsible for chemotactic towards certain hydrocarbons. This way, we will have three bacteria strains and its mutants; nonmotile, motile with defects in chemotaxis, and motile with chemotaxis.

In our previous trials, we attempted to introduce plasmid using commonly used method of electroporation and chemical method. Both methods failed to introduce the plasmid into the bacteria. Conjugation method was previously used for this strain by other research group.[282] Conjugation is a unidirectional transfer of gene from one

bacterium to another bacterium. For this, we are using *E. coli* S17-1 λpir (ATCC 47055) as a donor bacteria strain to transfer pBBR1MCS-2 plasmid into the SP17.

After successful transformation of nonmotile *Marinobacter hydrocarbonoclasticus* into motile *Marinobacter* mutants with and without chemotaxis, we aim to compare the effect of chemotaxis, and bacteria motility on bacteria adhesion on oil droplets. Because transformation of marine bacteria is known to be relatively more complex, this work would also contribute to the molecular biology methods. Because this bacteria strain is an alkane degrader, transforming this into a motile strain would further enhance adhesion to oil droplet and biofilm formation and this would likely enhance the biodegradation of oil.

References

(1) Koo, H.; Allan, R. N.; Howlin, R. P.; Stoodley, P.; Hall-Stoodley, L. Targeting Microbial Biofilms: Current and Prospective Therapeutic Strategies. *Nature Reviews Microbiology* **2017**, *15* (12), 740–755. https://doi.org/10.1038/nrmicro.2017.99.

(2) Brown, D. C.; Turner, R. J. Biofilms and Microbiologically Influenced Corrosion in the Petroleum Industry. In *Introduction to Biofilm Engineering*; ACS Symposium Series; American Chemical Society, 2019; Vol. 1323, pp 187–203. https://doi.org/10.1021/bk-2019-1323.ch009.

(3) Prieto, D. M.; Devesa-Rey, R.; Rubinos, D. A.; Díaz-Fierros, F.; Barral, M. T. Biofilm Formation on River Sediments Under Different Light Intensities and Nutrient Inputs: A Flume Mesocosm Study. *Environmental Engineering Science* **2016**, *33* (4), 250–260. https://doi.org/10.1089/ees.2015.0427.

(4) Carvalho, D.; R, C. C. C. Marine Biofilms: A Successful Microbial Strategy With Economic Implications. *Front. Mar. Sci.* **2018**, *5*. https://doi.org/10.3389/fmars.2018.00126.

(5) McBain, A. J.; Bartolo, R. G.; Catrenich, C. E.; Charbonneau, D.; Ledder, R. G.; Rickard, A. H.; Symmons, S. A.; Gilbert, P. Microbial Characterization of Biofilms in Domestic Drains and the Establishment of Stable Biofilm Microcosms. *Appl Environ Microbiol* **2003**, *69* (1), 177–185. https://doi.org/10.1128/AEM.69.1.177-185.2003.

(6) Bogino, P. C.; de las Mercedes Oliva, M.; Sorroche, F. G.; Giordano, W. The Role of Bacterial Biofilms and Surface Components in Plant-Bacterial Associations. *Int J Mol Sci* **2013**, *14* (8), 15838–15859. https://doi.org/10.3390/ijms140815838.

(7) Jiao, Y.; Tay, F. R.; Niu, L.; Chen, J. Advancing Antimicrobial Strategies for Managing Oral Biofilm Infections. *International Journal of Oral Science* **2019**, *11* (3), 1–11. https://doi.org/10.1038/s41368-019-0062-1.

(8) Arciola, C. R.; Campoccia, D.; Montanaro, L. Implant Infections: Adhesion, Biofilm Formation and Immune Evasion. *Nature Reviews Microbiology* **2018**, *16* (7), 397–409. https://doi.org/10.1038/s41579-018-0019-y.

(9) Prince, R. C.; Nash, G. W.; Hill, S. J. The Biodegradation of Crude Oil in the Deep Ocean. *Marine Pollution Bulletin* **2016**, *111* (1), 354–357. https://doi.org/10.1016/j.marpolbul.2016.06.087.

(10) Xu, X.; Liu, W.; Tian, S.; Wang, W.; Qi, Q.; Jiang, P.; Gao, X.; Li, F.; Li, H.; Yu, H. Petroleum Hydrocarbon-Degrading Bacteria for the Remediation of Oil Pollution Under Aerobic Conditions: A Perspective Analysis. *Front. Microbiol.* **2018**, *9*. https://doi.org/10.3389/fmicb.2018.02885.

(11) Prince, R. C. Oil Spill Dispersants: Boon or Bane? *Environ. Sci. Technol.* **2015**, *49* (11), 6376–6384. https://doi.org/10.1021/acs.est.5b00961.

(12) Mulkins-Phillips, G. J.; Stewart, J. E. Effect of Four Dispersants on Biodegradation and Growth of Bacteria on Crude Oil. *Appl Microbiol* **1974**, *28* (4), 547–552.

(13) Prince, R. C.; Coolbaugh, T. S.; Parkerton, T. F. Oil Dispersants Do Facilitate Biodegradation of Spilled Oil. *PNAS* **2016**, *113* (11), E1421–E1421. https://doi.org/10.1073/pnas.1525333113.

(14) Ferguson, R. M. W.; Gontikaki, E.; Anderson, J. A.; Witte, U. The Variable Influence of Dispersant on Degradation of Oil Hydrocarbons in Subarctic Deep-Sea Sediments at Low Temperatures (0–5 °C). *Scientific Reports* **2017**, *7* (1), 2253. https://doi.org/10.1038/s41598-017-02475-9.

(15) Sun, X.; Chu, L.; Mercando, E.; Romero, I.; Hollander, D.; Kostka, J. E. Dispersant Enhances Hydrocarbon Degradation and Alters the Structure of Metabolically Active Microbial Communities in Shallow Seawater From the Northeastern Gulf of Mexico. *Front. Microbiol.* **2019**, *10*. https://doi.org/10.3389/fmicb.2019.02387.

(16) Bayoudh, S.; Othmane, A.; Mora, L.; Ben Ouada, H. Assessing Bacterial Adhesion Using DLVO and XDLVO Theories and the Jet Impingement Technique. *Colloids and Surfaces B: Biointerfaces* **2009**, *73* (1), 1–9. https://doi.org/10.1016/j.colsurfb.2009.04.030.

(17) Bookstaver, M.; Bose, A.; Tripathi, A. Interaction of Alcanivorax Borkumensis with a Surfactant Decorated Oil–Water Interface. *Langmuir* **2015**, *31* (21), 5875–5881. https://doi.org/10.1021/acs.langmuir.5b00688.

(18) Godfrin, M. P.; Sihlabela, M.; Bose, A.; Tripathi, A. Behavior of Marine Bacteria in Clean Environment and Oil Spill Conditions. *Langmuir* **2018**, *34* (30), 9047–9053. https://doi.org/10.1021/acs.langmuir.8b01319.

(19) Omarova, M.; Swientoniewski, L. T.; Mkam Tsengam, I. K.; Blake, D. A.; John, V.; McCormick, A.; Bothun, G. D.; Raghavan, S. R.; Bose, A. Biofilm Formation by Hydrocarbon-Degrading Marine Bacteria and Its Effects on Oil Dispersion. *ACS Sustainable Chem. Eng.* **2019**, *7* (17), 14490–14499. https://doi.org/10.1021/acssuschemeng.9b01923.

(20) Panchal, A.; Swientoniewski, L. T.; Omarova, M.; Yu, T.; Zhang, D.; Blake, D. A.; John, V.; Lvov, Y. M. Bacterial Proliferation on Clay Nanotube Pickering Emulsions for Oil Spill Bioremediation. *Colloids and Surfaces B: Biointerfaces* **2018**, *164*, 27–33. https://doi.org/10.1016/j.colsurfb.2018.01.021.

(21) Oh, J. K.; Yegin, Y.; Yang, F.; Zhang, M.; Li, J.; Huang, S.; Verkhoturov, S. V.; Schweikert, E. A.; Perez-Lewis, K.; Scholar, E. A.; Taylor, T. M.; Castillo, A.; Cisneros-Zevallos, L.; Min, Y.; Akbulut, M. The Influence of Surface Chemistry on the Kinetics and Thermodynamics of Bacterial Adhesion. *Scientific Reports* **2018**, *8* (1), 17247. https://doi.org/10.1038/s41598-018-35343-1.

(22) Forson, A. M.; van der Mei, H. C.; Sjollema, J. Impact of Solid Surface Hydrophobicity and Micrococcal Nuclease Production on Staphylococcus Aureus Newman Biofilms. *Scientific Reports* **2020**, *10* (1), 12093. https://doi.org/10.1038/s41598-020-69084-x.

(23) Yuan, Y.; P. Hays, M.; R. Hardwidge, P.; Kim, J. Surface Characteristics Influencing Bacterial Adhesion to Polymeric Substrates. *RSC Advances* **2017**, *7* (23), 14254–14261. https://doi.org/10.1039/C7RA01571B.

(24) Yadav, V.; Jaimes-Lizcano, Y. A.; Dewangan, N. K.; Park, N.; Li, T.-H.; Robertson, M. L.; Conrad, J. C. Tuning Bacterial Attachment and Detachment via the Thickness and Dispersity of a PH-Responsive Polymer Brush. *ACS Appl. Mater. Interfaces* **2017**, *9* (51), 44900–44910. https://doi.org/10.1021/acsami.7b14416.

(25) Wang, Y.; Wu, J.; Zhang, D.; Chen, F.; Fan, P.; Zhong, M.; Xiao, S.; Chang, Y.; Gong, X.; Yang, J.; Zheng, J. Design of Salt-Responsive and Regenerative Antibacterial Polymer Brushes with Integrated Bacterial Resistance, Killing, and

Release Properties. *J. Mater. Chem. B* **2019**, *7* (38), 5762–5774. https://doi.org/10.1039/C9TB01313J.

(26) Encinas, N.; Yang, C.-Y.; Geyer, F.; Kaltbeitzel, A.; Baumli, P.; Reinholz, J.; Mailänder, V.; Butt, H.-J.; Vollmer, D. Submicrometer-Sized Roughness Suppresses Bacteria Adhesion. *ACS Appl. Mater. Interfaces* **2020**, *12* (19), 21192–21200. https://doi.org/10.1021/acsami.9b22621.

(27) Cheng, Y.; Feng, G.; Moraru, C. I. Micro- and Nanotopography Sensitive Bacterial Attachment Mechanisms: A Review. *Front Microbiol* **2019**, *10*. https://doi.org/10.3389/fmicb.2019.00191.

(28) Godoy-Gallardo, M.; Guillem-Marti, J.; Sevilla, P.; Manero, J. M.; Gil, F. J.; Rodriguez, D. Anhydride-Functional Silane Immobilized onto Titanium Surfaces Induces Osteoblast Cell Differentiation and Reduces Bacterial Adhesion and Biofilm Formation. *Mater Sci Eng C Mater Biol Appl* **2016**, *59*, 524–532. https://doi.org/10.1016/j.msec.2015.10.051.

(29) Vaccari, L.; Allan, D. B.; Sharifi-Mood, N.; Singh, A. R.; Leheny, R. L.; Stebe, K. J. Films of Bacteria at Interfaces: Three Stages of Behaviour. *Soft Matter* **2015**, *11* (30), 6062–6074. https://doi.org/10.1039/C5SM00696A.

(30) Omarova, M.; Swientoniewski, L. T.; Mkam Tsengam, I. K.; Blake, D. A.; John, V.; McCormick, A.; Bothun, G. D.; Raghavan, S. R.; Bose, A. Biofilm Formation by Hydrocarbon-Degrading Marine Bacteria and Its Effects on Oil Dispersion. *ACS Sustainable Chem. Eng.* **2019**, *7* (17), 14490–14499. https://doi.org/10.1021/acssuschemeng.9b01923.

(31) Vaccari, L.; Molaei, M.; Niepa, T. H. R.; Lee, D.; Leheny, R. L.; Stebe, K. J. Films of Bacteria at Interfaces. *Advances in Colloid and Interface Science* **2017**, *247*, 561–572. https://doi.org/10.1016/j.cis.2017.07.016.

(32) Subbiahdoss, G.; Reimhult, E. Biofilm Formation at Oil-Water Interfaces Is Not a Simple Function of Bacterial Hydrophobicity. *Colloids and Surfaces B: Biointerfaces* **2020**, *194*, 111163. https://doi.org/10.1016/j.colsurfb.2020.111163.

(33) Conrad, J. C. Biophysical Methods to Quantify Bacterial Behaviors at Oil–Water Interfaces. *J Ind Microbiol Biotechnol* **2020**. https://doi.org/10.1007/s10295-020-02293-5.

(34) Niepa, T. H. R.; Vaccari, L.; Leheny, R. L.; Goulian, M.; Lee, D.; Stebe, K. J. Films of Bacteria at Interfaces (FBI): Remodeling of Fluid Interfaces by Pseudomonas Aeruginosa. *Scientific Reports* **2017**, *7* (1), 17864. https://doi.org/10.1038/s41598-017-17721-3.

(35) Morelli, M. N.; Ibañez, M.; Leonardi, R. J.; Santiago, L. G.; Irazoqui, H.; Heinrich, J. M. Design of a Biodegradable Carrier for the Application of Controller Bacteria on Air–Water Interfaces. *Pest Management Science* **2020**, *76* (1), 296–303. https://doi.org/10.1002/ps.5514.

(36) National Research Council (US) Committee on Oil in the Sea: Inputs, F. *Input of Oil to the Sea*; National Academies Press (US), 2003.

(37) Rahman, K. S. M.; Thahira-Rahman, J.; Lakshmanaperumalsamy, P.; Banat, I. M. Towards Efficient Crude Oil Degradation by a Mixed Bacterial Consortium. *Bioresource Technology* **2002**, *85* (3), 257–261. https://doi.org/10.1016/S0960-8524(02)00119-0.

(38) Brooijmans, R. J. W.; Pastink, M. I.; Siezen, R. J. Hydrocarbon-Degrading Bacteria: The Oil-Spill Clean-up Crew. *Microbial Biotechnology* **2009**, *2* (6), 587–594. https://doi.org/10.1111/j.1751-7915.2009.00151.x.

(39) Kostka, J. E.; Prakash, O.; Overholt, W. A.; Green, S. J.; Freyer, G.; Canion, A.; Delgardio, J.; Norton, N.; Hazen, T. C.; Huettel, M. Hydrocarbon-Degrading Bacteria and the Bacterial Community Response in Gulf of Mexico Beach Sands Impacted by the Deepwater Horizon Oil Spill. *Applied and Environmental Microbiology* **2011**, *77* (22), 7962–7974. https://doi.org/10.1128/AEM.05402-11.

(40) Prince, R. C.; McFarlin, K. M.; Butler, J. D.; Febbo, E. J.; Wang, F. C. Y.; Nedwed, T. J. The Primary Biodegradation of Dispersed Crude Oil in the Sea. *Chemosphere* **2013**, *90* (2), 521–526. https://doi.org/10.1016/j.chemosphere.2012.08.020.

(41) McFarlin, K. M.; Prince, R. C.; Perkins, R.; Leigh, M. B. Biodegradation of Dispersed Oil in Arctic Seawater at -1°C. *PLoS ONE* **2014**, *9* (1), e84297. https://doi.org/10.1371/journal.pone.0084297.

(42) Mahmoudi, N.; Porter, T. M.; Zimmerman, A. R.; Fulthorpe, R. R.; Kasozi, G. N.; Silliman, B. R.; Slater, G. F. Rapid Degradation of Deepwater Horizon Spilled Oil by Indigenous Microbial Communities in Louisiana Saltmarsh Sediments. *Environ. Sci. Technol.* **2013**, *47* (23), 13303–13312. https://doi.org/10.1021/es4036072.

(43) Bagby, S. C.; Reddy, C. M.; Aeppli, C.; Fisher, G. B.; Valentine, D. L. Persistence and Biodegradation of Oil at the Ocean Floor Following Deepwater Horizon. *Proc. Natl. Acad. Sci. U.S.A.* **2017**, *114* (1), E9–E18. https://doi.org/10.1073/pnas.1610110114.

(44) Bostic, J. T.; Aeppli, C.; Swarthout, R. F.; Reddy, C. M.; Ziolkowski, L. A. Ongoing Biodegradation of Deepwater Horizon Oil in Beach Sands: Insights from Tracing Petroleum Carbon into Microbial Biomass. *Mar. Pollut. Bull.* **2018**, *126*, 130–136. https://doi.org/10.1016/j.marpolbul.2017.10.058.

(45) Place, B.; Anderson, B.; Mekebri, A.; Furlong, E. T.; Gray, J. L.; Tjeerdema, R.; Field, J. A Role for Analytical Chemistry in Advancing Our Understanding of the Occurrence, Fate, and Effects of Corexit Oil Dispersants. *Environ. Sci. Technol.* **2010**, *44* (16), 6016–6018. https://doi.org/10.1021/es102319w.

(46) Brakstad, O. G.; Nordtug, T.; Throne-Holst, M. Biodegradation of Dispersed Macondo Oil in Seawater at Low Temperature and Different Oil Droplet Sizes. *Marine Pollution Bulletin* **2015**, *93* (1), 144–152. https://doi.org/10.1016/j.marpolbul.2015.02.006.

(47) Hamdan LJ; Fulmer PA. Effects of COREXIT® EC9500A on Bacteria from a Beach Oiled by the Deepwater Horizon Spill. *Aquat Microb Ecol* **2011**, *63* (2), 101–109. https://doi.org/10.3354/ame01482.

(48) Zahed, M. A.; Aziz, H. A.; Isa, M. H.; Mohajeri, L.; Mohajeri, S.; Kutty, S. R. M. Kinetic Modeling and Half Life Study on Bioremediation of Crude Oil Dispersed by Corexit 9500. *Journal of Hazardous Materials* **2011**, *185* (2), 1027–1031. https://doi.org/10.1016/j.jhazmat.2010.10.009.

(49) Chakraborty, R.; Borglin, S. E.; Dubinsky, E. A.; Andersen, G. L.; Hazen, T. C. Microbial Response to the MC-252 Oil and Corexit 9500 in the Gulf of Mexico. *Frontiers in Microbiology* **2012**, *3*, 357. https://doi.org/10.3389/fmicb.2012.00357.

(50) Kleindienst, S.; Seidel, M.; Ziervogel, K.; Grim, S.; Loftis, K.; Harrison, S.; Malkin, S. Y.; Perkins, M. J.; Field, J.; Sogin, M. L.; Dittmar, T.; Passow, U.; Medeiros, P. M.; Joye, S. B. Chemical Dispersants Can Suppress the Activity of Natural Oil-Degrading Microorganisms. *Proc Natl Acad Sci U S A* **2015**, *112* (48), 14900–14905. https://doi.org/10.1073/pnas.1507380112.

(51) Khakpay, A.; Abolghasemi, H.; Montazer-Rahmati, M. M. The Effect of Sodium Dodecyl Sulfate on Mean Drop Size in a Horizontal Mixer–Settler Extractor. *The Canadian Journal of Chemical Engineering* **2010**, *88* (1), 101–108. https://doi.org/10.1002/cjce.20252.

(52) Xue, Y.-Q.; Yang, X.-C.; Cui, Z.-X.; Lai, W.-P. The Effect of Microdroplet Size on the Surface Tension and Tolman Length. *J. Phys. Chem. B* **2011**, *115* (1), 109–112. https://doi.org/10.1021/jp1084313.

(53) O'Toole, G.; Kaplan, H. B.; Kolter, R. Biofilm Formation as Microbial Development. *Annu. Rev. Microbiol.* **2000**, *54* (1), 49–79. https://doi.org/10.1146/annurev.micro.54.1.49.

(54) Katsikogianni, M.; Missirlis, Y. F. Concise Review of Mechanisms of Bacterial Adhesion to Biomaterials and of Techniques Used in Estimating Bacteria-Material Interactions. *Eur Cell Mater* **2004**, *8*, 37–57. https://doi.org/10.22203/eCM.v008a05.

(55) Kim, J.; Park, H.-D.; Chung, S. Microfluidic Approaches to Bacterial Biofilm Formation. *Molecules* **2012**, *17* (8), 9818–9834. https://doi.org/10.3390/molecules17089818.

(56) Persat, A.; Nadell, C. D.; Kim, M. K.; Ingremeau, F.; Siryaporn, A.; Drescher, K.; Wingreen, N. S.; Bassler, B. L.; Gitai, Z.; Stone, H. A. The Mechanical World of Bacteria. *Cell 161* (5), 988–997. https://doi.org/10.1016/j.cell.2015.05.005.

(57) Absolom, D. R.; Lamberti, F. V.; Policova, Z.; Zingg, W.; van Oss, C. J.; Neumann, A. W. Surface Thermodynamics of Bacterial Adhesion. *Applied and Environmental Microbiology* **1983**, *46* (1), 90–97.

(58) Sharma, S.; Conrad, J. C. Attachment from Flow of Escherichia Coli Bacteria onto Silanized Glass Substrates. *Langmuir* **2014**, *30* (37), 11147–11155. https://doi.org/10.1021/la502313y.

(59) Sharma, S.; Jaimes-Lizcano, Y. A.; McLay, R. B.; Cirino, P. C.; Conrad, J. C. Subnanometric Roughness Affects the Deposition and Mobile Adhesion of Escherichia Coli on Silanized Glass Surfaces. *Langmuir* **2016**, *32* (21), 5422–5433. https://doi.org/10.1021/acs.langmuir.6b00883.

(60) Liu, Y.; Zhao, Q. Influence of Surface Energy of Modified Surfaces on Bacterial Adhesion. *Biophys. Chem.* **2005**, *117* (1), 39–45. https://doi.org/10.1016/j.bpc.2005.04.015.

(61) Maestro, A.; Santini, E.; Zabiegaj, D.; Llamas, S.; Ravera, F.; Liggieri, L.; Ortega, F.; Rubio, R. G.; Guzman, E. Particle and Particle-Surfactant Mixtures at Fluid Interfaces: Assembly, Morphology, and Rheological Description. *Advances in Condensed Matter Physics* **2015**, *2015*, 17.

(62) Rekvig, L.; Kranenburg, M.; Hafskjold, B.; Smit, B. Effect of Surfactant Structure on Interfacial Properties. *EPL (Europhysics Letters)* **2003**, *63* (6), 902.

(63) Adkins, S. S.; Chen, X.; Nguyen, Q. P.; Sanders, A. W.; Johnston, K. P. Effect of Branching on the Interfacial Properties of Nonionic Hydrocarbon Surfactants at the Air–Water and Carbon Dioxide–Water Interfaces. *Journal of Colloid and Interface Science* **2010**, *346* (2), 455–463. https://doi.org/10.1016/j.jcis.2009.12.059.

(64) Farrow, M. R.; Camp, P. J.; Dowding, P. J.; Lewtas, K. The Effects of Surface Curvature on the Adsorption of Surfactants at the Solid-Liquid Interface. *Phys. Chem. Chem. Phys.* **2013**, *15* (28), 11653–11660. https://doi.org/10.1039/C3CP50585E.

(65) Utada, A. S.; Fernandez-Nieves, A.; Stone, H. A.; Weitz, D. A. Dripping to Jetting Transitions in Coflowing Liquid Streams. *Phys. Rev. Lett.* **2007**, *99* (9), 094502. https://doi.org/10.1103/PhysRevLett.99.094502.

(66) Shah, R. K.; Shum, H. C.; Rowat, A. C.; Lee, D.; Agresti, J. J.; Utada, A. S.; Chu, L.-Y.; Kim, J.-W.; Fernandez-Nieves, A.; Martinez, C. J.; Weitz, D. A. Designer Emulsions Using Microfluidics. *Materials Today* **2008**, *11* (4), 18–27. https://doi.org/10.1016/S1369-7021(08)70053-1.

(67) van Hoeve, W.; Dollet, B.; Gordillo, J. M.; Versluis, M.; Lohse, D. Bubble Size Prediction in Co-Flowing Streams. *EPL (Europhysics Letters)* **2011**, *94* (6), 64001. https://doi.org/10.1209/0295-5075/94/64001.

(68) Chandradoss, S. D.; Haagsma, A. C.; Lee, Y. K.; Hwang, J.-H.; Nam, J.-M.; Joo, C. Surface Passivation for Single-Molecule Protein Studies. *Journal of Visualized Experiments : JoVE* **2014**, No. 86, 50549. https://doi.org/10.3791/50549.

(69) Gauthier, M. J.; Lafay, B.; Christen, R.; Fernandez, L.; Acquaviva, M.; Bonin, P.; Bertrand, J. C. Marinobacter Hydrocarbonoclasticus Gen. Nov., Sp. Nov., a New,

Extremely Halotolerant, Hydrocarbon-Degrading Marine Bacterium. *Int J Syst Bacteriol* **1992**, *42* (4), 568–576. https://doi.org/10.1099/00207713-42-4-568.

(70) Gerdes, B.; Brinkmeyer, R.; Dieckmann, G.; Helmke, E. Influence of Crude Oil on Changes of Bacterial Communities in Arctic Sea-Ice. *FEMS Microbiol Ecol* **2005**, *53* (1), 129–139. https://doi.org/10.1016/j.femsec.2004.11.010.

(71) Reid, G.; Cuperus, P. L.; Bruce, A. W.; van der Mei, H. C.; Tomeczek, L.; Khoury, A. H.; Busscher, H. J. Comparison of Contact Angles and Adhesion to Hexadecane of Urogenital, Dairy, and Poultry Lactobacilli: Effect of Serial Culture Passages. *Appl. Environ. Microbiol.* **1992**, *58* (5), 1549–1553.

(72) McLay, R. B.; Nguyen, H. N.; Jaimes-Lizcano, Y. A.; Dewangan, N. K.; Alexandrova, S.; Rodrigues, D. F.; Cirino, P. C.; Conrad, J. C. Level of Fimbriation Alters the Adhesion of Escherichia Coli Bacteria to Interfaces. *Langmuir* **2018**, *34* (3), 1133–1142. https://doi.org/10.1021/acs.langmuir.7b02447.

(73) Wu, S. Calculation of Interfacial Tension in Polymer Systems. *Journal of Polymer Science Part C: Polymer Symposia* **1971**, *34* (1), 19–30. https://doi.org/10.1002/polc.5070340105.

(74) Wu, S. Polar and Nonpolar Interactions in Adhesion. *The Journal of Adhesion* **1973**, *5* (1), 39–55. https://doi.org/10.1080/00218467308078437.

(75) Wu, S. Surface and Interfacial Tensions of Polymer Melts. II. Poly(Methyl Methacrylate), Poly(n-Butyl Methacrylate), and Polystyrene. *J. Phys. Chem.* **1970**, *74* (3), 632–638. https://doi.org/10.1021/j100698a026.

(76) Berry, J. D.; Neeson, M. J.; Dagastine, R. R.; Chan, D. Y. C.; Tabor, R. F. Measurement of Surface and Interfacial Tension Using Pendant Drop Tensiometry.

Journal of Colloid and Interface Science **2015**, *454*, 226–237. https://doi.org/10.1016/j.jcis.2015.05.012.

(77) Chakraborty, T.; Chakraborty, I.; Ghosh, S. The Methods of Determination of Critical Micellar Concentrations of the Amphiphilic Systems in Aqueous Medium. *Arabian Journal of Chemistry* **2011**, *4* (3), 265–270. https://doi.org/10.1016/j.arabjc.2010.06.045.

(78) Crocker, J. C.; Grier, D. G. Methods of Digital Video Microscopy for Colloidal Studies. *Journal of Colloid and Interface Science* **1996**, *179* (1), 298–310. https://doi.org/10.1006/jcis.1996.0217.

(79) Mohraz, A.; Solomon, M. J. Direct Visualization of Colloidal Rod Assembly by Confocal Microscopy. *Langmuir* **2005**, *21* (12), 5298–5306. https://doi.org/10.1021/la046908a.

(80) Baroud, C. N.; Gallaire, F.; Dangla, R. Dynamics of Microfluidic Droplets. *Lab Chip* **2010**, *10* (16), 2032–2045. https://doi.org/10.1039/C001191F.

(81) Driessen, T.; Jeurissen, R.; Wijshoff, H.; Toschi, F.; Lohse, D. Stability of Viscous Long Liquid Filaments. *Physics of Fluids* **2013**, *25* (6), 062109. https://doi.org/10.1063/1.4811849.

(82) Li, Z.; Lee, K.; Kepkey, P. E.; Mikkelsen, O.; Pottsmith, C. Monitoring Dispersed Oil Droplet Size Distribution at the Gulf of Mexico Deepwater Horizon Spill Site. *International Oil Spill Conference Proceedings* **2011**, *2011* (1), abs377. https://doi.org/10.7901/2169-3358-2011-1-377.

(83) Harris, J. M.; Martin, L. F. An in Vitro Study of the Properties Influencing Staphylococcus Epidermidis Adhesion to Prosthetic Vascular Graft Materials. *Ann Surg* **1987**, *206* (5), 612–620.

(84) Liu, Y.; Shen, L. From Langmuir Kinetics to First- and Second-Order Rate Equations for Adsorption. *Langmuir* **2008**, *24* (20), 11625–11630. https://doi.org/10.1021/la801839b.

(85) Al-Rashed, S. M.; Al-Gaid, A. A. Kinetic and Thermodynamic Studies on the Adsorption Behavior of Rhodamine B Dye on Duolite C-20 Resin. *Journal of Saudi Chemical Society* **2012**, *16* (2), 209–215. https://doi.org/10.1016/j.jscs.2011.01.002.

(86) Kankare, J.; Vinokurov, I. A. Kinetics of Langmuirian Adsorption onto Planar, Spherical, and Cylindrical Surfaces. *Langmuir* **1999**, *15* (17), 5591–5599. https://doi.org/10.1021/la981642r.

(87) Dasgupta, S.; Katava, M.; Faraj, M.; Auth, T.; Gompper, G. Capillary Assembly of Microscale Ellipsoidal, Cuboidal, and Spherical Particles at Interfaces. *Langmuir* **2014**, *30* (40), 11873–11882. https://doi.org/10.1021/la502627h.

(88) Coertjens, S.; De Dier, R.; Moldenaers, P.; Isa, L.; Vermant, J. Adsorption of Ellipsoidal Particles at Liquid–Liquid Interfaces. *Langmuir* **2017**, *33* (11), 2689–2697. https://doi.org/10.1021/acs.langmuir.6b03534.

(89) Marshall, K. C.; Cruickshank, R. H. Cell Surface Hydrophobicity and the Orientation of Certain Bacteria at Interfaces. *Archiv. Mikrobiol.* **1973**, *91* (1), 29–40. https://doi.org/10.1007/BF00409536.

(90) Abdel-Fattah, A. I.; El-Genk, M. S. Sorption of Hydrophobic, Negatively Charged Microspheres onto a Stagnant Air/Water Interface. *Journal of Colloid and Interface Science* **1998**, *202* (2), 417–429. https://doi.org/10.1006/jcis.1998.5442.

(91) Levine, S.; Bowen, B. D.; Partridge, S. J. Stabilization of Emulsions by Fine Particles I. Partitioning of Particles between Continuous Phase and Oil/Water Interface. *Colloids and Surfaces* **1989**, *38* (2), 325–343. https://doi.org/10.1016/0166-6622(89)80271-9.

(92) Loudet, J. C.; Alsayed, A. M.; Zhang, J.; Yodh, A. G. Capillary Interactions Between Anisotropic Colloidal Particles. *Phys. Rev. Lett.* **2005**, *94* (1), 018301. https://doi.org/10.1103/PhysRevLett.94.018301.

(93) Madivala, B.; Fransaer, J.; Vermant, J. Self-Assembly and Rheology of Ellipsoidal Particles at Interfaces. *Langmuir* **2009**, *25* (5), 2718–2728. https://doi.org/10.1021/la803554u.

(94) Lewandowski, E. P.; Searson, P. C.; Stebe, K. J. Orientation of a Nanocylinder at a Fluid Interface. *J. Phys. Chem. B* **2006**, *110* (9), 4283–4290. https://doi.org/10.1021/jp0563282.

(95) Adams, D. J.; Adams, S.; Melrose, J.; Weaver, A. C. Influence of Particle Surface Roughness on the Behaviour of Janus Particles at Interfaces. *Colloids and Surfaces A: Physicochemical and Engineering Aspects* **2008**, *317* (1–3), 360–365. https://doi.org/10.1016/j.colsurfa.2007.11.004.

(96) San-Miguel, A.; Behrens, S. H. Influence of Nanoscale Particle Roughness on the Stability of Pickering Emulsions. *Langmuir* **2012**, *28* (33), 12038–12043. https://doi.org/10.1021/la302224v.

(97) Isa, L.; Lucas, F.; Wepf, R.; Reimhult, E. Measuring Single-Nanoparticle Wetting Properties by Freeze-Fracture Shadow-Casting Cryo-Scanning Electron Microscopy. *Nature Communications* **2011**, *2* (1), 438. https://doi.org/10.1038/ncomms1441.

(98) Park, B. J.; Lee, D. Equilibrium Orientation of Nonspherical Janus Particles at Fluid–Fluid Interfaces. *ACS Nano* **2012**, *6* (1), 782–790. https://doi.org/10.1021/nn204261w.

(99) Park, B. J.; Lee, D. Configuration of Nonspherical Amphiphilic Particles at a Fluid–Fluid Interface. *Soft Matter* **2012**, *8* (29), 7690–7698. https://doi.org/10.1039/C2SM25775K.

(100) Isa, L.; Samudrala, N.; Dufresne, E. R. Adsorption of Sub-Micron Amphiphilic Dumbbells to Fluid Interfaces. *Langmuir* **2014**, *30* (18), 5057–5063. https://doi.org/10.1021/la500463m.

(101) Zanini, M.; Marschelke, C.; Anachkov, S. E.; Marini, E.; Synytska, A.; Isa, L. Universal Emulsion Stabilization from the Arrested Adsorption of Rough Particles at Liquid-Liquid Interfaces. *Nature Communications* **2017**, *8* (1), 15701. https://doi.org/10.1038/ncomms15701.

(102) van der Vegt, W.; Norde, W.; van der Mei, H. C.; Busscher, H. J. Kinetics of Interfacial Tension Changes during Protein Adsorption from Sessile Droplets on FEP–Teflon. *Journal of Colloid and Interface Science* **1996**, *179* (1), 57–65. https://doi.org/10.1006/jcis.1996.0188.

(103) Nave, S.; Eastoe, J.; Heenan, R. K.; Steytler, D.; Grillo, I. What Is So Special about Aerosol-OT? 2. Microemulsion Systems. *Langmuir* **2000**, *16* (23), 8741–8748. https://doi.org/10.1021/la000342i.

(104) Dey, J.; Bhattacharjee, J.; Hassan, P. A.; Aswal, V. K.; Das, S.; Ismail, K. Micellar Shape Driven Counterion Binding. Small-Angle Neutron Scattering Study of AOT Micelle. *Langmuir* **2010**, *26* (20), 15802–15806. https://doi.org/10.1021/la1027652.

(105) Nakahara, H.; Shibata, O.; Moroi, Y. Examination of Surface Adsorption of Cetyltrimethylammonium Bromide and Sodium Dodecyl Sulfate. *The Journal of Physical Chemistry B* **2011**, *115* (29), 9077–9086. https://doi.org/10.1021/jp202940p.

(106) Hildebrandt, E.; Sommerling, J.-H.; Guthausen, G.; Zick, K.; Stürmer, J.; Nirschl, H.; Leneweit, G. Phospholipid Adsorption at Oil in Water versus Water in Oil Interfaces: Implications for Interfacial Densities and Bulk Solubilities. *Colloids and Surfaces A: Physicochemical and Engineering Aspects* **2016**, *505*, 56–63. https://doi.org/10.1016/j.colsurfa.2015.12.024.

(107) Nave, S.; Eastoe, J.; Penfold, J. What Is So Special about Aerosol-OT? 1. Aqueous Systems. *Langmuir* **2000**, *16* (23), 8733–8740. https://doi.org/10.1021/la000341q.

(108) McEldowney, S.; Fletcher, M. Variability of the Influence of Physicochemical Factors Affecting Bacterial Adhesion to Polystyrene Substrata. *Appl Environ Microbiol* **1986**, *52* (3), 460–465.

(109) Thaveesri, J.; Daffonchio, D.; Liessens, B.; Vandermeren, P.; Verstraete, W. Granulation and Sludge Bed Stability in Upflow Anaerobic Sludge Bed Reactors in Relation to Surface Thermodynamics. *Appl Environ Microbiol* **1995**, *61* (10), 3681–3686.

(110) Zhang, X.; Zhang, Q.; Yan, T.; Jiang, Z.; Zhang, X.; Zuo, Y. Y. Quantitatively Predicting Bacterial Adhesion Using Surface Free Energy Determined with a Spectrophotometric Method. *Environ. Sci. Technol.* **2015**, *49* (10), 6164–6171. https://doi.org/10.1021/es5050425.

(111) Singh, O. G.; Ismail, K. Effect of Sodium Chloride on the Aggregation, Adsorption and Counterion Binding Behavior of Mixtures of Sodium Dioctylsulfosuccinate and Sodium Dodecylsulfate in Water. *Colloids and Surfaces A: Physicochemical and Engineering Aspects* **2012**, *414*, 209–215. https://doi.org/10.1016/j.colsurfa.2012.08.025.

(112) Abbasi, A.; Bothun, G. D.; Bose, A. Attachment of Alcanivorax Borkumensis to Hexadecane-In-Artificial Sea Water Emulsion Droplets. *Langmuir* **2018**, *34* (18), 5352–5357. https://doi.org/10.1021/acs.langmuir.8b00082.

(113) Zenati, B.; Chebbi, A.; Badis, A.; Eddouaouda, K.; Boutoumi, H.; El Hattab, M.; Hentati, D.; Chelbi, M.; Sayadi, S.; Chamkha, M.; Franzetti, A. A Non-Toxic Microbial Surfactant from Marinobacter Hydrocarbonoclasticus SdK644 for Crude Oil Solubilization Enhancement. *Ecotoxicology and Environmental Safety* **2018**, *154*, 100–107. https://doi.org/10.1016/j.ecoenv.2018.02.032.

(114) R, R.; R, S. Microbes in Flow. *Curr Opin Microbiol* **2015**, *25*, 1–8. https://doi.org/10.1016/j.mib.2015.03.003.

(115) Conrad, J. C.; Poling-Skutvik, R. Confined Flow: Consequences and Implications for Bacteria and Biofilms. *Annu. Rev. Chem. Biomol. Eng.* **2018**, *9* (1), 175–200. https://doi.org/10.1146/annurev-chembioeng-060817-084006.

(116) Kaminski, T. S.; Scheler, O.; Garstecki, P. Droplet Microfluidics for Microbiology: Techniques, Applications and Challenges. *Lab Chip* **2016**, *16* (12), 2168–2187. https://doi.org/10.1039/C6LC00367B.

(117) Cydzik-Kwiatkowska, A.; Zielińska, M. Bacterial Communities in Full-Scale Wastewater Treatment Systems. *World J Microbiol Biotechnol* **2016**, *32*. https://doi.org/10.1007/s11274-016-2012-9.

(118) Ramaswamy, S. The Mechanics and Statistics of Active Matter. *Annual Review of Condensed Matter Physics* **2010**, *1* (1), 323–345. https://doi.org/10.1146/annurev-conmatphys-070909-104101.

(119) Koenderink, G. H.; Dogic, Z.; Nakamura, F.; Bendix, P. M.; MacKintosh, F. C.; Hartwig, J. H.; Stossel, T. P.; Weitz, D. A. An Active Biopolymer Network Controlled by Molecular Motors. *PNAS* **2009**, *106* (36), 15192–15197. https://doi.org/10.1073/pnas.0903974106.

(120) Thoresen, T.; Lenz, M.; Gardel, M. L. Reconstitution of Contractile Actomyosin Bundles. *Biophys. J.* **2011**, *100* (11), 2698–2705. https://doi.org/10.1016/j.bpj.2011.04.031.

(121) Sanchez, T.; Chen, D. T. N.; DeCamp, S. J.; Heymann, M.; Dogic, Z. Spontaneous Motion in Hierarchically Assembled Active Matter. *Nature* **2012**, *491* (7424), 431–434. https://doi.org/10.1038/nature11591.

(122) Keber, F. C.; Loiseau, E.; Sanchez, T.; DeCamp, S. J.; Giomi, L.; Bowick, M. J.; Marchetti, M. C.; Dogic, Z.; Bausch, A. R. Topology and Dynamics of Active Nematic Vesicles. *Science* **2014**, *345* (6201), 1135–1139. https://doi.org/10.1126/science.1254784.

(123) Manson, M. D.; Tedesco, P.; Berg, H. C.; Harold, F. M.; Drift, C. V. der. A Protonmotive Force Drives Bacterial Flagella. *PNAS* **1977**, *74* (7), 3060–3064. https://doi.org/10.1073/pnas.74.7.3060.

(124) Owen, D.; Ballard, M.; Alexeev, A.; Hesketh, P. J. Rapid Microfluidic Mixing via Rotating Magnetic Microbeads. *Sensors and Actuators A: Physical* **2016**, *251*, 84–91. https://doi.org/10.1016/j.sna.2016.09.040.

(125) Akin, D.; Sturgis, J.; Ragheb, K.; Sherman, D.; Burkholder, K.; Robinson, J. P.; Bhunia, A. K.; Mohammed, S.; Bashir, R. Bacteria-Mediated Delivery of Nanoparticles and Cargo into Cells. *Nature Nanotechnology* **2007**, *2* (7), 441–449. https://doi.org/10.1038/nnano.2007.149.

(126) Felfoul, O.; Mohammadi, M.; Taherkhani, S.; de Lanauze, D.; Xu, Y. Z.; Loghin, D.; Essa, S.; Jancik, S.; Houle, D.; Lafleur, M.; Gaboury, L.; Tabrizian, M.; Kaou, N.; Atkin, M.; Vuong, T.; Batist, G.; Beauchemin, N.; Radzioch, D.; Martel, S. Magneto-Aerotactic Bacteria Deliver Drug-Containing Nanoliposomes to Tumour Hypoxic Regions. *Nat Nanotechnol* **2016**, *11* (11), 941–947. https://doi.org/10.1038/nnano.2016.137.

(127) Park, B.-W.; Zhuang, J.; Yasa, O.; Sitti, M. Multifunctional Bacteria-Driven Microswimmers for Targeted Active Drug Delivery. *ACS Nano* **2017**, *11* (9), 8910–8923. https://doi.org/10.1021/acsnano.7b03207.

(128) Darnton, N.; Turner, L.; Breuer, K.; Berg, H. C. Moving Fluid with Bacterial Carpets. *Biophys J* **2004**, *86* (3), 1863–1870.

(129) Behkam, B.; Sitti, M. Bacterial Flagella-Based Propulsion and on/off Motion Control of Microscale Objects. *Appl. Phys. Lett.* **2007**, *90* (2), 023902. https://doi.org/10.1063/1.2431454.

(130) Behkam, B.; Sitti, M. Effect of Quantity and Configuration of Attached Bacteria on Bacterial Propulsion of Microbeads. *Appl. Phys. Lett.* **2008**, *93* (22), 223901. https://doi.org/10.1063/1.3040318.

(131) Steager, E. B.; Sakar, M. S.; Kim, D. H.; Kumar, V.; Pappas, G. J.; Kim, M. J. Electrokinetic and Optical Control of Bacterial Microrobots. *J. Micromech. Microeng.* **2011**, *21* (3), 035001. https://doi.org/10.1088/0960-1317/21/3/035001.

(132) Sahari, A.; Traore, M. A.; Scharf, B. E.; Behkam, B. Directed Transport of Bacteria-Based Drug Delivery Vehicles: Bacterial Chemotaxis Dominates Particle Shape. *Biomed Microdevices* **2014**, *16* (5), 717–725. https://doi.org/10.1007/s10544-014-9876-y.

(133) Wong, D.; Beattie, E. E.; Steager, E. B.; Kumar, V. Effect of Surface Interactions and Geometry on the Motion of Micro Bio Robots. *Appl. Phys. Lett.* **2013**, *103* (15), 153707. https://doi.org/10.1063/1.4824840.

(134) Stanton, M. M.; Sánchez, S. Pushing Bacterial Biohybrids to In Vivo Applications. *Trends in Biotechnology* **2017**, *35* (10), 910–913. https://doi.org/10.1016/j.tibtech.2017.04.008.

(135) Vaccari, L.; Molaei, M.; Leheny, R. L.; Stebe, K. J. Cargo Carrying Bacteria at Interfaces. *Soft Matter* **2018**, *14* (27), 5643–5653. https://doi.org/10.1039/C8SM00481A.

(136) Hiratsuka, Y.; Miyata, M.; Tada, T.; Uyeda, T. Q. P. A Microrotary Motor Powered by Bacteria. *PNAS* **2006**, *103* (37), 13618–13623. https://doi.org/10.1073/pnas.0604122103.

(137) Sokolov, A.; Apodaca, M. M.; Grzybowski, B. A.; Aranson, I. S. Swimming Bacteria Power Microscopic Gears. *PNAS* **2010**, *107* (3), 969–974. https://doi.org/10.1073/pnas.0913015107.

(138) Leonardo, R. D.; Angelani, L.; Dell'Arciprete, D.; Ruocco, G.; Iebba, V.; Schippa, S.; Conte, M. P.; Mecarini, F.; Angelis, F. D.; Fabrizio, E. D. Bacterial Ratchet Motors. *PNAS* **2010**, *107* (21), 9541–9545. https://doi.org/10.1073/pnas.0910426107.

(139) Vizsnyiczai, G.; Frangipane, G.; Maggi, C.; Saglimbeni, F.; Bianchi, S.; Di Leonardo, R. Light Controlled 3D Micromotors Powered by Bacteria. *Nature Communications* **2017**, *8*, 15974. https://doi.org/10.1038/ncomms15974.

(140) Kojima, M.; Miyamoto, T.; Nakajima, M.; Homma, M.; Arai, T.; Fukuda, T. Bacterial Sheet-Powered Rotation of a Micro-Object. *Sensors and Actuators B: Chemical* **2016**, *222*, 1220–1225. https://doi.org/10.1016/j.snb.2015.07.071.

(141) Cates, M. E. Diffusive Transport without Detailed Balance in Motile Bacteria: Does Microbiology Need Statistical Physics? *Rep. Prog. Phys.* **2012**, *75* (4), 042601. https://doi.org/10.1088/0034-4885/75/4/042601.

(142) Brochard, F. Motions of Droplets on Solid Surfaces Induced by Chemical or Thermal Gradients. *Langmuir* **1989**, *5* (2), 432–438. https://doi.org/10.1021/la00086a025.

(143) Toyota, T.; Tsuha, H.; Yamada, K.; Takakura, K.; Ikegami, T.; Sugawara, T. *Listeria* -like Motion of Oil Droplets. *Chem. Lett.* **2006**, *35* (7), 708–709. https://doi.org/10.1246/cl.2006.708.

(144) Thutupalli, S.; Seemann, R.; Herminghaus, S. Swarming Behavior of Simple Model Squirmers. *New J. Phys.* **2011**, *13* (7), 073021. https://doi.org/10.1088/1367-2630/13/7/073021.

(145) Banno, T.; Kuroha, R.; Toyota, T. PH-Sensitive Self-Propelled Motion of Oil Droplets in the Presence of Cationic Surfactants Containing Hydrolyzable Ester Linkages. *Langmuir* **2012**, *28* (2), 1190–1195. https://doi.org/10.1021/la2045338.

(146) Peddireddy, K.; Kumar, P.; Thutupalli, S.; Herminghaus, S.; Bahr, C. Solubilization of Thermotropic Liquid Crystal Compounds in Aqueous Surfactant Solutions. *Langmuir* **2012**, *28* (34), 12426–12431. https://doi.org/10.1021/la3015817.

(147) Herminghaus, S.; Maass, C. C.; Krüger, C.; Thutupalli, S.; Goehring, L.; Bahr, C. Interfacial Mechanisms in Active Emulsions. *Soft Matter* **2014**, *10* (36), 7008–7022. https://doi.org/10.1039/C4SM00550C.

(148) Tanaka, S.; Sogabe, Y.; Nakata, S. Spontaneous Change in Trajectory Patterns of a Self-Propelled Oil Droplet at the Air-Surfactant Solution Interface. *Phys. Rev. E* **2015**, *91* (3), 032406. https://doi.org/10.1103/PhysRevE.91.032406.

(149) Jin, C.; Krüger, C.; Maass, C. C. Chemotaxis and Autochemotaxis of Self-Propelling Droplet Swimmers. *Proc Natl Acad Sci U S A* **2017**, *114* (20), 5089–5094. https://doi.org/10.1073/pnas.1619783114.

(150) Nagasaka, Y.; Tanaka, S.; Nehira, T.; Amimoto, T. Spontaneous Emulsification and Self-Propulsion of Oil Droplets Induced by the Synthesis of Amino Acid-Based Surfactants. *Soft Matter* **2017**, *13* (37), 6450–6457. https://doi.org/10.1039/C7SM01117B.

(151) Čejková, J.; Banno, T.; Hanczyc, M. M.; Štěpánek, F. Droplets As Liquid Robots. *Artificial life* **2017**, *23* (4), 528–549. https://doi.org/10.1162/ARTL_a_00243.

(152) Suga, M.; Suda, S.; Ichikawa, M.; Kimura, Y. Self-Propelled Motion Switching in Nematic Liquid Crystal Droplets in Aqueous Surfactant Solutions. *Phys. Rev. E* **2018**, *97* (6), 062703. https://doi.org/10.1103/PhysRevE.97.062703.

(153) Krüger, C.; Klös, G.; Bahr, C.; Maass, C. C. Curling Liquid Crystal Microswimmers: A Cascade of Spontaneous Symmetry Breaking. *Phys. Rev. Lett.* **2016**, *117* (4), 048003. https://doi.org/10.1103/PhysRevLett.117.048003.

(154) Suzuki, K.; Miyazaki, M.; Takagi, J.; Itabashi, T.; Ishiwata, S. Spatial Confinement of Active Microtubule Networks Induces Large-Scale Rotational Cytoplasmic Flow. *PNAS* **2017**, *114* (11), 2922–2927. https://doi.org/10.1073/pnas.1616001114.

(155) Lushi, E.; Wioland, H.; Goldstein, R. E. Fluid Flows Created by Swimming Bacteria Drive Self-Organization in Confined Suspensions. *PNAS* **2014**, *111* (27), 9733–9738. https://doi.org/10.1073/pnas.1405698111.

(156) Lee, J.-C.; Kim, Y.-S.; Yun, B.-S.; Whang, K.-S. Halomonas Salicampi Sp. Nov., a Halotolerant and Alkalitolerant Bacterium Isolated from a Saltern Soil. *International Journal of Systematic and Evolutionary Microbiology* **2015**, *65* (12), 4792–4799. https://doi.org/10.1099/ijsem.0.000650.

(157) Kim, D.; Baik, K. S.; Kim, M. S.; Jung, B.-M.; Shin, T.-S.; Chung, G.-H.; Rhee, M. S.; Seong, C. N. Shewanella Haliotis Sp. Nov., Isolated from the Gut Microflora of Abalone, Haliotis Discus Hannai. *International Journal of Systematic and Evolutionary Microbiology* **2007**, *57* (12), 2926–2931. https://doi.org/10.1099/ijs.0.65257-0.

(158) Verma, P.; Pandey, P. K.; Gupta, A. K.; Kim, H. J.; Baik, K. S.; Seong, C. N.; Patole, M. S.; Shouche, Y. S. Shewanella Indica Sp. Nov., Isolated from Sediment of the Arabian Sea. *International Journal of Systematic and Evolutionary Microbiology,* **2011**, *61* (9), 2058–2064. https://doi.org/10.1099/ijs.0.026310-0.

(159) Kim, S.-J.; Park, S.-J.; Oh, Y.-S.; Lee, S.-A.; Shin, K.-S.; Roh, D.-H.; Rhee, S.-K. Shewanella Arctica Sp. Nov., an Iron-Reducing Bacterium Isolated from Arctic Marine Sediment. *International Journal of Systematic and Evolutionary Microbiology* **2012**, *62* (Pt_5), 1128–1133. https://doi.org/10.1099/ijs.0.031401-0.

(160) Dewangan, N. K.; Conrad, J. C. Adhesion of Marinobacter Hydrocarbonoclasticus to Surfactant-Decorated Dodecane Droplets. *Langmuir* **2018**, *34* (46), 14012–14021. https://doi.org/10.1021/acs.langmuir.8b02071.

(161) Lemelle, L.; Palierne, J.-F.; Chatre, E.; Vaillant, C.; Place, C. Curvature Reversal of the Circular Motion of Swimming Bacteria Probes for Slip at Solid/Liquid

Interfaces. *Soft Matter* **2013**, *9* (41), 9759–9762. https://doi.org/10.1039/C3SM51426A.

(162) Lemelle, L.; Palierne, J.-F.; Chatre, E.; Place, C. Counterclockwise Circular Motion of Bacteria Swimming at the Air-Liquid Interface. *J. Bacteriol.* **2010**, *192* (23), 6307–6308. https://doi.org/10.1128/JB.00397-10.

(163) Schwarz-Linek, J.; Valeriani, C.; Cacciuto, A.; Cates, M. E.; Marenduzzo, D.; Morozov, A. N.; Poon, W. C. K. Phase Separation and Rotor Self-Assembly in Active Particle Suspensions. *PNAS* **2012**, *109* (11), 4052–4057. https://doi.org/10.1073/pnas.1116334109.

(164) Lamb, H. Hydrodynamics | Fluid dynamics and solid mechanics https://www.cambridge.org/us/academic/subjects/mathematics/fluid-dynamics-and-solid-mechanics/hydrodynamics-6th-edition, https://www.cambridge.org/us/academic/subjects/mathematics/fluid-dynamics-and-solid-mechanics (accessed Jul 10, 2020).

(165) Rubinow, S. I.; Keller, J. B. The Transverse Force on a Spinning Sphere Moving in a Viscous Fluid. *Journal of Fluid Mechanics* **1961**, *11* (3), 447–459. https://doi.org/10.1017/S0022112061000640.

(166) Hatwalne, Y.; Ramaswamy, S.; Rao, M.; Simha, R. A. Rheology of Active-Particle Suspensions. *Phys. Rev. Lett.* **2004**, *92* (11), 118101. https://doi.org/10.1103/PhysRevLett.92.118101.

(167) Baskaran, A.; Marchetti, M. C. Statistical Mechanics and Hydrodynamics of Bacterial Suspensions. *PNAS* **2009**, *106* (37), 15567–15572. https://doi.org/10.1073/pnas.0906586106.

(168) Jeffery, G. B. On the Steady Rotation of a Solid of Revolution in a Viscous Fluid. *Proceedings of the London Mathematical Society* **1915**, *14* (1), 327–338. https://doi.org/10.1112/plms/s2_14.1.327.

(169) Liu, Q.; Prosperetti, A. Wall Effects on a Rotating Sphere. *Journal of Fluid Mechanics* **2010**, *657*, 1–21. https://doi.org/10.1017/S002211201000128X.

(170) Darnton, N. C.; Turner, L.; Rojevsky, S.; Berg, H. C. On Torque and Tumbling in Swimming Escherichia Coli. *J. Bacteriol.* **2007**, *189* (5), 1756–1764. https://doi.org/10.1128/JB.01501-06.

(171) Nguyen, F. T. M.; Graham, M. D. Impacts of Multiflagellarity on Stability and Speed of Bacterial Locomotion. *Phys. Rev. E* **2018**, *98* (4), 042419. https://doi.org/10.1103/PhysRevE.98.042419.

(172) Stanton, M. M.; Simmchen, J.; Ma, X.; Miguel-López, A.; Sánchez, S. Biohybrid Janus Motors Driven by Escherichia Coli. *Advanced Materials Interfaces* **2016**, *3* (2), 1500505. https://doi.org/10.1002/admi.201500505.

(173) Angeles, O.; Medina-Moreno, S. A.; Jiménez-González, A.; Coreño-Alonso, A.; Lizardi-Jiménez, M. A. Predominant Mode of Diesel Uptake: Direct Interfacial versus Emulsification in Multiphase Bioreactor. *Chemical Engineering Science* **2017**, *165*, 108–112. https://doi.org/10.1016/j.ces.2017.02.046.

(174) Sokolov, A.; Aranson, I. S. Rapid Expulsion of Microswimmers by a Vortical Flow. *Nature Communications* **2016**, *7*, 11114. https://doi.org/10.1038/ncomms11114.

(175) Sokolov, A.; Rubio, L. D.; Brady, J. F.; Aranson, I. S. Instability of Expanding Bacterial Droplets. *Nature Communications* **2018**, *9* (1), 1322. https://doi.org/10.1038/s41467-018-03758-z.

(176) Krüger, C.; Bahr, C.; Herminghaus, S.; Maass, C. C. Dimensionality Matters in the Collective Behaviour of Active Emulsions. *Eur. Phys. J. E* **2016**, *39* (6), 64. https://doi.org/10.1140/epje/i2016-16064-y.

(177) Seemann, R.; Fleury, J.-B.; Maass, C. C. Self-Propelled Droplets. *Eur. Phys. J. Spec. Top.* **2016**, *225* (11), 2227–2240. https://doi.org/10.1140/epjst/e2016-60061-7.

(178) Abbasnezhad, H.; Foght, J. M.; Gray, M. R. Adhesion to the Hydrocarbon Phase Increases Phenanthrene Degradation by Pseudomonas Fluorescens LP6a. *Biodegradation* **2011**, *22* (3), 485–496. https://doi.org/10.1007/s10532-010-9421-5.

(179) Morrish, J. L. E.; Brennan, E. T.; Dry, H. C.; Daugulis, A. J. Enhanced Bioproduction of Carvone in a Two-Liquid-Phase Partitioning Bioreactor with a Highly Hydrophobic Biocatalyst. *Biotechnology and Bioengineering* **2008**, *101* (4), 768–775. https://doi.org/10.1002/bit.21941.

(180) Oda, S. Microbial Transformation of Water-Insoluble Substrates by Two Types of Novel Interface Bioprocesses, Tacky Liquid–Liquid Interface Bioreactor and Non-Aqueous Sporular Bioconversion System. *World J Microbiol Biotechnol* **2020**, *36* (4), 57. https://doi.org/10.1007/s11274-020-02834-1.

(181) MARSHALL, K. C.; STOUT, R.; MITCHELL, R. Mechanism of the Initial Events in the Sorption of Marine Bacteria to Surfaces. *Microbiology,* **1971**, *68* (3), 337–348. https://doi.org/10.1099/00221287-68-3-337.

(182) Bolster, C. H.; Mills, A. L.; Hornberger, G. M.; Herman, J. S. Effect of Surface Coatings, Grain Size, and Ionic Strength on the Maximum Attainable Coverage of Bacteria on Sand Surfaces. *Journal of Contaminant Hydrology* **2001**, *50* (3), 287–305. https://doi.org/10.1016/S0169-7722(01)00106-1.

(183) de Kerchove, A. J.; Weroński, P.; Elimelech, M. Adhesion of Nonmotile Pseudomonas Aeruginosa on "Soft" Polyelectrolyte Layer in a Radial Stagnation Point Flow System: Measurements and Model Predictions. *Langmuir* **2007**, *23* (24), 12301–12308. https://doi.org/10.1021/la701936x.

(184) Chakraborty, S.; Mukherji, S.; Mukherji, S. Surface Hydrophobicity of Petroleum Hydrocarbon Degrading Burkholderia Strains and Their Interactions with NAPLs and Surfaces. *Colloids and Surfaces B: Biointerfaces* **2010**, *78* (1), 101–108. https://doi.org/10.1016/j.colsurfb.2010.02.019.

(185) Berg, H. C.; Brown, D. A. Chemotaxis in Escherichia Coli Analysed by Three-Dimensional Tracking. *Nature* **1972**, *239* (5374), 500–504. https://doi.org/10.1038/239500a0.

(186) Blair, D. F. How Bacteria Sense and Swim. *Annu. Rev. Microbiol.* **1995**, *49* (1), 489–520. https://doi.org/10.1146/annurev.mi.49.100195.002421.

(187) Berg, H. C. The Rotary Motor of Bacterial Flagella. *Annu. Rev. Biochem.* **2003**, *72*, 19–54. https://doi.org/10.1146/annurev.biochem.72.121801.161737.

(188) Harshey, R. M. Bacterial Motility on a Surface: Many Ways to a Common Goal. *Annu. Rev. Microbiol.* **2003**, *57* (1), 249–273. https://doi.org/10.1146/annurev.micro.57.030502.091014.

(189) Szurmant, H.; Ordal, G. W. Diversity in Chemotaxis Mechanisms among the Bacteria and Archaea. *Microbiol Mol Biol Rev* **2004**, *68* (2), 301–319. https://doi.org/10.1128/MMBR.68.2.301-319.2004.

(190) Desai, N.; Shaik, V. A.; Ardekani, A. M. Hydrodynamic Interaction Enhances Colonization of Sinking Nutrient Sources by Motile Microorganisms. *Front Microbiol* **2019**, *10*. https://doi.org/10.3389/fmicb.2019.00289.

(191) Shaik, V. A.; Vasani, V.; Ardekani, A. M. Locomotion inside a Surfactant-Laden Drop at Low Surface Péclet Numbers. *Journal of Fluid Mechanics* **2018**, *851*, 187–230. https://doi.org/10.1017/jfm.2018.491.

(192) Wheeler, J. D.; Secchi, E.; Rusconi, R.; Stocker, R. Not Just Going with the Flow: The Effects of Fluid Flow on Bacteria and Plankton. *Annu. Rev. Cell Dev. Biol.* **2019**, *35* (1), 213–237. https://doi.org/10.1146/annurev-cellbio-100818-125119.

(193) Korber, D. R.; Lawrence, J. R.; Caldwell, D. E. Effect of Motility on Surface Colonization and Reproductive Success of Pseudomonas Fluorescens in Dual-Dilution Continuous Culture and Batch Culture Systems. *Appl. Environ. Microbiol.* **1994**, *60* (5), 1421–1429.

(194) Kogure, K.; Ikemoto, E.; Morisaki, H. Attachment of Vibrio Alginolyticus to Glass Surfaces Is Dependent on Swimming Speed. *J Bacteriol* **1998**, *180* (4), 932–937.

(195) Camesano, T. A.; Logan, B. E. Influence of Fluid Velocity and Cell Concentration on the Transport of Motile and Nonmotile Bacteria in Porous Media. *Environ. Sci. Technol.* **1998**, *32* (11), 1699–1708. https://doi.org/10.1021/es970996m.

(196) Morisaki, H.; Nagai, S.; Ohshima, H.; Ikemoto, E.; Kogure, K. The Effect of Motility and Cell-Surface Polymers on Bacterial Attachment. *Microbiology* **1999**, *145* (10), 2797–2802.

(197) Vigeant, M. A.-S.; Ford, R. M.; Wagner, M.; Tamm, L. K. Reversible and Irreversible Adhesion of Motile Escherichia Coli Cells Analyzed by Total Internal Reflection Aqueous Fluorescence Microscopy. *Appl. Environ. Microbiol.* **2002**, *68* (6), 2794–2801. https://doi.org/10.1128/AEM.68.6.2794-2801.2002.

(198) Kerchove, A. J. de; Elimelech, M. Impact of Alginate Conditioning Film on Deposition Kinetics of Motile and Nonmotile Pseudomonas Aeruginosa Strains. *Appl. Environ. Microbiol.* **2007**, *73* (16), 5227–5234. https://doi.org/10.1128/AEM.00678-07.

(199) Kerchove, A. J. de; Elimelech, M. Bacterial Swimming Motility Enhances Cell Deposition and Surface Coverage. *Environ. Sci. Technol.* **2008**, *42* (12), 4371–4377. https://doi.org/10.1021/es703028u.

(200) Tamar, E.; Koler, M.; Vaknin, A. The Role of Motility and Chemotaxis in the Bacterial Colonization of Protected Surfaces. *Scientific Reports* **2016**, *6*, 19616. https://doi.org/10.1038/srep19616.

(201) Jindai, K.; Nakade, K.; Masuda, K.; Sagawa, T.; Kojima, H.; Shimizu, T.; Shingubara, S.; Ito, T. Adhesion and Bactericidal Properties of Nanostructured Surfaces Dependent on Bacterial Motility. *RSC Adv.* **2020**, *10* (10), 5673–5680. https://doi.org/10.1039/C9RA08282D.

(202) Deng, J.; Molaei, M.; Chisholm, N. G.; Stebe, K. J. Motile Bacteria at Oil-Water Interfaces: Pseudomonas Aeruginosa. *Langmuir* **2020**. https://doi.org/10.1021/acs.langmuir.9b03578.

(203) Dewangan, N. K.; Conrad, J. C. Rotating Oil Droplets Driven by Motile Bacteria at Interfaces. *Soft Matter* **2019**, *15* (45), 9368–9375. https://doi.org/10.1039/C9SM01570A.

(204) Ramos, G.; Cordero, M. L.; Soto, R. Bacteria Driving Droplets. *Soft Matter* **2020**, *16* (5), 1359–1365. https://doi.org/10.1039/C9SM01839E.

(205) Gosink, K. K.; Häse, C. C. Requirements for Conversion of the Na+-Driven Flagellar Motor of Vibrio Cholerae to the H+-Driven Motor of Escherichia Coli. *Journal of Bacteriology* **2000**, *182* (15), 4234–4240. https://doi.org/10.1128/JB.182.15.4234-4240.2000.

(206) Eisenbach, M.; Adler, J. Bacterial Cell Envelopes with Functional Flagella. *J. Biol. Chem.* **1981**, *256* (16), 8807–8814.

(207) Myerthall, D. L.; Thomas, T. H. Kinetics of Adherence of Actinomyces Viscosus to Saliva-Coated Silica and Hydroxyapatite Beads. *J. Gen. Microbiol.* **1983**, *129* (5), 1387–1395. https://doi.org/10.1099/00221287-129-5-1387.

(208) Pacha-Olivenza, M. Á.; Rodríguez-Cano, A.; González-Martín, M. L.; Gallardo-Moreno, A. M. Kinetic of Adhesion of S. Epidermidis with Different EPS Production on Ti6Al4V Surfaces. *Biomed Res Int* **2019**, *2019*, 1437806. https://doi.org/10.1155/2019/1437806.

(209) Carniello, V.; Peterson, B. W.; van der Mei, H. C.; Busscher, H. J. Physico-Chemistry from Initial Bacterial Adhesion to Surface-Programmed Biofilm Growth.

Advances in Colloid and Interface Science **2018**, *261*, 1–14. https://doi.org/10.1016/j.cis.2018.10.005.

(210) Power, L.; Itier, S.; Hawton, M.; Schraft, H. Time Lapse Confocal Microscopy Studies of Bacterial Adhesion to Self-Assembled Monolayers and Confirmation of a Novel Approach to the Thermodynamic Model. *Langmuir* **2007**, *23* (10), 5622–5629. https://doi.org/10.1021/la070099o.

(211) He, L.; Niemeyer, B. A Novel Correlation for Protein Diffusion Coefficients Based on Molecular Weight and Radius of Gyration. *Biotechnology Progress* **2003**, *19* (2), 544–548. https://doi.org/10.1021/bp0256059.

(212) Liu, J.; Xu, Y.; Sun, H. Diffusion-Controlled Adsorption Kinetics of Surfactant at Air/Solution Interface. *Chinese Journal of Chemical Engineering* **2013**, *21* (9), 953–958. https://doi.org/10.1016/S1004-9541(13)60562-5.

(213) Rudzinski, W.; Plazinski, W. Studies of the Kinetics of Solute Adsorption at Solid/Solution Interfaces: On the Possibility of Distinguishing between the Diffusional and the Surface Reaction Kinetic Models by Studying the Pseudo-First-Order Kinetics. *J. Phys. Chem. C* **2007**, *111* (41), 15100–15110. https://doi.org/10.1021/jp073249c.

(214) Rudzinski, W.; Plazinski, W. Kinetics of Solute Adsorption at Solid/Solution Interfaces: On the Special Features of the Initial Adsorption Kinetics. *Langmuir* **2008**, *24* (13), 6738–6744. https://doi.org/10.1021/la800743a.

(215) Taktikos, J.; Stark, H.; Zaburdaev, V. How the Motility Pattern of Bacteria Affects Their Dispersal and Chemotaxis. *PLOS ONE* **2013**, *8* (12), e81936. https://doi.org/10.1371/journal.pone.0081936.

(216) Kim, M. J.; Breuer, K. S. Enhanced Diffusion Due to Motile Bacteria. *Physics of Fluids* **2004**, *16* (9), L78–L81. https://doi.org/10.1063/1.1787527.

(217) Licata, N. A.; Mohari, B.; Fuqua, C.; Setayeshgar, S. Diffusion of Bacterial Cells in Porous Media. *Biophys J* **2016**, *110* (1), 247–257. https://doi.org/10.1016/j.bpj.2015.09.035.

(218) Berg, H. C. *Random Walks in Biology*; Princeton University Press, 1993.

(219) Kaczorek, E.; Olszanowski, A. Uptake of Hydrocarbon by Pseudomonas Fluorescens (P1) and Pseudomonas Putida (K1) Strains in the Presence of Surfactants: A Cell Surface Modification. *Water Air Soil Pollut* **2011**, *214* (1–4), 451–459. https://doi.org/10.1007/s11270-010-0436-7.

(220) Zhang, D.; Zhu, L.; Li, F. Influences and Mechanisms of Surfactants on Pyrene Biodegradation Based on Interactions of Surfactant with a Klebsiella Oxytoca Strain. *Bioresource Technology* **2013**, *142*, 454–461. https://doi.org/10.1016/j.biortech.2013.05.077.

(221) Lin, W.; Liu, S.; Tong, L.; Zhang, Y.; Yang, J.; Liu, W.; Guo, C.; Xie, Y.; Lu, G.; Dang, Z. Effects of Rhamnolipids on the Cell Surface Characteristics of Sphingomonas Sp. GY2B and the Biodegradation of Phenanthrene. *RSC Advances* **2017**, *7* (39), 24321–24330. https://doi.org/10.1039/C7RA02576A.

(222) Dey, J.; Thapa, U.; Ismail, K. Aggregation and Adsorption of Sodium Dioctylsulfosuccinate in Aqueous Ammonium Chloride Solution: Role of Mixed Counterions. *Journal of Colloid and Interface Science* **2012**, *367* (1), 305–310. https://doi.org/10.1016/j.jcis.2011.10.055.

(223) Wouters, T. de; Jans, C.; Niederberger, T.; Fischer, P.; Rühs, P. A. Adhesion Potential of Intestinal Microbes Predicted by Physico-Chemical Characterization Methods. *PLOS ONE* **2015**, *10* (8), e0136437. https://doi.org/10.1371/journal.pone.0136437.

(224) Yuan, Y.; P. Hays, M.; R. Hardwidge, P.; Kim, J. Surface Characteristics Influencing Bacterial Adhesion to Polymeric Substrates. *RSC Advances* **2017**, *7* (23), 14254–14261. https://doi.org/10.1039/C7RA01571B.

(225) Gao, Z. P.; Nie, P.; Lu, J. F.; Liu, L. Y.; Xiao, T. Y.; Liu, W.; Liu, J. S.; Xie, H. X. Type III Secretion System Translocon Component EseB Forms Filaments on and Mediates Autoaggregation of and Biofilm Formation by Edwardsiella Tarda. *Appl Environ Microbiol* **2015**, *81* (17), 6078–6087. https://doi.org/10.1128/AEM.01254-15.

(226) Kragh, K. N.; Hutchison, J. B.; Melaugh, G.; Rodesney, C.; Roberts, A. E. L.; Irie, Y.; Jensen, P. Ø.; Diggle, S. P.; Allen, R. J.; Gordon, V.; Bjarnsholt, T. Role of Multicellular Aggregates in Biofilm Formation. *mBio* **2016**, *7* (2). https://doi.org/10.1128/mBio.00237-16.

(227) Sorroche, F. G.; Spesia, M. B.; Zorreguieta, Á.; Giordano, W. A Positive Correlation between Bacterial Autoaggregation and Biofilm Formation in Native Sinorhizobium Meliloti Isolates from Argentina. *Appl Environ Microbiol* **2012**, *78* (12), 4092–4101. https://doi.org/10.1128/AEM.07826-11.

(228) Cruz, L. F.; Cobine, P. A.; De La Fuente, L. Calcium Increases Xylella Fastidiosa Surface Attachment, Biofilm Formation, and Twitching Motility. *Appl Environ Microbiol* **2012**, *78* (5), 1321–1331. https://doi.org/10.1128/AEM.06501-11.

(229) Foster, L. L.; Yusa, S.; Kuroda, K. Solution-Mediated Modulation of Pseudomonas Aeruginosa Biofilm Formation by a Cationic Synthetic Polymer. *Antibiotics (Basel)* **2019**, *8* (2). https://doi.org/10.3390/antibiotics8020061.

(230) Das, T.; Sehar, S.; Koop, L.; Wong, Y. K.; Ahmed, S.; Siddiqui, K. S.; Manefield, M. Influence of Calcium in Extracellular DNA Mediated Bacterial Aggregation and Biofilm Formation. *PLoS One* **2014**, *9* (3). https://doi.org/10.1371/journal.pone.0091935.

(231) Jiang, H.-L.; Tay, J.-H.; Maszenan, A. M.; Tay, S. T.-L. Enhanced Phenol Biodegradation and Aerobic Granulation by Two Coaggregating Bacterial Strains. *Environmental Science and Technology* **2006**, *40*, 6137–6142. https://doi.org/10.1021/es0609295.

(232) Mack, D.; Siemssen, N.; Laufs, R. Parallel Induction by Glucose of Adherence and a Polysaccharide Antigen Specific for Plastic-Adherent Staphylococcus Epidermidis: Evidence for Functional Relation to Intercellular Adhesion. *Infect Immun* **1992**, *60* (5), 2048–2057.

(233) Ochiai, K.; Kurita-Ochiai, T.; Kamino, Y.; Ikeda, T. Effect of Co-Aggregation on the Pathogenicity of Oral Bacteria. *J Med Microbiol* **1993**, *39* (3), 183–190. https://doi.org/10.1099/00222615-39-3-183.

(234) Montero, D. A.; Velasco, J.; Del Canto, F.; Puente, J. L.; Padola, N. L.; Rasko, D. A.; Farfán, M.; Salazar, J. C.; Vidal, R. Locus of Adhesion and Autoaggregation (LAA), a Pathogenicity Island Present in Emerging Shiga Toxin–Producing Escherichia Coli Strains. *Scientific Reports* **2017**, *7* (1), 7011. https://doi.org/10.1038/s41598-017-06999-y.

(235) Bossier, P.; Verstraete, W. Triggers for Microbial Aggregation in Activated Sludge? *Appl Microbiol Biotechnol* **1996**, *45* (1), 1–6. https://doi.org/10.1007/s002530050640.

(236) Monier, J.-M.; Lindow, S. E. Differential Survival of Solitary and Aggregated Bacterial Cells Promotes Aggregate Formation on Leaf Surfaces. *Proc Natl Acad Sci U S A* **2003**, *100* (26), 15977–15982. https://doi.org/10.1073/pnas.2436560100.

(237) Corno, G.; Coci, M.; Giardina, M.; Plechuk, S.; Campanile, F.; Stefani, S. Antibiotics Promote Aggregation within Aquatic Bacterial Communities. *Front. Microbiol.* **2014**, *5*. https://doi.org/10.3389/fmicb.2014.00297.

(238) Eboigbodin, K. E.; Newton, J. R. A.; Routh, A. F.; Biggs, C. A. Role of Nonadsorbing Polymers in Bacterial Aggregation. *Langmuir* **2005**, *21* (26), 12315–12319. https://doi.org/10.1021/la051740u.

(239) Dorken, G.; Ferguson, G. P.; French, C. E.; Poon, W. C. K. Aggregation by Depletion Attraction in Cultures of Bacteria Producing Exopolysaccharide. *J R Soc Interface* **2012**, *9* (77), 3490–3502. https://doi.org/10.1098/rsif.2012.0498.

(240) Secor, P. R.; Michaels, L. A.; Ratjen, A.; Jennings, L. K.; Singh, P. K. Entropically Driven Aggregation of Bacteria by Host Polymers Promotes Antibiotic Tolerance in Pseudomonas Aeruginosa. *PNAS* **2018**, *115* (42), 10780–10785. https://doi.org/10.1073/pnas.1806005115.

(241) Porter, M. K.; Steinberg, A. P.; Ismagilov, R. F. Interplay of Motility and Polymer-Driven Depletion Forces in the Initial Stages of Bacterial Aggregation. *Soft Matter* **2019**, *15* (35), 7071–7079. https://doi.org/10.1039/C9SM00791A.

(242) Schwarz-Linek, J.; Winkler, A.; G. Wilson, L.; T. Pham, N.; Schilling, T.; K. Poon, W. C. Polymer -Induced Phase Separation in Escherichia Coli Suspensions. *Soft Matter* **2010**, *6* (18), 4540–4549. https://doi.org/10.1039/C0SM00214C.

(243) Marenduzzo, D.; Finan, K.; Cook, P. R. The Depletion Attraction: An Underappreciated Force Driving Cellular Organization. *J Cell Biol* **2006**, *175* (5), 681–686. https://doi.org/10.1083/jcb.200609066.

(244) González García, Á.; Nagelkerke, M. M. B.; Tuinier, R.; Vis, M. Polymer-Mediated Colloidal Stability: On the Transition between Adsorption and Depletion. *Advances in Colloid and Interface Science* **2020**, *275*, 102077. https://doi.org/10.1016/j.cis.2019.102077.

(245) Disney, M. D.; Zheng, J.; Swager, T. M.; Seeberger, P. H. Detection of Bacteria with Carbohydrate-Functionalized Fluorescent Polymers. *J. Am. Chem. Soc.* **2004**, *126* (41), 13343–13346. https://doi.org/10.1021/ja047936i.

(246) Arenas, J.; Nijland, R.; Rodriguez, F. J.; Bosma, T. N. P.; Tommassen, J. Involvement of Three Meningococcal Surface-Exposed Proteins, the Heparin-Binding Protein NhbA, the α-Peptide of IgA Protease and the Autotransporter Protease NalP, in Initiation of Biofilm Formation. *Mol Microbiol* **2013**, *87* (2), 254–268. https://doi.org/10.1111/mmi.12097.

(247) Rose, R. K. The Role of Calcium in Oral Streptococcal Aggregation and the Implications for Biofilm Formation and Retention. *Biochimica et Biophysica Acta (BBA) - General Subjects* **2000**, *1475* (1), 76–82. https://doi.org/10.1016/S0304-4165(00)00048-9.

(248) Leite, B.; Ishida, M. L.; Alves, E.; Carrer, H.; Pascholati, S. F.; Kitajima, E. W. Genomics and X-Ray Microanalysis Indicate That Ca2+ and Thiols Mediate the Aggregation and Adhesion of Xylella Fastidiosa. *Brazilian Journal of Medical and Biological Research* **2002**, *35* (6), 645–650. https://doi.org/10.1590/S0100-879X2002000600003.

(249) Das, T.; Sharma, P. K.; Busscher, H. J.; van der Mei, H. C.; Krom, B. P. Role of Extracellular DNA in Initial Bacterial Adhesion and Surface Aggregation. *Appl Environ Microbiol* **2010**, *76* (10), 3405–3408. https://doi.org/10.1128/AEM.03119-09.

(250) Das, T.; Krom, B. P.; Mei, H. C. van der; Busscher, H. J.; Sharma, P. K. DNA-Mediated Bacterial Aggregation Is Dictated by Acid–Base Interactions. *Soft Matter* **2011**, *7* (6), 2927–2935. https://doi.org/10.1039/C0SM01142H.

(251) Gestwicki, J. E.; Strong, L. E.; Cairo, C. W.; Boehm, F. J.; Kiessling, L. L. Cell Aggregation by Scaffolded Receptor Clusters. *Chem Biol* **2002**, *9* (2), 163–169. https://doi.org/10.1016/s1074-5521(02)00102-3.

(252) Harris, R. H.; Mitchell, R. The Role of Polymers in Microbial Aggregation. *Annual Review of Microbiology* **1973**, *27* (1), 27–50. https://doi.org/10.1146/annurev.mi.27.100173.000331.

(253) Qin, Z.; Ou, Y.; Yang, L.; Zhu, Y.; Tolker-Nielsen, T.; Molin, S.; Qu, D. Role of Autolysin-Mediated DNA Release in Biofilm Formation of Staphylococcus Epidermidis. *Microbiology (Reading)* **2007**, *153* (Pt 7), 2083–2092. https://doi.org/10.1099/mic.0.2007/006031-0.

(254) Caldara, M.; Friedlander, R. S.; Kavanaugh, N. L.; Aizenberg, J.; Foster, K. R.; Ribbeck, K. Mucin Biopolymers Prevent Bacterial Aggregation by Retaining Cells in the Free-Swimming State. *Curr Biol* **2012**, *22* (24), 2325–2330. https://doi.org/10.1016/j.cub.2012.10.028.

(255) De La Fuente, L.; Burr, T. J.; Hoch, H. C. Autoaggregation of Xylella Fastidiosa Cells Is Influenced by Type I and Type IV Pili. *AEM* **2008**, *74* (17), 5579–5582. https://doi.org/10.1128/AEM.00995-08.

(256) Guerry, P. Campylobacter Flagella: Not Just for Motility. *Trends in Microbiology* **2007**, *15* (10), 456–461. https://doi.org/10.1016/j.tim.2007.09.006.

(257) Hoeflinger, J. L.; Miller, M. J. Cronobacter Sakazakii ATCC 29544 Autoaggregation Requires FliC Flagellation, Not Motility. *Front Microbiol* **2017**, *8*. https://doi.org/10.3389/fmicb.2017.00301.

(258) Olsén, A.; Jonsson, A.; Normark, S. Fibronectin Binding Mediated by a Novel Class of Surface Organelles on Escherichia Coll. *Nature* **1989**, *338* (6217), 652–655. https://doi.org/10.1038/338652a0.

(259) Arnqvist, A.; Olsén, A.; Pfeifer, J.; Russell, D. G.; Normark, S. The Crl Protein Activates Cryptic Genes for Curli Formation and Fibronectin Binding in Escherichia Coli HB101. *Molecular Microbiology* **1992**, *6* (17), 2443–2452. https://doi.org/10.1111/j.1365-2958.1992.tb01420.x.

(260) Tree, J. J.; Ulett, G. C.; Hobman, J. L.; Constantinidou, C.; Brown, N. L.; Kershaw, C.; Schembri, M. A.; Jennings, M. P.; McEwan, A. G. The Multicopper Oxidase (CueO) and Cell Aggregation in Escherichia Coli. *Environ Microbiol* **2007**, *9* (8), 2110–2116. https://doi.org/10.1111/j.1462-2920.2007.01320.x.

(261) Klebensberger, J.; Lautenschlager, K.; Bressler, D.; Wingender, J.; Philipp, B. Detergent-Induced Cell Aggregation in Subpopulations of Pseudomonas Aeruginosa as a Preadaptive Survival Strategy. *Environ Microbiol* **2007**, *9* (9), 2247–2259. https://doi.org/10.1111/j.1462-2920.2007.01339.x.

(262) Passow, U.; Sweet, J.; Quigg, A. How the Dispersant Corexit Impacts the Formation of Sinking Marine Oil Snow. *Marine Pollution Bulletin* **2017**, *125* (1), 139–145. https://doi.org/10.1016/j.marpolbul.2017.08.015.

(263) Zhong, Z.-P.; Liu, Y.; Liu, H.-C.; Wang, F.; Zhou, Y.-G.; Liu, Z.-P. Marinobacter Halophilus Sp. Nov., a Halophilic Bacterium Isolated from a Salt Lake. *Int J Syst Evol Microbiol* **2015**, *65* (9), 2838–2845. https://doi.org/10.1099/ijs.0.000338.

(264) Trunk, T.; Khalil, H. S.; Leo, J. C. Bacterial Autoaggregation. *AIMS Microbiol* **2018**, *4* (1), 140–164. https://doi.org/10.3934/microbiol.2018.1.140.

(265) Swinehart, D. F. The Beer-Lambert Law. *J. Chem. Educ.* **1962**, *39* (7), 333.

(266) Sun, J.; Goldys, E. M. Linear Absorption and Molar Extinction Coefficients in Direct Semiconductor Quantum Dots. *J. Phys. Chem. C* **2008**, *112* (25), 9261–9266. https://doi.org/10.1021/jp800700m.

(267) Alhede, M.; Lorenz, M.; Fritz, B. G.; Jensen, P. Ø.; Ring, H. C.; Bay, L.; Bjarnsholt, T. Bacterial Aggregate Size Determines Phagocytosis Efficiency of Polymorphonuclear Leukocytes. *Med Microbiol Immunol* **2020**, *209* (6), 669–680. https://doi.org/10.1007/s00430-020-00691-1.

(268) Mondain-Monval, O.; Leal-Calderon, F.; Phillip, J.; Bibette, J. Depletion Forces in the Presence of Electrostatic Double Layer Repulsion. *Phys. Rev. Lett.* **1995**, *75* (18), 3364–3367. https://doi.org/10.1103/PhysRevLett.75.3364.

(269) Patrauchan, M. A.; Sarkisova, S.; Sauer, K.; Franklin, M. J. Calcium Influences Cellular and Extracellular Product Formation during Biofilm-Associated Growth of a Marine Pseudoalteromonas Sp. *Microbiology (Reading)* **2005**, *151* (Pt 9), 2885–2897. https://doi.org/10.1099/mic.0.28041-0.

(270) de Kerchove, A. J.; Elimelech, M. Calcium and Magnesium Cations Enhance the Adhesion of Motile and Nonmotile Pseudomonas Aeruginosa on Alginate Films. *Langmuir* **2008**, *24* (7), 3392–3399. https://doi.org/10.1021/la7036229.

(271) Abdel-Nour, M.; Duncan, C.; Prashar, A.; Rao, C.; Ginevra, C.; Jarraud, S.; Low, D. E.; Ensminger, A. W.; Terebiznik, M. R.; Guyard, C. The Legionella Pneumophila Collagen-Like Protein Mediates Sedimentation, Autoaggregation, and Pathogen-Phagocyte Interactions. *Appl Environ Microbiol* **2014**, *80* (4), 1441–1454. https://doi.org/10.1128/AEM.03254-13.

(272) King, M. M.; Kayastha, B. B.; Franklin, M. J.; Patrauchan, M. A. Calcium Regulation of Bacterial Virulence. In *Calcium Signaling*; Islam, Md. S., Ed.; Advances in Experimental Medicine and Biology; Springer International Publishing: Cham, 2020; pp 827–855. https://doi.org/10.1007/978-3-030-12457-1_33.

(273) Lopez, J. M.; Hirsa, A. H. Coupling of the Interfacial and Bulk Flow in Knife-Edge Viscometers. *Physics of Fluids* **2015**, *27* (4), 042102. https://doi.org/10.1063/1.4916619.

(274) Flemming, H.-C.; Wingender, J. The Biofilm Matrix. *Nature Reviews Microbiology* **2010**, *8* (9), 623–633. https://doi.org/10.1038/nrmicro2415.

(275) Costa, O. Y. A.; Raaijmakers, J. M.; Kuramae, E. E. Microbial Extracellular Polymeric Substances: Ecological Function and Impact on Soil Aggregation. *Front Microbiol* **2018**, *9*. https://doi.org/10.3389/fmicb.2018.01636.

(276) Lattner, D.; Flemming, H.-C.; Mayer, C. 13C-NMR Study of the Interaction of Bacterial Alginate with Bivalent Cations. *International Journal of Biological Macromolecules* **2003**, *33* (1), 81–88. https://doi.org/10.1016/S0141-8130(03)00070-9.

(277) Ennouri, H.; d'Abzac, P.; Hakil, F.; Branchu, P.; Naïtali, M.; Lomenech, A.-M.; Oueslati, R.; Desbrières, J.; Sivadon, P.; Grimaud, R. The Extracellular Matrix of the Oleolytic Biofilms of Marinobacter Hydrocarbonoclasticus Comprises Cytoplasmic Proteins and T2SS Effectors That Promote Growth on Hydrocarbons and Lipids. *Environ Microbiol* **2017**, *19* (1), 159–173. https://doi.org/10.1111/1462-2920.13547.

(278) Laganenka, L.; Colin, R.; Sourjik, V. Chemotaxis towards Autoinducer 2 Mediates Autoaggregation in Escherichia Coli. *Nature Communications* **2016**, *7* (1), 1–11. https://doi.org/10.1038/ncomms12984.

(279) Re, B. D.; Busetto, A.; Vignola, G.; Sgorbati, B.; Palenzona, D. L. Autoaggregation and Adhesion Ability in a Bifidobacterium Suis Strain. *Letters in Applied Microbiology* **1998**, *27* (5), 307–310. https://doi.org/10.1046/j.1472-765X.1998.t01-1-00449.x.

(280) Re, B. D.; Sgorbati, B.; Miglioli, M.; Palenzona, D. Adhesion, Autoaggregation and Hydrophobicity of 13 Strains of Bifidobacterium Longum. *Letters in Applied*

Microbiology **2000**, *31* (6), 438–442. https://doi.org/10.1046/j.1365-2672.2000.00845.x.

(281) Dewangan, N. K.; Conrad, J. C. Bacterial Motility Enhances Adhesion to Oil Droplets. *Soft Matter* **2020**, *16* (35), 8237–8244. https://doi.org/10.1039/D0SM00944J.

(282) Mounier, J.; Hakil, F.; Branchu, P.; Naïtali, M.; Goulas, P.; Sivadon, P.; Grimaud, R. AupA and AupB Are Outer and Inner Membrane Proteins Involved in Alkane Uptake in Marinobacter Hydrocarbonoclasticus SP17. *mBio* **2018**, *9* (3), e00520-18. https://doi.org/10.1128/mBio.00520-18.

Disclosure

1. *Chapter 2 has been published in the journal 'Langmuir'*

   Dewangan, N.K. and Conrad, J.C., Langmuir, 2018, 34(46), pp.14012-14021

2. *Chapter 3 has been published in the journal 'Soft Matter'*

   Dewangan, N.K. and Conrad, J.C., Soft Matter, 2019, 15(45), pp.9368-9375

3. *Chapter 4 has been published in the journal 'Soft Matter'*

   Dewangan, N.K. and Conrad, J.C., Soft Matter, 2020, 16, pp.8237-8244